HOKKAIDO UNIVERSITY

Title	Experimental study for modeling unloading behavior of marine clays
Author(s)	樊, ソウ
Degree Grantor	北海道大学
Degree Name	博士(工学)
Dissertation Number	甲第16538号
Issue Date	2025-06-30
DOI	https://doi.org/10.14943/doctoral.k16538
Doc URL	https://hdl.handle.net/2115/95708
Type	doctoral thesis
File Information	Zheng_Fan.pdf

Hokkaido University Collection of Scholarly and Academic Papers : HUSCAP

令和 7 年度博士論文

Experimental study for modeling unloading behavior of marine clays

海成粘土における除荷挙動の実験研究とモデル化

Graduate School of Engineering
Division of Field Engineering for the Environment
FAN Zheng
Supervisor: WATABE Yoichi

Abstract

There is a rising demand for land reclamation in coastal cities with economic and demographic growth in East and Southeast Asia. Marine clays play a critical role in these projects, as their deformation characteristics significantly impact subsoil quality. The long-term loading behavior of marine clays has been studied by many researchers. However, there are relatively few existing studies focusing on the unloading behavior after preloading, and strain rate dependency on the unloading behavior of marine clays remains unclear.

This study aims to accumulate experimental data on the unloading behavior of marine clays and develop a strain rate-based model for improving the prediction accuracy for marine clays' unloading behavior. The authors conducted a series of constant rate of strain (CRS) consolidation tests from loading to unloading, and long-term unloading oedometer tests for marine clays to observe the unloading behavior. Controlling the preloading duration corresponding to different strain rates at the end of preloading to elucidate the stress history's effect.

Moreover, instead of a parameter σ'_p (preconsolidation pressure) for normal consolidation visco-plastic behavior, the authors develop and propose a new visco-plastic model by introducing a concept of plastic rebound boundary and a new parameter R for swelling behavior in unloading. This parameter R represents the normalized distance from the current stress state to the plastic rebound boundary in logarithmic effective consolidation stress. Therefore, the visco-plastic model for behavior in the loading stage has been developed into the swelling visco-plastic behavior in the unloading stage of marine clay. Comparing the simulation and test results, the simplified visco-plastic swelling model shows great agreement with the test results.

This thesis provides a novel perspective on the unloading behavior of marine clays and experimentally validates the efficacy of a strain rate-based model in describing their swelling behavior. The new model offers significant theoretical support for optimizing foundation design and prediction in future coastal land reclamation projects.

The thesis is composed of 8 chapters. Chapter 1 introduces the study's background, objectives, and the need for improving the accuracy of prediction for unloading behavior

of marine clay. Chapter 2 provides a literature review of experimental research, such as incremental loading (IL) oedometer tests, constant rate of strain (CRS) consolidation tests and inter-connected consolidation tests, on the loading and unloading behavior of marine clays, as well as some recent constitutive models developed to simulate unloading behavior. Chapter 3 introduces the physical properties of Ariake clay, Louiseville clay and Onsøy clay, respectively. The consolidation characteristics of the three marine clays are compared based on their compression curves. Chapter 4 describes two types of CRS consolidation test methodologies: constant unloading strain rate consolidation test and multi-stepwise unloading strain rate consolidation test. The experimental results demonstrate the direct influence of unloading strain rate on the unloading behavior. In addition, the strain rate dependency is compared between loading and unloading stages. Chapter 5 presents two types of incremental loading oedometer test methodologies: four-stage unloading oedometer test and long-term unloading oedometer test. The influence of overconsolidation ratio (OCR) and preloading duration on the unloading behavior is investigated, and the strain rate dependency during unloading is quantitatively evaluated. Chapter 6 describes the proposed model's development process in detail and presents its simulation results based on the experimental data. First, the loading behavior of the new model adopts the formulation proposed by Watabe et al. (2008; 2012). Then, a new strain-rate-based swelling model for unloading is developed by incorporating the concept of a plastic unloading boundary (Amerasinghe and Kraft, 1983; Tachibana et al., 2020) and reference overconsolidation ratio (OCR_{ref}). Finally, numerical simulations are conducted to evaluate the model's performance. The simulated results show good agreement with the observed unloading behavior of marine clays. Chapter 7 further discusses the new visco-plastic model, including a comparison between the swelling behavior during unloading and loading behavior. The advantages of introducing the reference overconsolidation ratio OCR_{ref} are elaborated, and the proposed model is systematically compared with some existing models. Finally, Chapter 8 summarizes the study's findings and provides some recommendations for further research.

Published works

1. **FAN Zheng**, WATABE Yoichi, Experimental study for modeling unloading swelling behavior of Ariake clay, Soils and Foundations.

2. **FAN Zheng**, WATABE Yoichi, Evaluation of marine clays' strain rate dependency during the unloading process, 2023-12, Geotec Hanoi 2023, Hanoi, Vietnam.

3. **FAN Zheng**, WATABE Yoichi, Strain rate dependency of Ariake clay during the unloading process measured by CRS test, 2021-07, 56th Japan National Conference on Geotechnical Engineering, Yamagata Prefecture.

4. **FAN Zheng**, WATABE Yoichi, Strain rate dependency of marine clays during the unloading process, 2022-07, 57th Japan National Conference on Geotechnical Engineering, Niigata Prefecture.

5. **FAN Zheng**, WATABE Yoichi, A simplified visco-plastic model for swelling behavior of marine clay in unloading, 2023-07, 58th Japan National Conference on Geotechnical Engineering, Fukuoka Prefecture.

6. ZHANG Sui, **FAN Zheng**, WATABE Yoichi, Influence of initial conditions on consolidation behaviors in hypotheses A and B examined by means of interconnected oedometer test, 23-01, The 63rd Hokkaido Regional Technical Committee, Hokkaido, Sapporo city.

7. YI Hanxiang, WATABE Yoichi, **FAN Zheng**, Application of C+S model to prediction of unloading swelling and recompression behaviors observed for Osaka Bay clay and Ariake clay, 23-01, The 63rd Hokkaido Regional Technical Committee, Hokkaido, Sapporo city.

Acknowledgments

First and foremost, I would like to express my deep gratitude to my supervisor, Professor Watabe Yoichi, for his invaluable guidance, continuous encouragement, and insightful advice throughout my doctoral studies. His expertise and unwavering support have been instrumental in shaping my research and academic development.

I am also profoundly grateful to Professor Nishimura and Assistant Professor Fukuda from our Soil Mechanics Laboratory for their generous support and constructive feedback, which have significantly contributed to the completion of my research.

Including both my master's and doctoral studies, I have spent five years in Soil Mechanics laboratory, and I feel fortunate to have had the opportunity to work with so many excellent students and technicians. Their collaboration and discussions have greatly enriched my academic career, making my time in the laboratory both productive and enjoyable.

Part of the experimental work in this study was conducted at the Soil Mechanics and Geo-Environment Group of the Port and Airport Research Institute (PARI). I am sincerely grateful for the kind support of the group members during my time there. In particular, I would like to express my heartfelt appreciation to Dr. Sugiyama and Ms. Asai for their assistance.

Lastly, I would like to extend my appreciation to my parents for their unwavering support, unconditional love, and sacrifices that have allowed me to pursue and complete my doctoral degree. Without their encouragement and belief in me, I cannot imagine reaching this milestone in my academic career.

This research project was supported by JST SPRING, Grant Number JPMJSP2119. I sincerely thank them for their generous financial support.

Contents

List of figures

List of tables

Chapter 1 Introduction

1.1 Background

In the past few decades, economic prosperity and demographic expansion have significantly escalated the demand for land reclamation in coastal cities of East and Southeast Asia, where flat land is scarce. Land reclamation emerges as a strategic solution, facilitating urban development by converting water-adjacent spaces into viable land. Typically, the process relies on geotechnical materials such as marine clays. Therefore, the deformation of marine clays becomes a crucial concern for the quality of subsoil conditions.

The swelling behavior of marine clay, especially its time-dependent characteristics, plays an important role in determining the long-term stability of reclaimed land. In the background of land reclamation, preloading and surcharging techniques are commonly used to accelerate consolidation and enhance soil strength. After the temporary surcharges are removed, the underlying clay layers often undergo swelling, which can lead to significant deformation and affect the serviceability of the reclaimed land. Therefore, understanding the time-dependent swelling behavior of marine clay under unloading conditions is essential for predicting post-construction settlement and designing effective ground improvement strategies.

Many researchers have studied the long-term consolidation behavior of marine clays using the isotache concept in which the effect of the strain rate on the compression characteristics is considered (Leroueil et al. 1985; Hinchberger and Rowe 1998; Rowe and Hinchberger 1998; Kim and Leroueil 2001; Den Haan and Kamao 2003; Tanaka et al. 2006; Watabe et al. 2008; 2012; Qu et al. 2010; Degago et al. 2011; Yuan and Whittle 2018; Yu et al. 2021). Most of these studies have focused on assessing secondary consolidation in consideration of the strain rate effect. Within this research realm, Watabe et al. (2008; 2012) proposed a strain rate-based model that applied a non-linear isotache relationship with a creep limit and the model excels in the compression field. However,

there are relatively few existing studies focusing on the unloading behavior after preloading (Mesri et al. 1978; Alonso and Navarro 2005). The unloading process is associated not only with recompression of clays but also with viscous swelling. Under a certain load, particularly when the load changes significantly, continuous swelling behavior is observed, and the deformation behavior after unloading is influenced by the preloading duration. Moreover, the strain rate dependency in the unloading behavior of marine clays remains unclear and requires further investigation (Tanaka et al. 2014). Figure 1-1 illustrates the strain rate dependency of clay during compression and swelling, respectively.

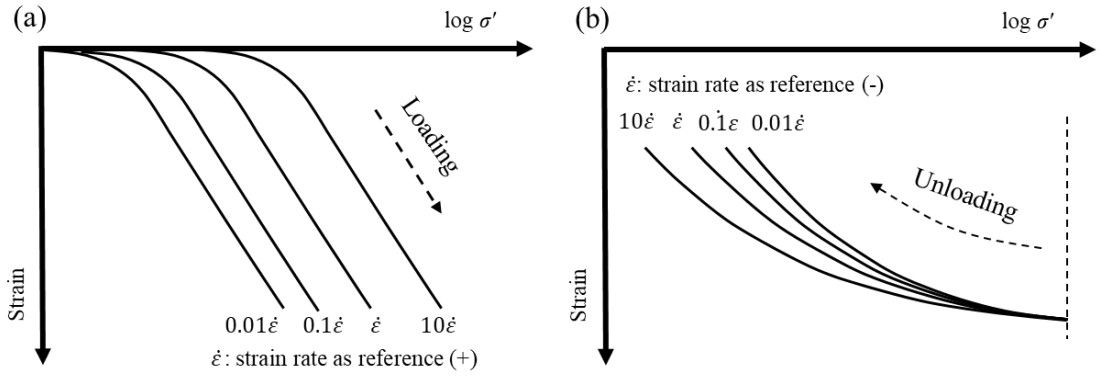

Figure 1-1 Strain rate dependency of clay in two stages (a) Compression stage; (b) Swelling stage.

1.2 Preloading with vertical drains (PVDs)

The PVDs method is one of the most widely used technologies on land and in coastal areas due to its proven efficiency in shortening the drainage path and accelerating the consolidation process. (Onoue, 1988; Chu et al., 2000, 2006; Indraratna et al., 2005; Laskar and Pal, 2016; Zhu et al., 2018; Zhou et al., 2023). Consolidation of compressible soil could take up to several years based on the thickness of the soft soil layer. Preloading is the process of placing additional vertical stress on compressible soil to reduce residual

settlement. In addition, the use of vertical drains to accelerate excess pore water pressure dissipation significantly shortens the time of the soil improvement.

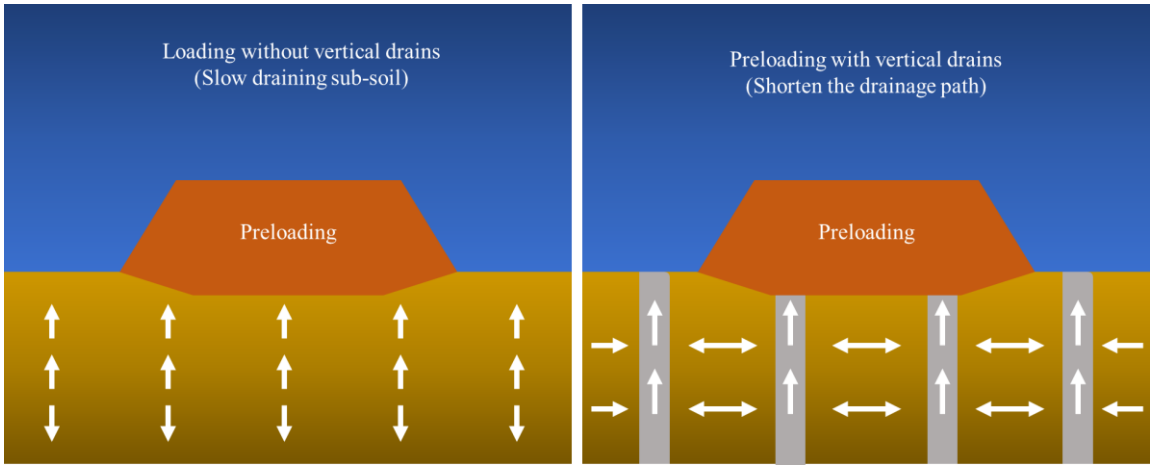

Figure 1-2 Diagrams of preloading

However, after removing the preload, a long-term viscous swelling occurs, and at the low *OCR* (over-consolidation ratio) condition, creep settlement will also happen even after swelling (Vergote et al. 2019). What's more, the unloading test results show that viscous swelling plays a prominent role in unloading behavior. Up to now, there is no model that can simulate the long-term unloading process well, including swelling at high *OCR* conditions. Also, the prediction of residual settlement is essential for land use in safety.

Therefore, the unloading behavior of clays is critical for preloading in large-scale reclamation projects. It is crucial to develop a method to improve the accuracy of unloading behavior prediction and establish a model for evaluating the unloading behavior of clay in the future.

1.3 Research objectives

The main objective of this study is to improve the accuracy of simulating the

unloading behavior of soil. Watabe et al. (2008) have demonstrated that a rate-dependent model based on the isotache concept is able to accurately predict the long-term loading behavior of soil. The isotache concept was proposed by Šuklje (1957), who introduced a unique relationship between the strain and the consolidation pressure corresponding to the strain rate associated with viscosity. Some researchers (Tanaka et al. 2014) have described a strain rate-dependent relationship will also play a significant role in the unloading behavior of marine clays. Therefore, a rate-dependent model based on the isotache concept will also play a significant role in predicting unloading behavior.

To achieve this, firstly, it is crucial to develop a method to quantitatively evaluate the strain rate dependency during the unloading behavior of clays. In this study, three kinds of marine clays, Ariake clay, Louiseville clay and Onsøy clay were examined by CRS consolidation test and incremental loading oedometer test to clarify the strain rate effect during the unloading behavior. The authors also evaluated a ratio ($C_{c\alpha}/C_c$ and $C_{s\alpha}/C_s$) to compare the strain rate dependency between loading and unloading. Secondly, based on the quantitative findings, the loading-phase model was extended to the unloading phase in order to simulate the experimental results. The individual objectives of this study are presented as follows:

- To clarify the shape of isotache lines during the unloading process and the location relationship between different isotache lines. Moreover, clarifying that the isotache lines are equally spaced, which is the same as the consolidation behavior or the difference between two neighboring isotache lines becomes larger with *OCR* (overconsolidation ratio, $OCR=\sigma'_{max}/\sigma'$) grows by CRS consolidation test.
- Try to develop a way that can evaluate the unloading strain rate dependency for one soil sample, similar to the approach proposed by (Watabe et al. 2020) for the loading process.
- To make clear the relationship between strain rate dependency and *OCR* during unloading process by incremental loading oedometer test.
- To generalize the isotache model that Watabe et al. (2008, 2021) proposed from loading into unloading conditions based on the result of this study.

1.4 Comparison between $C_{c\alpha}/C_c$ and $C_{s\alpha}/C_s$

The objective of this study is to quantitatively evaluate the strain rate dependency of the unloading behavior. For this reason, the author set a group of $C_{c\alpha}/C_c$ and $C_{s\alpha}/C_s$ in order to compare the strain rate dependency during loading and unloading. The values of $C_{c\alpha}/C_c$ and $C_{s\alpha}/C_s$ are able to estimate the strain rate dependency during compression and swelling respectively.

Geometrically, the values of $C_{c\alpha}/C_c$ and $C_{s\alpha}/C_s$ respectively represent the distance ($x_{\log p} = \Delta \log p'$) in above figures equals to increment of $\log p'$ for one log cycle of strain rate at a constant void ratio (Watabe et al. 2012), as shown in Figure 1-3 and Figure 1-4. The higher values of $C_{c\alpha}/C_c$ and $C_{s\alpha}/C_s$ means the stronger strain rate dependency when strain rate changes. (Here the $C_{c\alpha}$ is secondary consolidation index, generally expressed as C_α and $C_{s\alpha}$ is secondary swelling index.)

The formula derivation flow of loading behavior (Watabe et al. 2013) has been written hereunder:

As the Figure 1-3 shown, geometrically,

$$\frac{x}{x_{\log \mathrm{P}}} = \frac{C_\mathrm{c}}{1} \tag{1-1}$$

From the definition of secondary compression index in strain $C_{c\alpha}$:

$$\Delta e = C_{c\alpha} \Delta \log t \tag{1-2}$$

$$\dot{e} = \frac{\Delta \mathrm{e}}{\Delta t} = \frac{C_{c\alpha} \Delta \log t}{\Delta t} = \frac{C_{c\alpha}}{ln10} \frac{\Delta \ln t}{\Delta t} = \frac{C_{c\alpha}}{2.303} \frac{1}{t} \tag{1-3}$$

Eq. (1-3) means that the strain rate decreases with elapsed time in inverse proportion, indicating that the strain rate decreases by a factor of ten when elapsed time increases by 10 times ($\Delta \log t = 1$), if $C_{c\alpha}$ is constant during the time increment. From equation (2):

$$x = C_{c\alpha} \tag{1-4}$$

The distance $x_{\log \mathrm{P}}$ equals to increment of $\log p'$ for one log cycle of strain rate or void ratio rate,

$$x_{\log \mathrm{P}} = \frac{\Delta \log p\prime}{\Delta \log \dot{e}} \tag{1-5}$$

This equation is the exact definition of the parameter $C_{c\alpha}/C_c$:

$$\frac{C_{c\alpha}}{C_\mathrm{c}} = \frac{\Delta \log p\prime}{\Delta \log \dot{e}} \tag{1-6}$$

The formula derivation flow of unloading behavior is in line with the loading

behavior, so the derivation is omitted here. The equation for unloading behavior (Figure 1-4):

$$\frac{C_{s\alpha}}{C_s} = \frac{\Delta \log p\prime}{\Delta \log \dot{e}} \tag{1-7}$$

From the formulation, the forms of equation (1-6) for loading and equation (1-7) unloading seem similar, however, the data of $p', \dot{e}$ and e were derived from different processes, loading and unloading. Therefore, the value of $C_{c\alpha}/C_c$ is significantly larger than that of $C_{s\alpha}/C_s$.

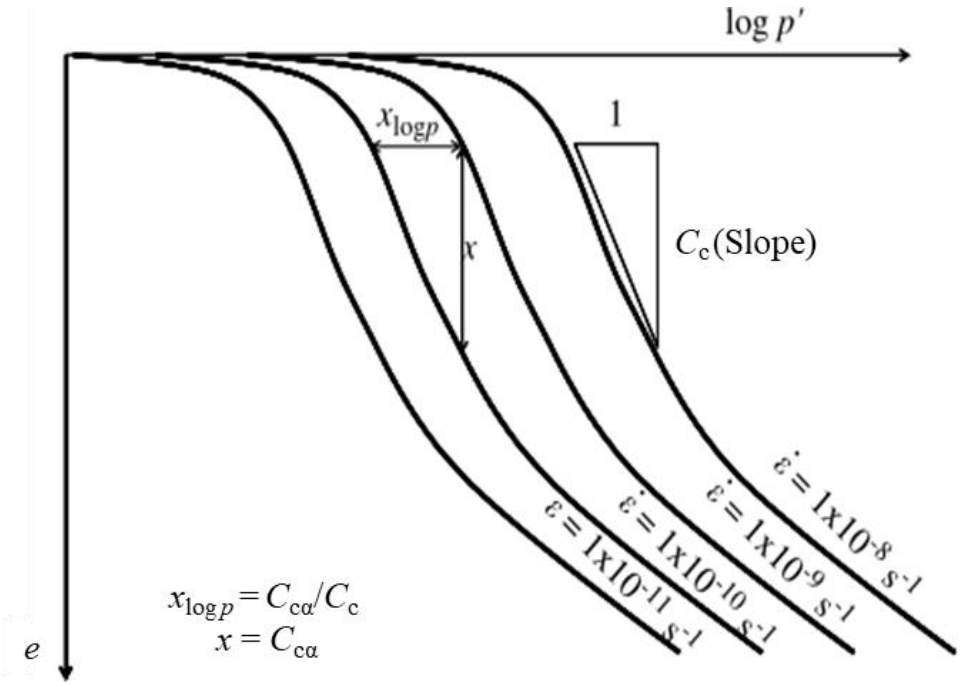

Figure 1-3 Illustration of geometrical relationship between the parameters (Loading)

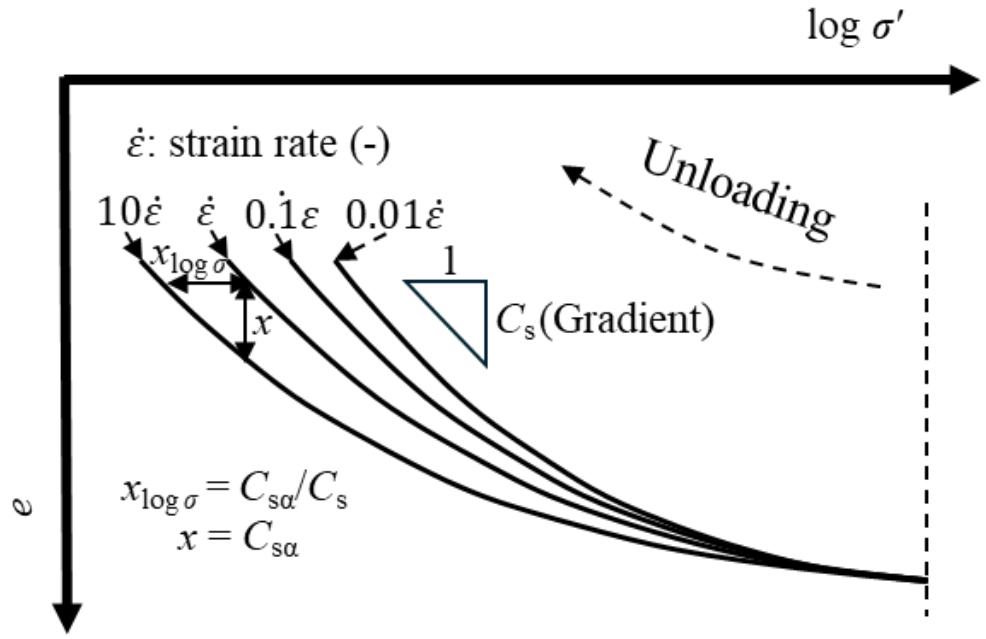

Figure 1-4 Illustration of geometrical relationship between the parameters (Unloading)

1.5 Introduction of this thesis

This study conducts constant rate of strain (CRS) unloading consolidation tests and a series of long-term oedometer tests on Ariake clay, Louisville clay, and Onsøy clay to address the insufficient understanding of time-dependent unloading behavior in marine clays. In particular, the strain-rate dependency of both recompression and viscous swelling during the unloading process remains unclear. The tests were designed to simulate the conditions typically encountered in land reclamation projects, where temporary surcharges are removed after consolidation. A new aspect of the experimental design is the variation in preloading durations, corresponding to different initial strain rates before the unloading process. Furthermore, the concept of plastic rebound (Amerasinghe and Kraft 1983; Tachibana et al. 2020) was applied to describe the mechanical behavior of marine clay during unloading. The proposed visco-plastic model, which was originally developed for the normal consolidation stage (Watabe et al. 2008; 2012) was modified to account for swelling behavior by introducing a new parameter, R,

representing the normalized distance from the current stress state to the plastic rebound boundary in logarithmic effective pressure. This enhancement aims to improve the precision in predicting marine clay's swelling behavior in unloading, which Yao and Fang (2020) named this behavior "negative creep".

Through this research, the modified model was applied to simulate the results of the long-term unloading oedometer test, contributing to a better understanding of the soil's response to loading history effects.

Due to the experimental design and model calculations of this study based on strain rate, for ease of description and computation, this paper similarly utilizes strain (ε) to characterize soil deformation behavior in the same manner as some scholars (Watabe et al. 2008; 2012, Yin and Tong 2011; Feng et al. 2017), rather than void ratio (e) (Yao and Fang 2020) and settlement (mm) (Alonso and Navarro 2005). Compression is designated as positive; swelling is designated as negative for strains according to the convention of soil mechanics.

Chapter 2 Literature review

2.1 Loading behavior

The one-dimensional sudden loading of a clay sample results in a time-dependent decrease in void ratio, as illustrated in Figure 2-1. During primary consolidation, settlement is governed by the dissipation of excess pore water pressures and Darcy's Law. During secondary consolidation, the rate of settlement is controlled by soil viscosity. Secondary consolidation is characterized by the slope of the consolidation curve, the secondary compression index $C_\alpha = \Delta e/\Delta \log t$.

Secondary consolidation of soils has achieved much importance as a significant contribution to soft clays' long-term settlements. There are three main approaches to evaluating the consolidation settlement, both practically and theoretically, and these are written as follows:

(1) The coupling of Terzaghi's one-dimensional consolidation theory and the constant C_α concept.

(2) The end of primary consolidation (EOP) concept (Mesri and Choi 1985) and the constant C_α/C_c concept (Mesri and Castro 1987).

(3) The isotache concept introduced by (Šuklje 1957).

where C_c denotes the consolidation index and C_α denotes the coefficient of secondary consolidation.

Approach (1): In practice, approach (1) is the most widely used. After the end of primary consolidation, the decremental void ratio induced by secondary consolidation varies linearly against the logarithmic elapsed time after loading, log t. The decremental void ratio corresponding to one cycle of logarithmic time during the secondary consolidation is expressed as C_α. In this approach, the secondary consolidation is calculated by taking C_α as a constant value.

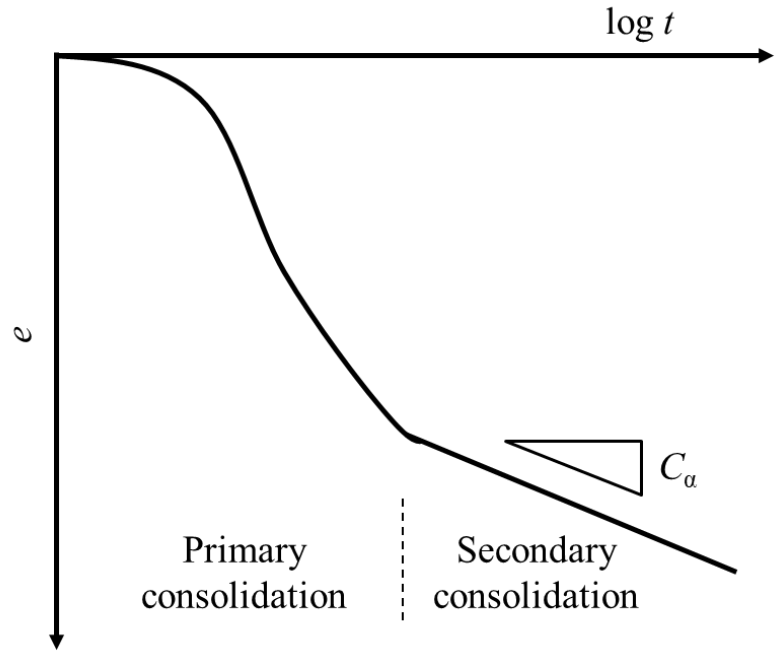

Figure 2-1 Illustration of primary and secondary consolidation

Approach (2): From the EOP compression curves, Mesri and Choi (1985) empirically determined that the consolidation yield stresses obtained in the laboratory and the field are equivalent. The constant C_α/C_c concept proposed by Mesri and Castro (1987) is useful to explain the secondary consolidation with regard to the delayed creep consolidation (Bjerrum 1967) in which the e-log p curve shifts downward with time. Because time is introduced explicitly as "elapsed time" rather than being implicitly denoted as "strain rate", this method is essentially the same as method (1), provided that the compression index C_c is constant (i.e., the NC-line is linear in the e–log$p$ space). However, if the NC-line exhibits a downward-convex shape (i.e., C_c decreases with increasing effective stress), then the two methods lead to different interpretations of the time-dependent behavior. The constant C_α/C_c concept is consistent with the isotache concept; nevertheless, its application is limited because secondary consolidation lasts infinitely against logarithmic time, in other words, the strain increases to infinity at infinite time. Moreover, Leroueil (2006) denied the generality of the EOP concept based on his experience in which the consolidation yield stress corresponding to the EOP

compression curve obtained in the laboratory is significantly larger than that observed in the field.

Approach (3): The isotache concept was first proposed by Šuklje (1957), which professed a unique relationship between the strains and the consolidation pressure corresponding to the strain rate in association with viscosity. Strain rate effect works as a key parameter here. This method states that the rate of change of void ratio is given by the prevailing void ratio and effective stress.

Leroueil et al. (1985) proposed one of the first isotache models. The parameters of this model are mostly based on CRS consolidation tests. It was found that CRS consolidation tests on the same soil with different strain rates are related to a different preconsolidation pressure. As such, in the constitutive model, given σ', ε and $\dot{\varepsilon}$, the preconsolidation pressure is determined and not an independent parameter:

$$\sigma'_{\mathrm{p}} = f(\dot{\varepsilon}) \tag{2-1}$$

This function illustrates the strain rate dependency. The function can be used to define the relation σ', ε, $\dot{\varepsilon}$ together by using a normalised reference compression line at a certain strain rate:

$$\sigma'_{\mathrm{v}}/\sigma'_{\mathrm{p}}(\dot{\varepsilon}) = g(\varepsilon) \tag{2-2}$$

Equation (2-2) shows that the compressibility can change over stress, but is the same for any strain rate. As σ'_{p} changes, the compression curve is simply translated.

This model was further developed by Leroueil (2006) and Watabe et al. (2008; 2012), with the difference that the visco-plastic component $\varepsilon_{\mathrm{vp}}$ was applied instead of the total strain ε.

Watabe et al. (2008; 2012) proposed a simplified method with the isotache concept using a reference compression curve and a function of the strain-rate dependency of the consolidation yield stress obtained from both constant rate of strain (CRS) tests and long-term consolidation (LT) tests under a constant stress. The equation is expressed as below,

$$\ln\frac{\sigma'_{\mathrm{p}}-\sigma'_{\mathrm{pL}}}{\sigma'_{\mathrm{pL}}} = c_1 + c_2\ln\dot{\varepsilon}_{vp} \tag{2-3}$$

Here c_1, c_2, σ'_{pL} are called isotache parameters. c_1 is equal to $\ln\frac{\sigma'_{\mathrm{p}}-\sigma'_{\mathrm{pL}}}{\sigma'_{\mathrm{pL}}}$ at $\dot{\varepsilon}_{\mathrm{vp}} = 1$, i.e., it expresses the relative position of the $\log\sigma'_{\mathrm{p}}$ - $\log\dot{\varepsilon}_{\mathrm{vp}}$ curve. c_2 expresses the level of strain-rate dependency. σ'_{pL} expresses the value of σ'_{p} when the strain rate is nearly

zero. c_1 and c_2 are constants and σ'_{pL} is the lower limit of σ'_p. Figure 2-2 shows the relationship among three parameters.

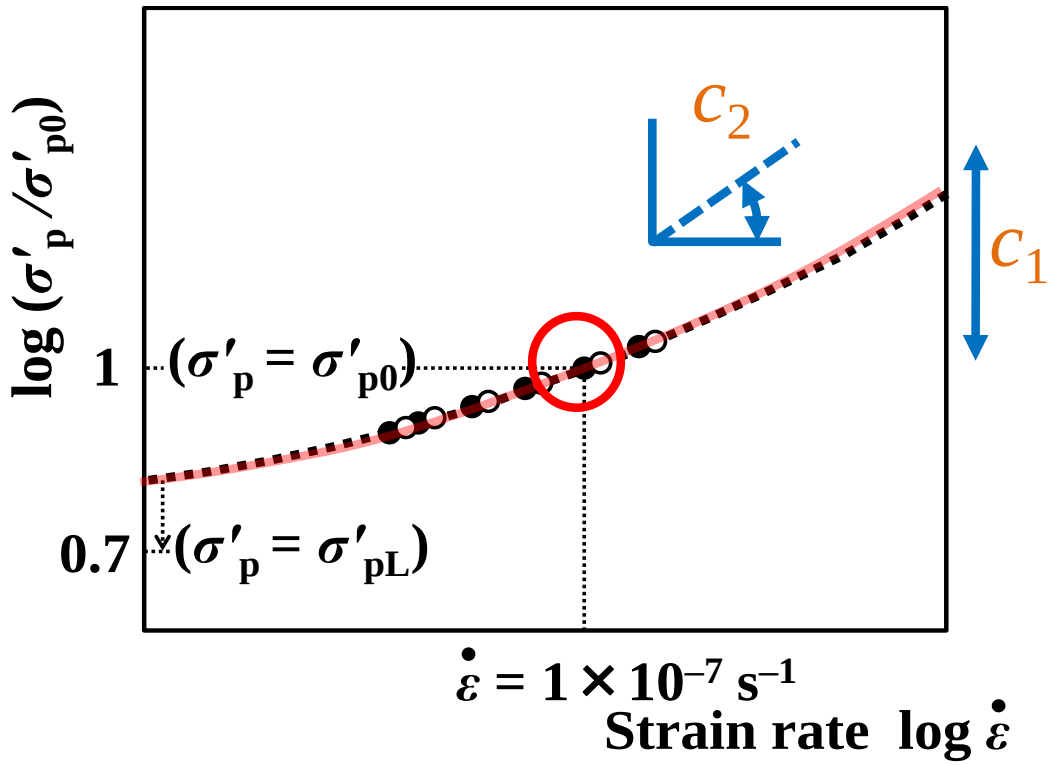

Figure 2-2 Relationship among three isotache parameters (Watabe et al., 2012)

2.2 Unloading behavior

Understanding the unloading behavior of clays is critical in geotechnical engineering, particularly in the context of ground improvement techniques such as surcharge method and preloading with vertical drains (PVDs) method. These methods are commonly employed to accelerate consolidation in soft clay deposits, and the subsequent removal of the surcharge load introduces an unloading stage that can significantly influence the deformation behavior of the soil. Such removal aims to bring the soft clay into an overconsolidated state, which enhances its mechanical properties and reduces the amount of residual settlement under service loads. Similarly, excavation activities also involve

unloading processes that will affect long-term ground deformation and overall stability. A thorough understanding of these unloading responses is essential for reliable prediction of clay behavior in both ground improvement and excavation scenarios. This section provides a concise review of previous studies on the unloading behavior of clays under various geotechnical conditions.

2.2.1 Experimental study on the unloading behavior of soils

Laboratory testing is indispensable for evaluating the unloading behavior of soils. To reliably assess such behavior, a substantial amount of experimental data is required. Unloading behavior is typically investigated through long-term oedometer tests, which are designed to examine the subsequent one-dimensional unloading response of soils after preloading. Some researchers have conducted such oedometer tests on marine clays (Feng 1991; Tanaka et al. 2014; Feng et al. 2017). Alonso and Navarro (2005) conducted oedometer tests following non-standard stress stages over several different durations on inorganic soils. Similar investigations have also been carried out on peat by Madaschi and Gajo (2015) and Yamazoe et al. (2025). As noted by Madaschi and Gajo (2017), the amount of published long-term unloading tests remains limited, and more experimental results are crucial for improving the generalization of conclusions.

Some studies have challenged the conventional assumption of purely elastic soil behavior during unloading, revealing more complex mechanical responses. It is commonly believed that soil under unloading behaves elastically, and only the dissipation of the negative pore water pressure should be considered. However, Mesri et al. (1978) investigated the unloading behavior of clays through constant loading oedometer tests and triaxial tests, and Tanaka et al. (2014) utilized a modified Constant Rate of Strain (CRS) consolidation test to examine unloading behavior in both reconstituted and intact clays. Their findings revealed that the swelling index (C_s) is not a constant parameter but tends to increase with overconsolidation ratio (OCR). Additionally, the effect of swelling is significant at large stress removals.

Previous research using incremental loading oedometer test

Alonso and Navarro (2005) conducted a series of oedometer tests on 8-mm high specimens of reconstituted Llobregat Delta silty clay. These tests followed various stress stages, distinguishing them from conventional preloading tests. In their procedure, the samples were preloaded to a target stress level based on a specified *OCR* and last for a fixed preloading duration. Subsequently, the samples were unloaded to a vertical effective stress of σ'_v = 200 kPa and maintained under that stress to evaluate swelling and recompression behavior. Totally nine tests were conducted, including *OCR* values of 1.05, 1.2, and 2.0, with preloading durations of 10 minutes, 100 hours, and 500 hours. The results are presented in Figure 2-3. Recompression behavior was observed in three test conditions: *OCR* 1.05 with a preloading duration of 10 minutes, *OCR* 1.2 with 10 minutes, and *OCR* 1.05 with 100 hours of preloading. At the *OCR* 2.0 condition, swelling was consistently observed. The swelling strain was strongly influenced by the duration of the preloading stage: the longer preloading duration, the greater swelling strain. This observation highlights the significance of swelling behavior, which is often ignored.

As shown in Figure 2-4, Tanaka et al. (2014) conducted a series of incremental loading oedometer test on 20-mm high specimens of Ma13 Osaka Bay clay. The overconsolidation ratio ranged from 1.14 to 3.0. Before unloading to the specified *OCR* levels, the samples were initially loaded to 90 kPa for 24 hours, followed by an additional loading stage to 330 kPa for 2 hours. The strain rate at the end of preloading 2h is 8×10^{-7} s^{-1}. Among the six test results, three exhibited recompression behavior at *OCRs* 1.14, 1.27, and 1.49. The remaining tests, conducted at *OCR* values greater than 2.0, resulted in long-term swelling.

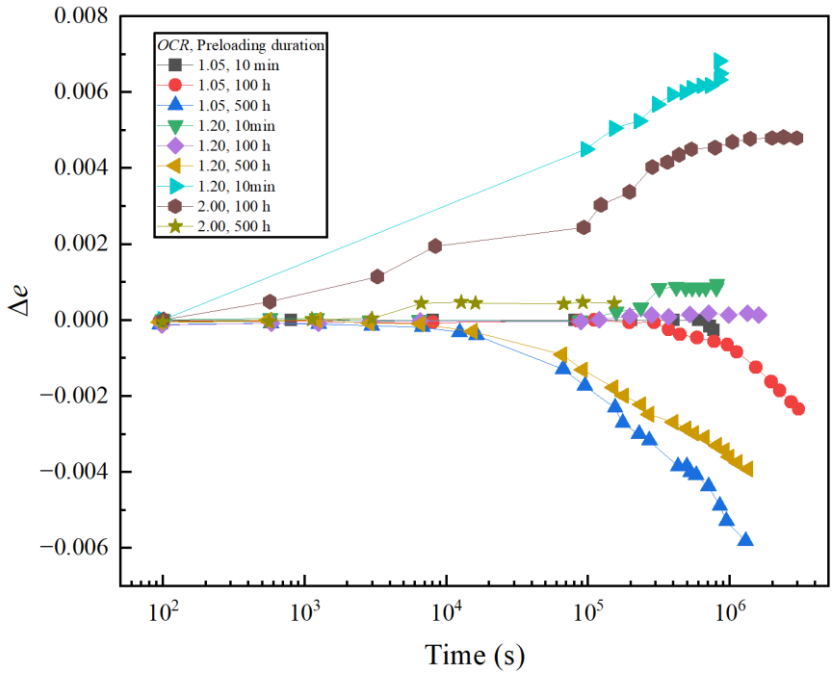

Figure 2-3 Relationship between displacement and elapsed time measured by constant load consolidation test (Alonso and Navarro 2005)

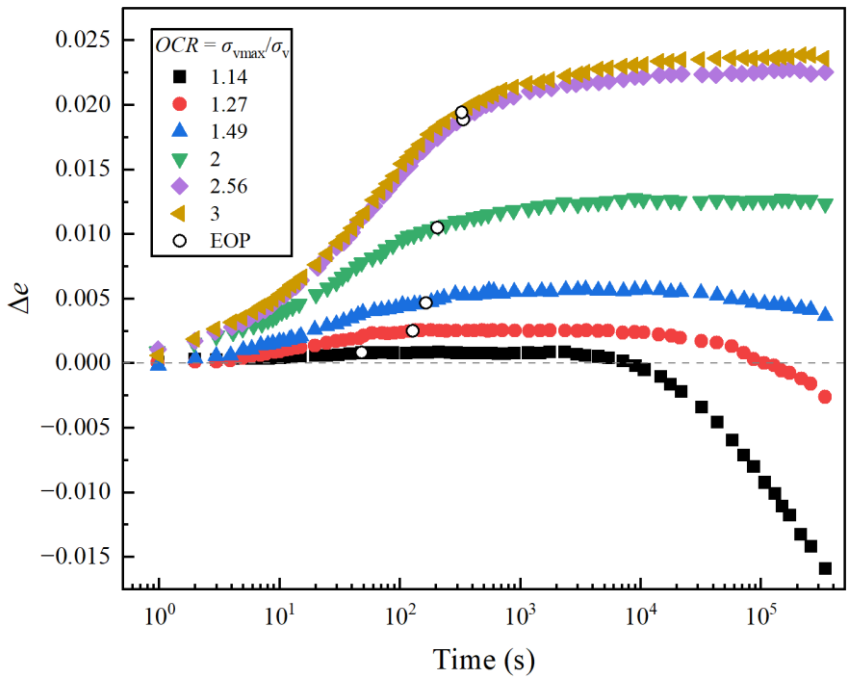

Figure 2-4 Relationship between Δ*e* and *t* measured by constant load test (Tanaka et al. 2014)

Previous research using CRS consolidation test

Watabe et al. (2010) conducted CRS consolidation tests on Ma12 Osaka Bay clay and Tanaka et al. (2014) performed a series of tests on Kasaoka clay, Louiseville clay and Ma13 Osaka Bay clay, as shown in Figure 2-5 and Figure 2-6, respectively. Both studies similarly adopted a multi-stepwise unloading approach, with steps corresponding to a range of strain rates. The aim was to examine the strain-rate dependency of the unloading behavior. However, in contrast to the loading behavior, lower strain rates during unloading resulted in higher stress at a given strain.

Tanaka et al. (2014) also conducted a series of unloading–reloading CRS consolidation tests on Louiseville clay, reconstituted Kasaoka clay, and reconstituted Ma13 Osaka bay clay to investigate the effect of the maximum consolidation stress ($\sigma'_{v,max}$) on unloading behavior. By comparing the relationship between the incremental void ratio after unloading and the normalized effective stress ($\sigma'_v/\sigma'_{v,max}$) under different levels of maximum consolidation stress, it was found that the unloading paths converge onto a unique curve. This relationship appeared to be independent of $\sigma'_{v,max}$, strain magnitude, or the compression index C_c. This finding supports the development of more general constitutive models and may contribute to improving the prediction of post-unloading deformation in soft clays.

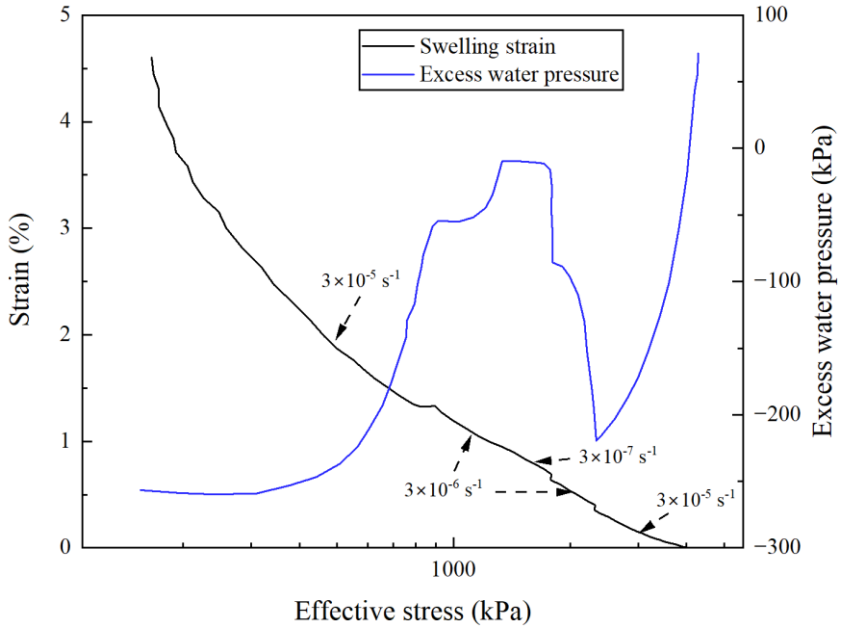

Figure 2-5 ε-p' relation at different strain rates (Watabe et al. 2010)

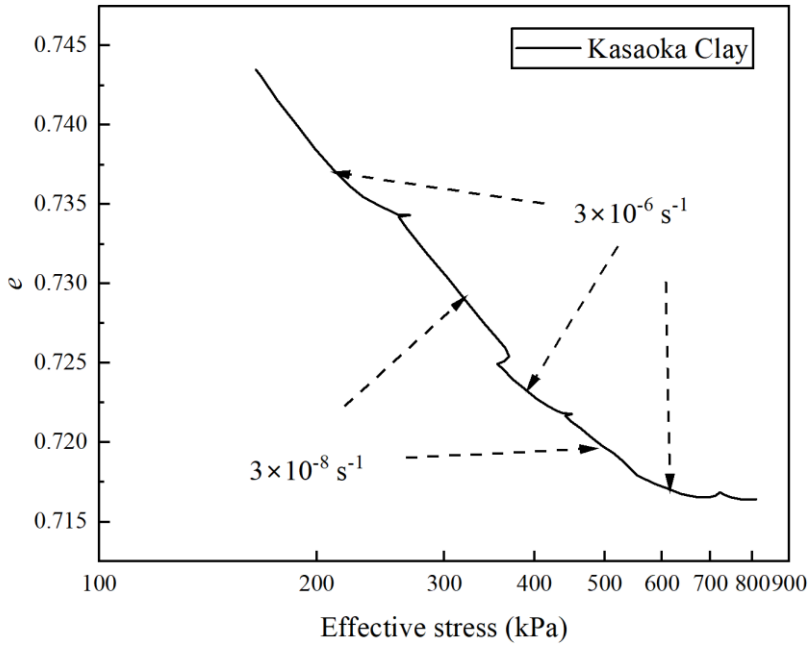

Figure 2-6 e–log p' relation at different strain rates (Tanaka et al. 2014)

Previous research using inter-connected consolidation test

The thickness effect during loading behavior of soil layer was investigated for the compressibility characteristics of clayey soils in the laboratory and field tests (Berre and Iversen 1972, Kabbaj et al. 1988, Watabe et al. 2008; 2009, Degago et al 2010).

Watabe et al. (2009) and Shirako et al. (2009) investigated the thickness effect and the distribution of excess pore water pressure during unloading using the inter-connected consolidation test. Figure 2-7 presents a conceptual diagram of the apparatus for the inter-connected consolidation test.

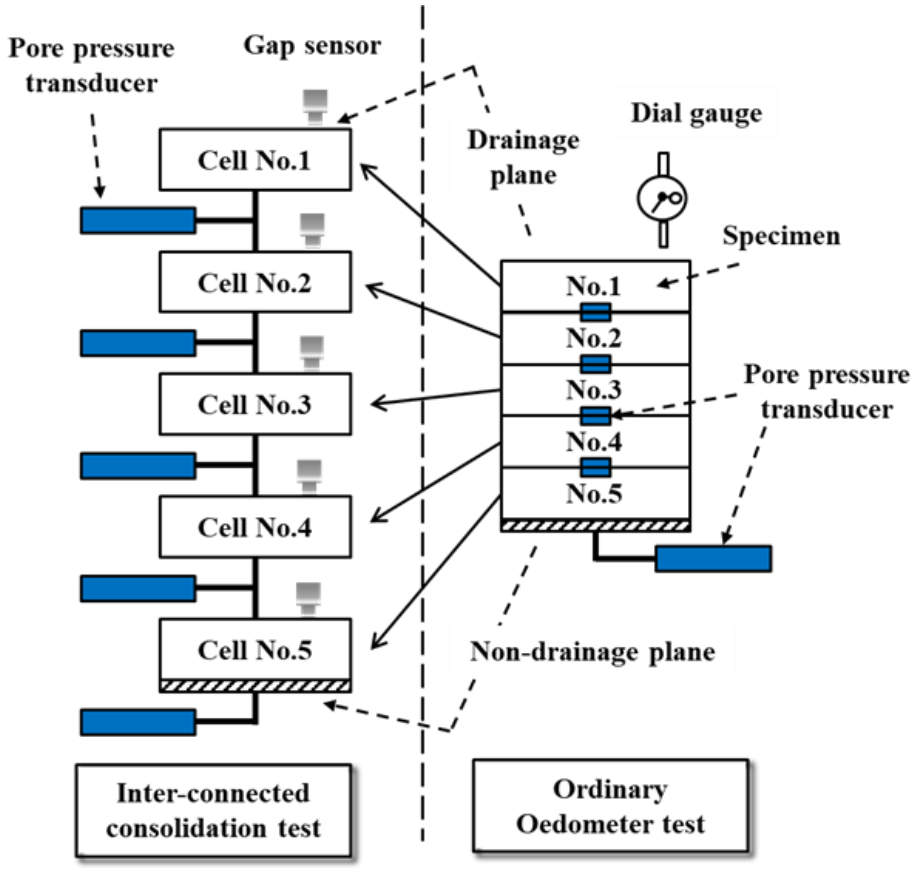

Figure 2-7 Diagram of the apparatus of inter-connected consolidation test (Kang et al. 2001)

In Figure 2-8, Watabe et al. (2009) initiated to unload from the secondary consolidation stage ($\Delta u = 0$). After unloading, negative excess pore water pressures were generated. From 0.5 minutes after unloading, the excess pore water pressure distribution began to approximate a parabolic shape, and by 6 minutes, the excess pore water pressures clearly followed a parabolic distribution. Shirako et al. (2009) initiated to unload from the primary consolidation stage, where excess pore water pressure was still positive ($\Delta u > 0$). Under this condition, the excess pore water pressure distribution became more complex, as illustrated in Figure 2-9. After unloading, negative excess pore water pressures were generated near the drainage boundary, while positive pressures remained in the regions farther from the drainage surface. In this condition, the excess pore water pressure distribution did not follow the conventional parabolic distribution predicted by classical consolidation theory.

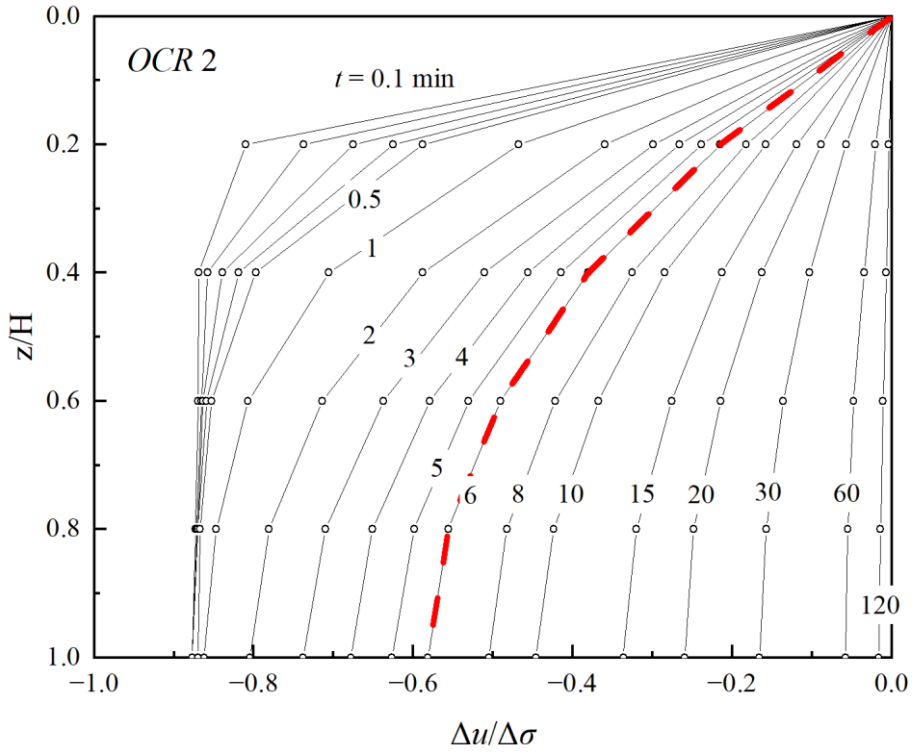

Figure 2-8 Isochrones of excess pore water pressure during unloading in secondary consolidation ($\Delta u = 0$) (Watabe et al. 2009)

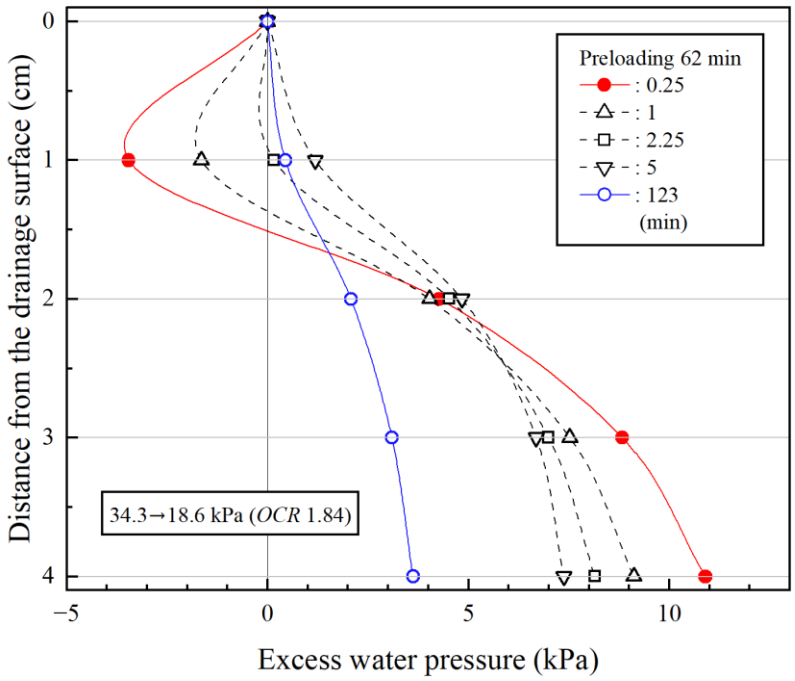

Figure 2-9 Isochrones of excess pore water pressure during unloading in primary consolidation ($\Delta u > 0$) (Shirako et al. 2009)

2.2.2 Existing models for unloading behavior of soils

There are many models for predicting long-term unloading behavior after removing the preload, and two recent models will be mentioned in this chapter. However, there is not enough focus on the swelling process of marine clay, which plays a crucial role in the unloading behavior. Although most of the current models pay more attention to the creep after the swelling process in order to calculate the residual settlement, they also cannot perform well at high overconsolidation ratios. Moreover, no models can perform long-term swelling behavior and fit the unloading CRS consolidation test greatly; almost all of them were proposed based only on the result of incremental loading oedometer tests.

The EVP (Elasto-Viscoplastic) model from Vergote et al. (2021) thought the creep after unloading was a strain rate-dependent behavior. The model is based on a rule that creep strain after unloading is linear with strain rate in the log scale. However, the model takes the swelling process as a transient behavior that plays a crucial role in the unloading behavior. As the data shown in Chapters 4 and 5, the experimental results support the swelling process as a strain rate-dependent and visco-plastic behavior. The model is also highly dependent on the initial strain rate of creep, it is difficult to find when the creep

after swelling starts.

The elastic visco-plastic (EVP) model of Yuan and Whittle (2018) can behave within hypotheses A or B (Ladd et al. 1977) by selecting a rate sensitivity parameter β. It can fit greatly at OCR<1.3 conditions. However, this model has many parameters and is difficult for engineers to apply.

From the field data, the relationship between *OCR* and depth does not follow a linear distribution (Cascone and Biondi 2013; Rujikiatkamjorn and Indraratna 2007), as shown in Figure 2-10. As the depth approaches the ground surface, the *OCR* increases to a high value.

In addition, all of the previous models are complex and have too many parameters, and some of them used the experimental data one decade ago without their own experimental data.

To improve the lack of current models, it is necessary to focus on the long-term swelling behavior and pay more attention to the high *OCR* conditions. Develop the model to fit the test results of the unloading CRS consolidation test. Design the experiment for the particular objective; as a researcher, it is convenient and reliable to research the experimental characteristics by their tests.

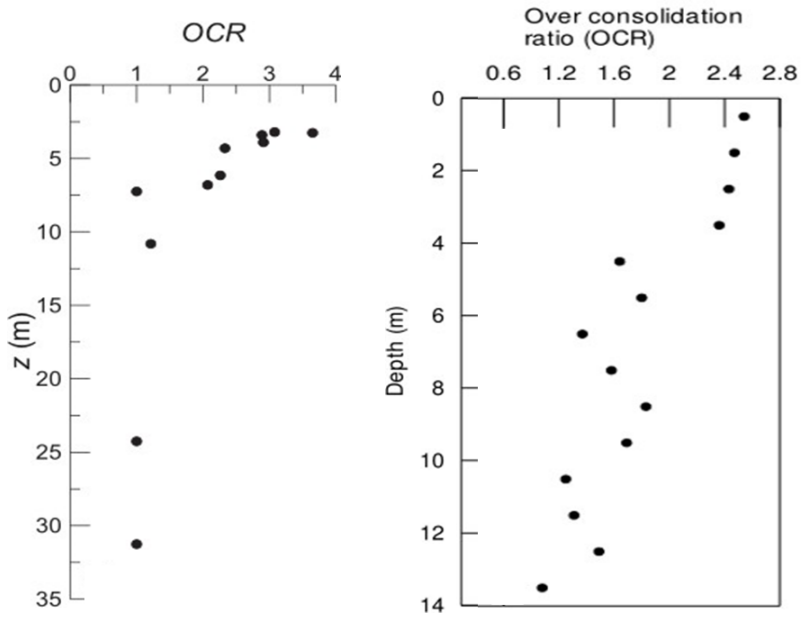

Figure 2-10 Relationship between *OCR* and depth from two case studies (Left: Rujikiatkamjorn et al. 2007, Right: Cascone et al. 2013)

Chapter 3 Marine clay samples

This study applied constant rate of strain (CRS) consolidation tests and incremental loading oedometer tests from loading to unloading on Ariake clay, Louiseville clay and Onsøy clay.

3.1 Ariake clay

Ariake clay is a well-known sensitive marine clay through previous studies (Ohtsubo et al. 1982; Hanzawa et al. 1990; Tanaka 2000; Tanaka et al. 2001; Hong et al. 2006; Watabe et al. 2012). The Ariake clay is a high-plastic marine clay around the Ariake Sea in Kyushu, Japan (Hanzawa et al. 1990). The Ariake clay in this study was sampled at the same location as Hanzawa et al. (1990). The physical properties of the clay samples are indicated in Table 3-1. Ariake clay, which has a significantly high initial void ratio (average e_0 = 3.37) sampled from G.L. -7.00 to -7.80 m, was mainly used in this study. Figure 3-1 shows the compression curves of Ariake clays and comparison with previous research. The samples from previous research were obtained at a shallower depth (G.L. -4.2 m). The discrepancy in compressibility observed in the two CRS consolidation tests can be attributed to two primary factors. First, the differences in natural water content (w_n) and plasticity index (I_p) between the different depths of the Ariake clay significantly influence compressibility (C_c) at various depths. Second, overconsolidation occurs due to different reasons: the upper layer (above -7.5 meters) exhibits quasi-overconsolidation due to chemical bonding, whereas the layer between -7.5 and -15 meters is predominantly influenced by secondary compression (Hanzawa et al. 1990). These distinct mechanisms lead to variations in compressibility characteristics.

Table 3-1 Physical properties of Aiake clay examined in this study

Sample	Depth (m)	Particle density ρ_s (Mg/m^3)	Natural water content w_n (%)	Liquid limit w_L (%)	Plastic limit w_p (%)	Plasticity index I_p	Clay fraction (%)	Silt fraction (%)	e_0
Ariake clay	7.00-7.80	2.605	129.5	115.5	45.2	70.3	62.0	36.0	3.37

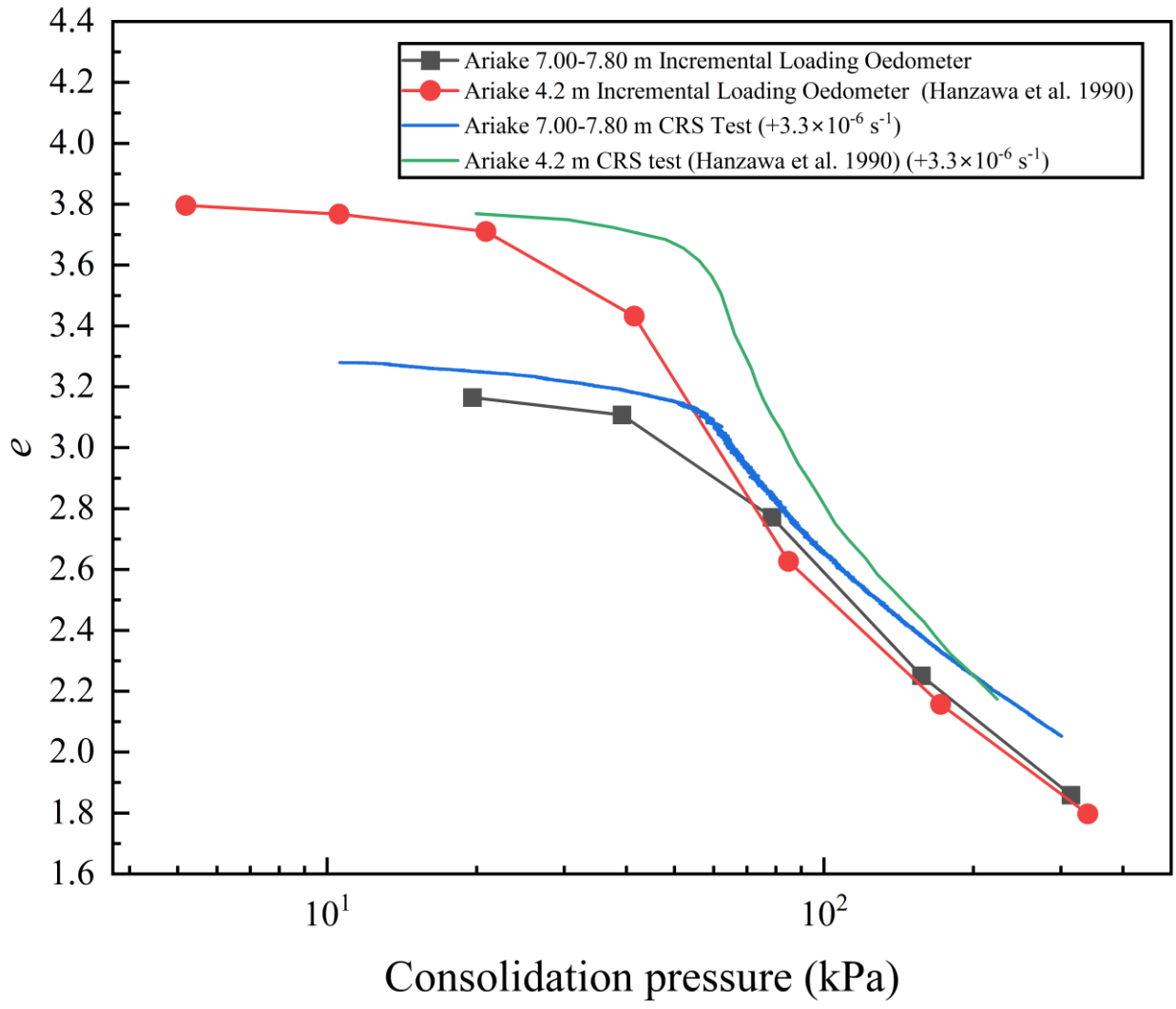

Figure 3-1 Compression curves of Ariake clays

3.2 Louiseville clay

The physical properties of Louiseville clay are shown in Table 3-2. Louiseville clay is a Champlain Sea clay widely distributed in Quebec, eastern Canada, and is a very sensitive clay with a significant cementation effect and mechanical overconsolidation. The main component of the clay particles is glacial rock flour mainly consisting of fine quartz. Louiseville clay's characteristics are described by Leroueil et al. (2003).

Table 3-2 Physical properties of Louiseville clay

Sample	Depth (m)	Particle density (g/cm^3)	w_n (%)	I_p	Clay fraction (%)	Silt fraction (%)	e_0
Louiseville	15.00-15.70	2.767	67.6	52.6	65.0	35.0	2.03

3.3 Onsøy clay

The physical properties of Onsøy clay are shown in Table 3-3. The Onsøy clay, sampled from Norway, is a very homogeneous clay with fine particles mainly consisting of glacial rock flour. The characteristics of this clay are described in Lunne et al. (2003). Onsøy clay has a large clay content (74.3%), and the water content and plastic index are the smallest among these three kinds of soil.

Table 3-3 Physical properties of Onsøy clay

Sample	Depth (m)	Particle density (g/cm^3)	w_n (%)	I_p	Clay fraction (%)	Silt fraction (%)	e_0
Onsøy	19.00-19.85	2.756	54.3	46.9	74.3	25.7	1.42

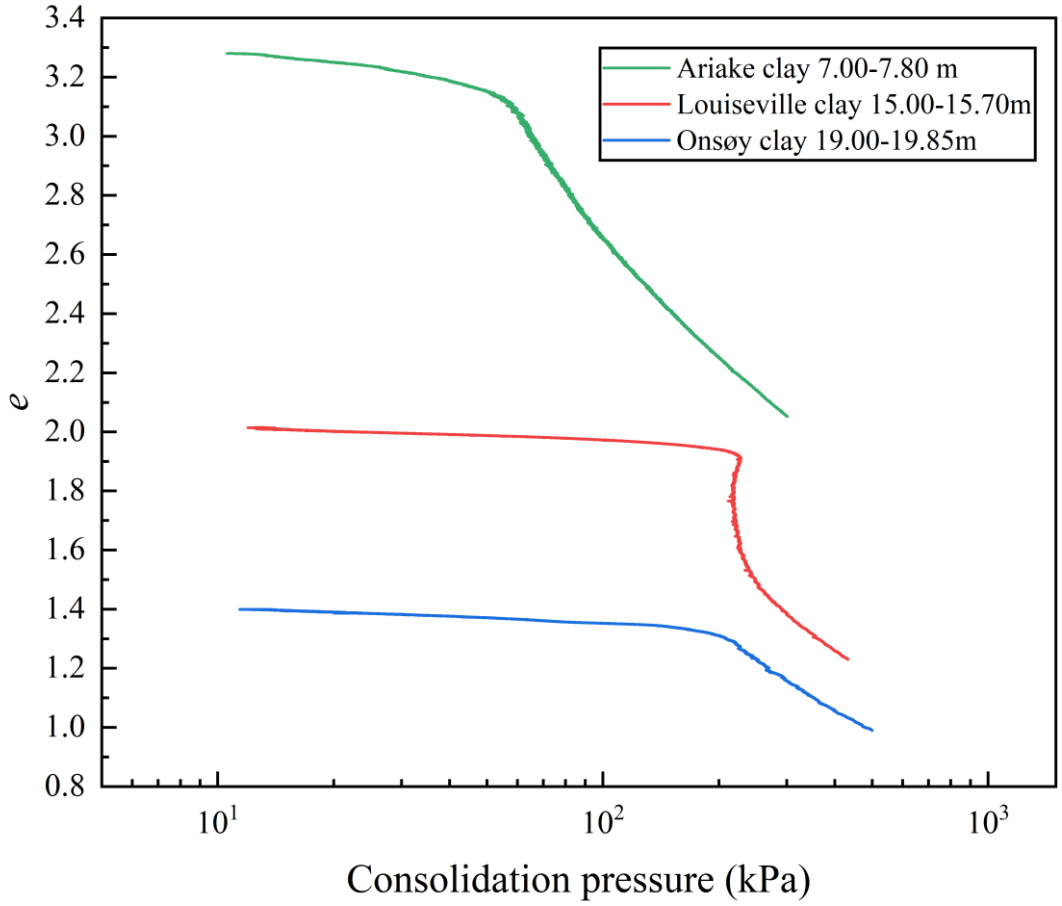

Figure 3-2 Compression curves of the three marine clays

Consolidation characteristics of marine clays

Figure 3-2 presents a comparison of the compression curves for the three marine clay samples, Ariake clay, Louiseville clay, and Onsøy clay, examined in this study. Among them, Ariake clay exhibits the highest compressibility, which is consistent with its higher water content and lower yield stress. Louiseville clay demonstrates a clear yield point, followed by a sharp increase in compressibility. This characteristic results from the effects of cementation and mechanical overconsolidation in a sensitive clay matrix. Onsøy clay displays intermediate behavior. Compared to Ariake clay, Onsøy clay has a lower compressibility and a higher yield stress.

Table 3-4 presents the hydraulic conductivity and coefficient of consolidation of the three marine clays. Among them, Ariake clay exhibits the highest compressibility and permeability, which can be attributed to its high water content and initial void ratio. Onsøy

clay, characterized by weak structural bonding, shows intermediate behavior in comparison with the other two clays.

Table 3-4 Hydraulic conductivity and coefficient of consolidation of marine clays

Sample	Ariake	Louiseville	Onsøy
c_v (cm^2/d)	220	23	39
k (m/s)	2.3×10^{-9}	3×10^{-10}	4×10^{-10}

Specimen preparation and controlled testing conditions

All the specimens for both CRS consolidation tests and incremental loading oedometer tests in this study were trimmed to a dimension of 60 mm in diameter and 20 mm in thickness. The specimens were placed into a rigid steel ring, and the internal surface of the ring was lubricated with grease to minimize the possible friction. Filter papers were used on the top and bottom of the specimen to avoid the entry of clay particles into the porous stones. During all the tests, the temperature in the laboratory was maintained at 25±1°C.

Chapter 4 CRS consolidation test

4.1 Apparatus

The set-up of the constant rate of strain (CRS) consolidation test is illustrated in Figure 4-1 and Figure 4-2. The specimen examined in this study possessed a diameter of 60 mm and an initial height of 20 mm. The device consists of axial displacement control and back-pressure application systems. Throughout the experimental procedure, the specimen's upper surface was maintained in a drained boundary condition, and the bottom of the specimen was in undrained boundary condition. Water pressure was measured at the bottom by connecting a porewater pressure transducer. A back pressure of 200 kPa was applied to enhance marine clay's high degree of saturation. The axial displacement, axial load and excess pore water pressure at the bottom of the specimen were recorded by data acquisition system. CRS consolidation tests were carried out according to Japanese Industrial Standard JIS A 1227 (JSA, 2000a).

For the CRS consolidation test, assuming that the distribution of excess pore water pressure within a specimen is in parabolic shape curve (JSA, 2000b), the average effective vertical stress σ_{v} in a specimen is calculated from the following Equation 4-1:

$$\sigma_{\mathrm{v}}' = \sigma_{\mathrm{v}} - \frac{2}{3}u_{\mathrm{b}} \tag{4-1}$$

where σ_{v} is the total vertical stress, and u_{b} is the excess pore water pressure at the bottom of the soil specimen.

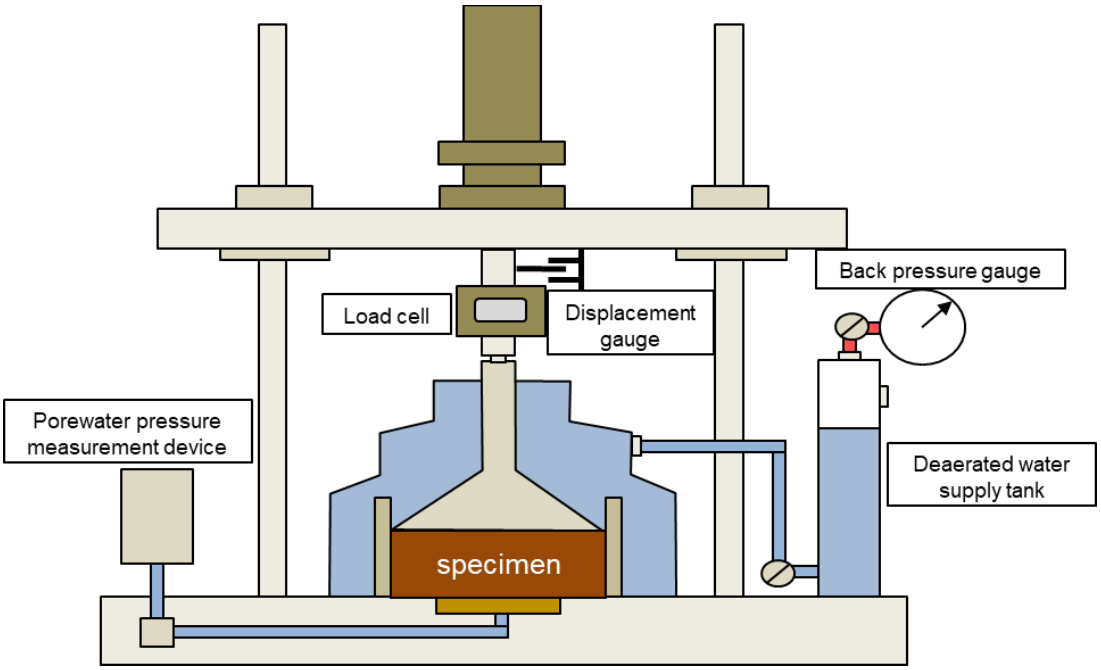

Figure 4-1 Schematic illustration of experimental setup (CRS consolidation test)

Figure 4-2 Photo of experimental setup (CRS consolidation test)

4.2 Constant unloading strain rate consolidation test

4.2.1 Test methods

First of all, to clarify the shape of isotache lines during the unloading process and the relationship between different isotache lines, the constant unloading strain rate consolidation test was applied to Ariake clay.

A series of CRS consolidation tests were carried out. For all the CRS consolidation tests in this study, the samples were compressed under a multi-stepwise strain rate ($+3.3\times10^{-6}$ s^{-1} → $+3.3\times10^{-7}$ s^{-1} → $+3.3\times10^{-8}$ s^{-1}) until approximately 550 kPa, then unloading tests were carried out.

As for the unloading process, constant unloading strain rate was used in the No. 1 and No. 2 tests, under a constant unloading strain rate of -3.3×10^{-6} s^{-1} and -3.3×10^{-8} s^{-1}, respectively, as shown in Figure 4-3.

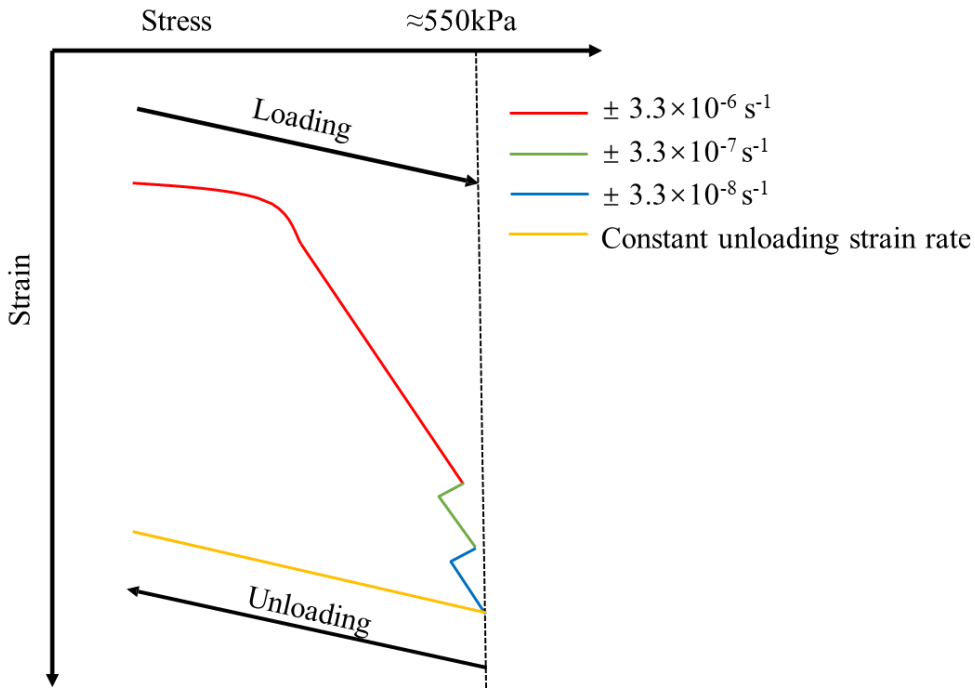

Figure 4-3 Diagram of experimental methods in constant unloading strain rate consolidation test

4.2.2 Test results

The experimental results obtained from the three tests measured by CRS consolidation tests of Ariake clay include relationships of strain and consolidation stress. Using the point where the unloading began as a reference point, the strain is transformed to the incremental void ratio, and the effective consolidation stress is normalized by the maximum one.

Figure 4-4 depicts an enlarged unloading section and a short section of compression near the reference point. Strain rate dependency is observed during unloading process. The curve of unloading at 3.3×10^{-8} s^{-1} (No. 2 test) is drawn at upper position than that of 3.3×10^{-6} s^{-1} (No. 1 test).

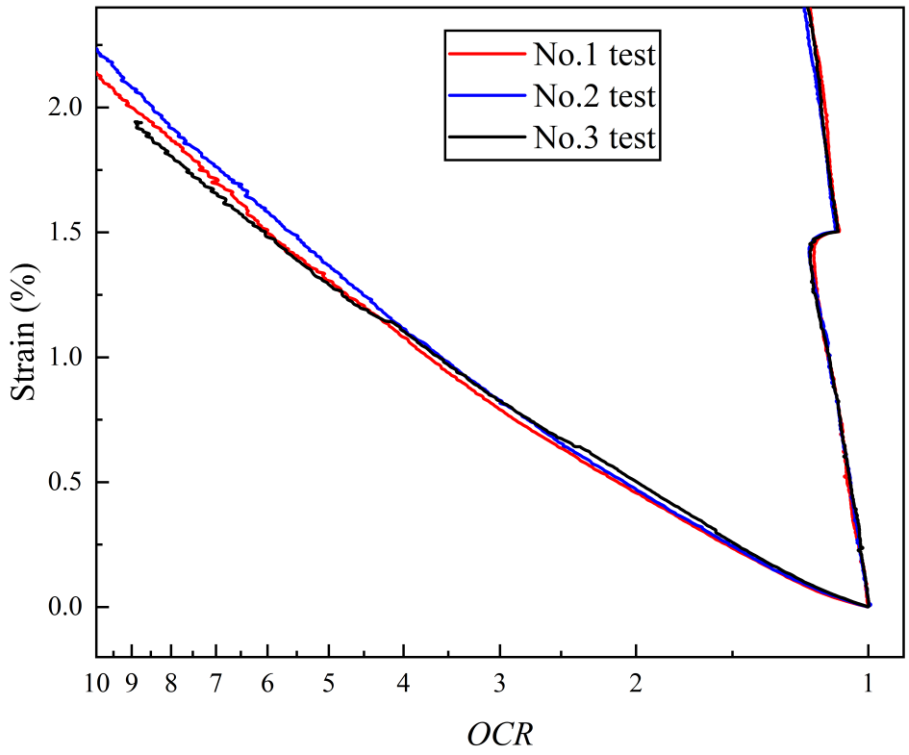

Figure 4-4 Enlarged the unloading part of the CRS consolidation tests

4.3 Multi-stepwise unloading strain rate consolidation test

4.3.1 Test methods

CRS consolidation test was carried out to make clear that the isotache lines are equally spaced, which is the same as the loading consolidation behavior or the difference between two neighboring isotache lines becomes larger with *OCR* (over-consolidation ratio, $OCR = \sigma'_{max}/\sigma'$) grows. Also, try to develop a way that can evaluate the strain rate dependency from the CRS consolidation test for one soil specimens.

In this study, CRS consolidation tests were conducted for the Ariake clay, Onsøy clay and Louiseville clay. The physical properties of the clay samples have been shown in Table 3-2 of Chapter 3.

For all of the three kinds of clays, the same method, as shown in Figure 4-5, was carried out. During the consolidation process, the samples were loaded under a multi-stepwise strain rate ($+3.3\times10^{-6}$ s^{-1} → $+3.3\times10^{-7}$ s^{-1} → $+3.3\times10^{-8}$ s^{-1}) until approximately 550 kPa, afterwards the unloading test was carried out. Using this method, the strain rate dependency is able to be evaluated. During the swelling process, the samples were unloaded under a series of strain rates (-3.3×10^{-7} s^{-1} → -3.3×10^{-8} s^{-1} → -3.3×10^{-7} s^{-1} → -3.3×10^{-6} s^{-1} → -3.3×10^{-7} s^{-1}). Same as the loading part, the strain rate dependency can also be evaluated during the unloading part.

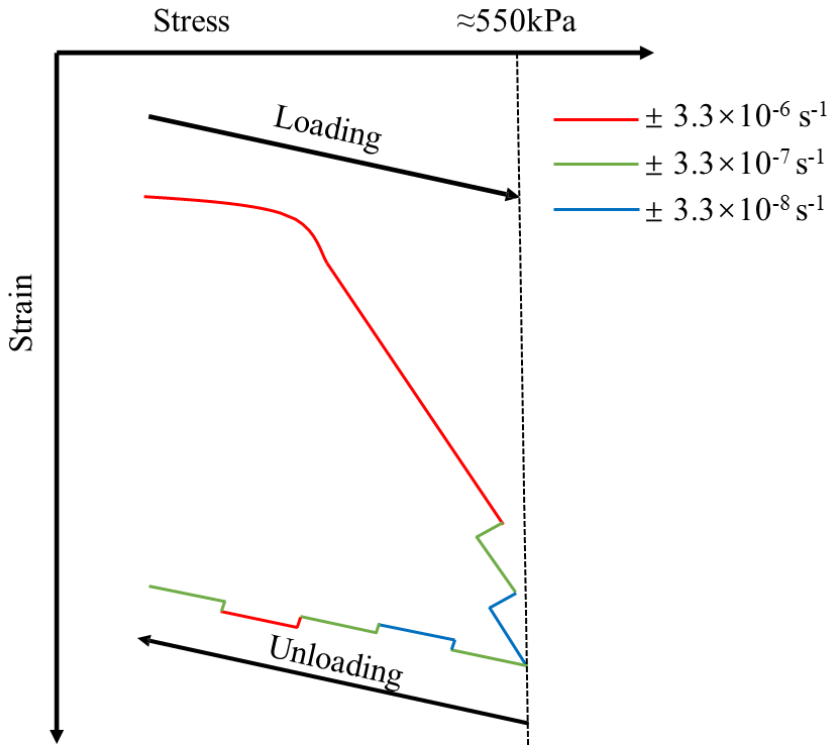

Figure 4-5 Diagram of experimental methods in multi-stepwise unloading strain rate consolidation test

4.3.2 Test results

Figure 4-6 shows the data of No. 3 test (multi-stepwise unloading tests at three different strain rates) in the same field as Figure 4-4. As the strain rate changes, the adjusted value during the unloading process is much smaller than that during the compression process. As shown in Figure 4-7 and Figure 4-8, enlarged different multi-stepwise unloading strain rate periods, the unloading curve rises as the unloading strain rate decreases, and it turns to the left as the unloading strain rate increases. Therefore, this result supports establishing a model based on the isotache concept. Also, contrary to the consolidation part, the lower strain rate line is upper on the higher strain rate line.

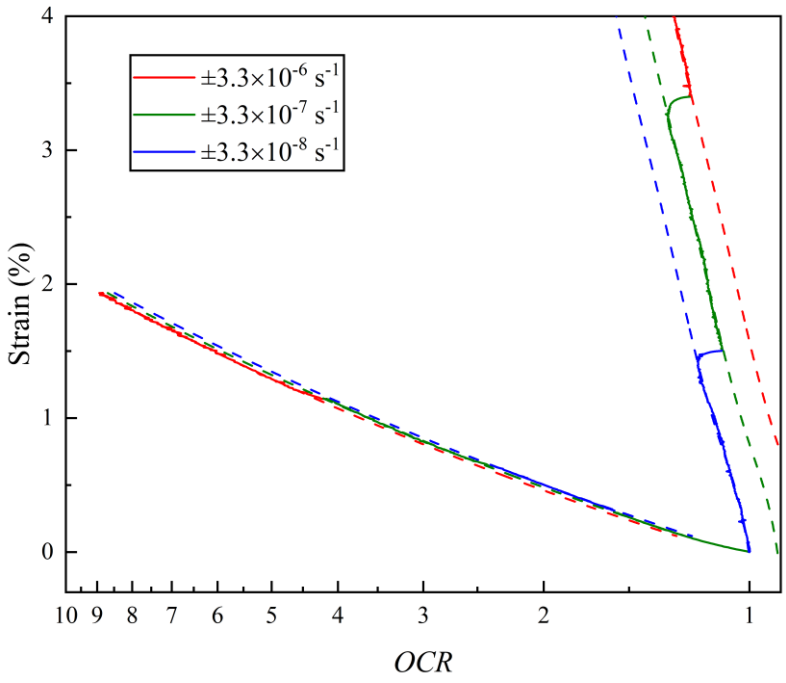

Figure 4-6 Relation of strain versus *OCR* of different unloading strain rates

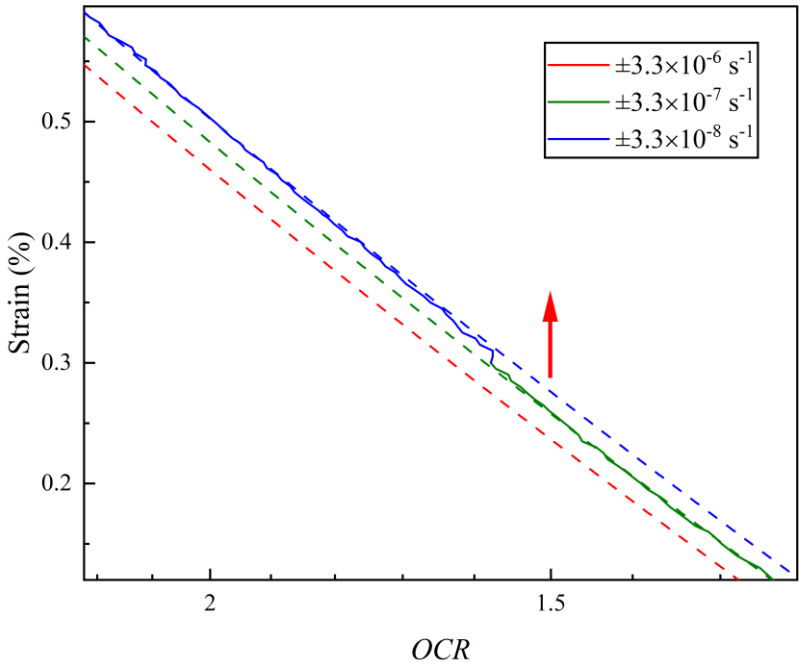

Figure 4-7 Enlarged varying unloading strain rate part (-3.3×10^{-7} s^{-1} → -3.3×10^{-8} s^{-1})

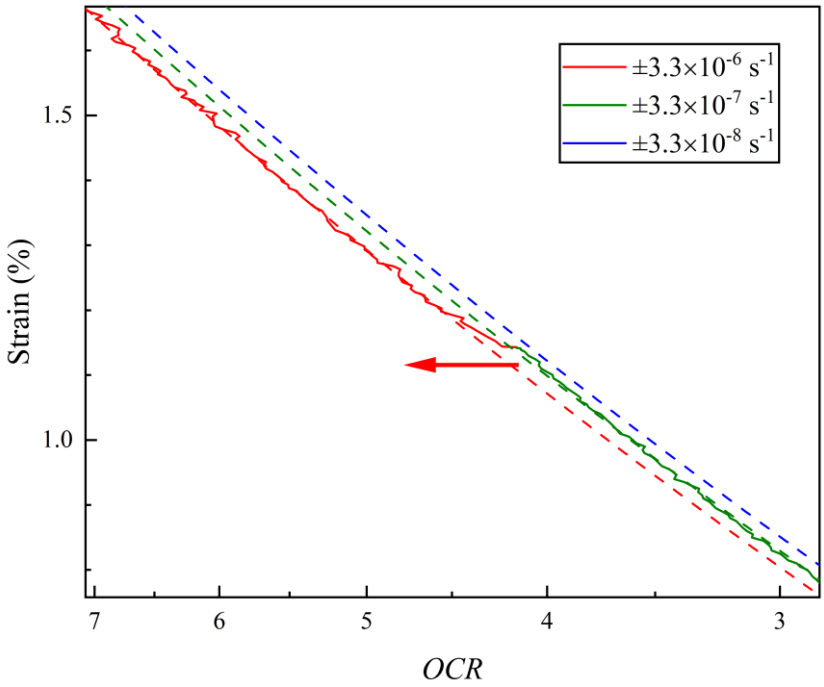

Figure 4-8 Enlarged varying unloading strain rate part (-3.3×10^{-7} s^{-1} → -3.3×10^{-6} s^{-1})

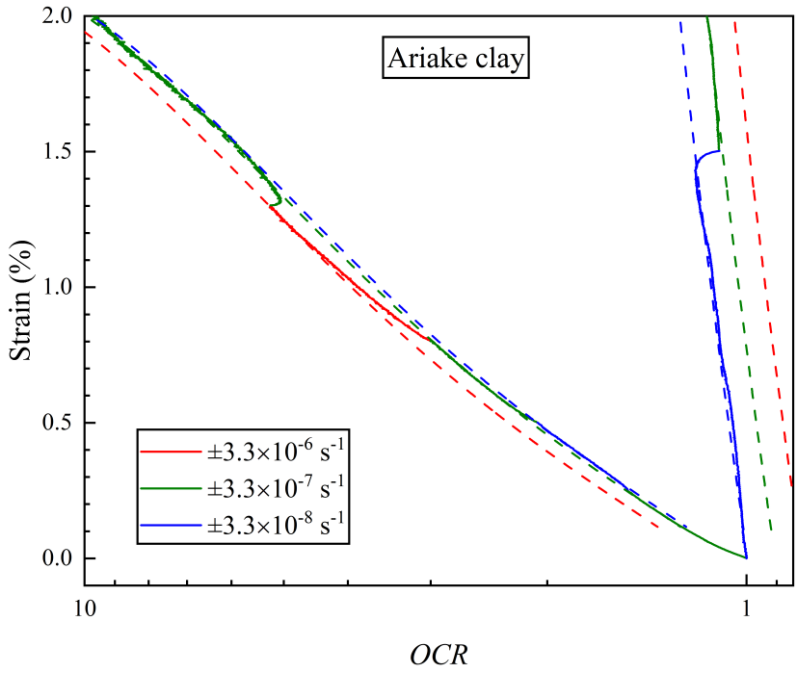

Figure 4-9 Compression and swelling curve for Ariake clay measured by unloading CRS consolidation test

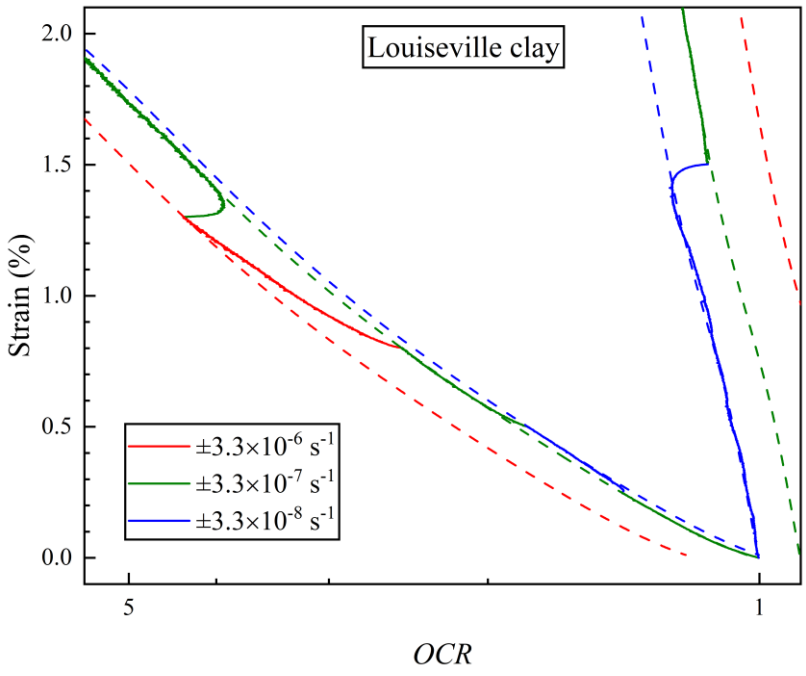

Figure 4-10 Compression and swelling curve for Louiseville clay measured by unloading CRS consolidation test

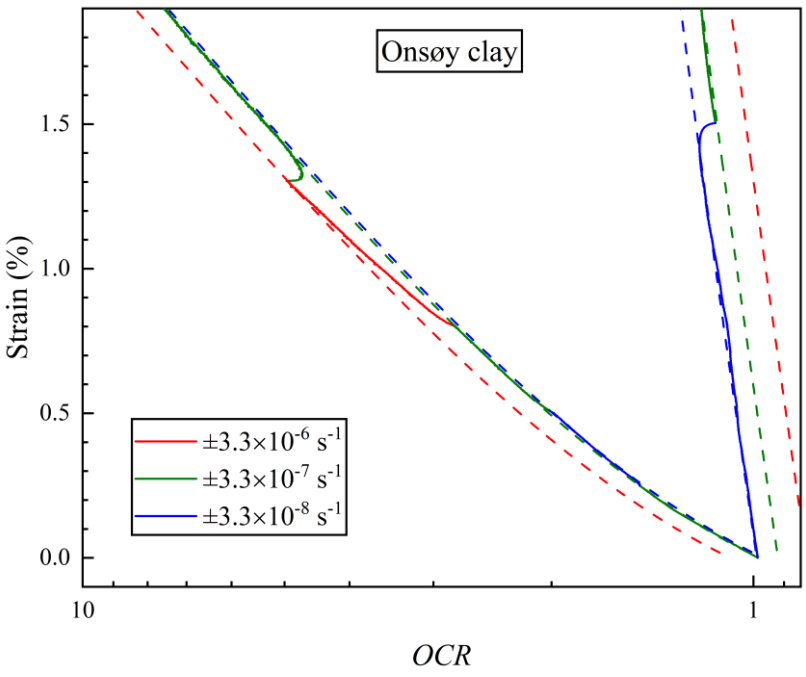

Figure 4-11 Compression and swelling curve for Onsøy clay measured by unloading CRS consolidation test

The test results of the multi-stepwise unloading strain rate consolidation tests are presented in Figure 4-9, Figure 4-10 and Figure 4-11. By magnifying the unloading stage, the effect of unloading strain rate variations on the behavior of the three clays can be clearly observed. The overall trends are generally consistent across the different soil types.

Computing method for isotache lines

Determining a fitting line according to the data of the middle strain rate ($\pm 3.3\times10^{-7}$ s^{-1}) as a reference isotache line of that strain rate (the green dotted line during the unloading stages in Figure 4-9 to Figure 4-11).

Afterwards, horizontally, moving this reference isotache line to fit the isotache lines of other strain rates.

Lastly, evaluating the values of $C_{s\alpha}/C_s$ or $C_{c\alpha}/C_c$, which is the distance between the neighboring isotache lines.

Using the ratio of $C_{s\alpha}/C_s$ to $C_{c\alpha}/C_c$ to compare the strain rate dependency

From the test results of the three kinds of marine clays, the ratios of $C_{s\alpha}/C_s$ to $C_{c\alpha}/C_c$ are from 0.25 to approximately 1.00 as shown in the Table 4-1. However, it seems the ratio between 3.3×10^{-6} s^{-1} and 3.3×10^{-7} s^{-1} is significantly larger. This may be because the unloading strain rate was changed at high *OCR*, and the details about the influence of *OCR* during the unloading process will be discussed in the next chapter. The CRS consolidation test results from these three kinds of marine clays appear to be within the same range.

The author also calculated the values of other clays, Ma12 Osaka Bay clay (Watabe et al., 2010), Ma13 Osaka Bay clay, and Kasaoka clay (Tanaka et al. 2014). The ratio of $C_{s\alpha}/C_s$ to $C_{c\alpha}/C_c$ is also from 1/4 to approximately 1, and the ratio tends to increase with *OCR* (σ'_{max}/σ') increasing. The results are similar to the range of the values of Ariake clay, Louiseville clay, and Onsøy clay. It means that in some marine clays, the strain rate dependency of compression and swelling has a similar relationship.

Table 4-1 Comparison between $C_{c\alpha}/C_c$ and $C_{s\alpha}/C_s$

	Strain rate ($\pm$ s^{-1})	Ariake	Louiseville	Onsøy
$C_{c\alpha}/C_c$ (Loading)	3.3×10^{-6}-3.3×10^{-7}	0.04035	0.06328	0.04287
$C_{c\alpha}/C_c$ (Loading)	3.3×10^{-7}-3.3×10^{-8}	0.04180	0.04658	0.03165
$C_{s\alpha}/C_s$ (Unloading)	3.3×10^{-6}-3.3×10^{-7}	0.03458	0.06810	0.04311
$C_{s\alpha}/C_s$ (Unloading)	3.3×10^{-7}-3.3×10^{-8}	0.00881	0.01299	0.00604
Ratio	3.3×10^{-6}-3.3×10^{-7}	0.85700	1.07617	1.00560
Ratio	3.3×10^{-7}-3.3×10^{-8}	0.21077	0.27888	0.19084

(Ratio in Table 4-1 equals to $\frac{C_{c\alpha}/C_c}{C_{s\alpha}/C_s}$)

Chapter 5 Incremental loading oedometer test

5.1 Apparatus

Incremental loading oedometer tests were conducted at two institutions: Hokkaido University and Port and Airport Research Institute (PARI). Figure 5-1 presents the experimental setup at Hokkaido University, while Figure 5-2 shows the apparatus used at PARI. A detailed schematic of the Incremental Loading (IL) oedometer test configuration at PARI is provided in Figure 5-3. The long-term unloading oedometer tests (preloading 4 hours and 36 hours) for Louiseville clay and Onsøy clay were conducted at PARI. The other tests were carried out at Hokkaido University.

All the soil samples had a diameter of 60 mm and a height of 20 mm. During the test, drainage was allowed at both the top and bottom surfaces of the specimen. Moreover, a data logger is recording the axial displacement and the elapsed time during the test.

Figure 5-1 Photo of experimental setup (IL test at Hokkaido University)

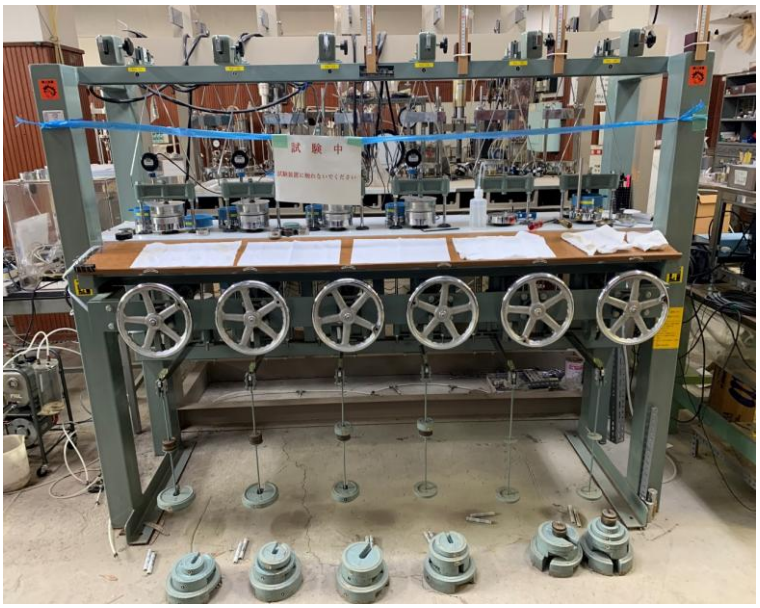

Figure 5-2 Photo of experimental setup (IL test at PARI)

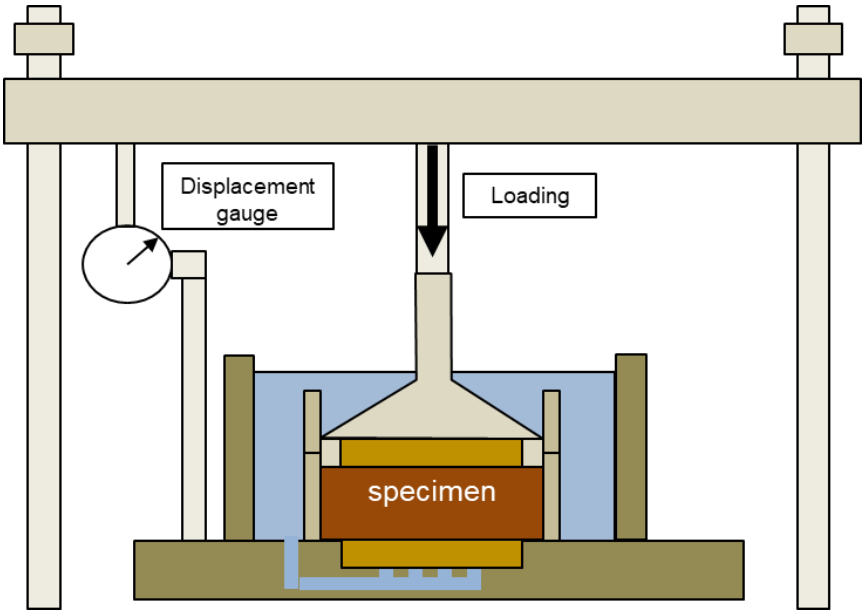

Figure 5-3 Diagram of experimental installation (IL oedometer test)

5.2 Four-stage unloading oedometer test

5.2.1 Test methods

To make clear the relationship between strain rate dependency and *OCR* (overconsolidation ratio = σ'_{max}/σ') during unloading process, incremental loading (IL) oedometer tests were carried out to Ariake clay, Louiseville clay and Onsøy clay. Moreover, compared to the CRS consolidation test, the incremental loading (IL) oedometer test can directly calculate the C_s and $C_{s\alpha}$ by the following equations instead of measuring the distance between two neighboring isotache lines as $C_{s\alpha}/C_s$.

$$C_s = \frac{\Delta e}{\Delta \log p}$$

$$C_{s\alpha} = \frac{\Delta e}{\Delta \log t}$$

In this series of tests, as shown in Figure 5-4, Incremental loading oedometer test was conducted following JIS A 1217 (JSA, 2000b) except the final loading step and the unloading process. Incremental stress ratio was unity, and every step lasted 24 hours. The soil sample is 60 mm in diameter and typically 20 mm in height.

According to the previous research (Vergote et al. 2019, 2022), the unloading behavior is strongly affected by the longer preloading time, which also affects the strain rate at the end of preloading. To avoid this effect from the final loading step, the final step of loading was defined to take 36h, including creep, and the final strain rate is about 3.3×10^{-8} s^{-1}, which is the same as the strain rate where CRS consolidation test started to unload. What's more, the applied pressure in the final step of loading is 549.5 kPa which is close to the maximum pressure in CRS consolidation test. The same applies to the loading process, and every step takes 24 hours during the unloading process.

Table 5-1 Applied loads and corresponding vertical pressures during loading stage

Loaded mass (kg)	0.1	0.2	0.4	0.8	1.6	3.2	5.6 (36h)
Loading stress (kPa)	9.8	19.6	39.2	78.5	157	314	549.5

Table 5-2 Unloading path and corresponding *OCR* values

Loaded mass (kg)	5.6 (36h)	4.0	2.4	1.6	0.8
Unloading stress (kPa)	549.5	392.5	235.5	157	78.5
OCR	1	1.4	2.33	3.5	7

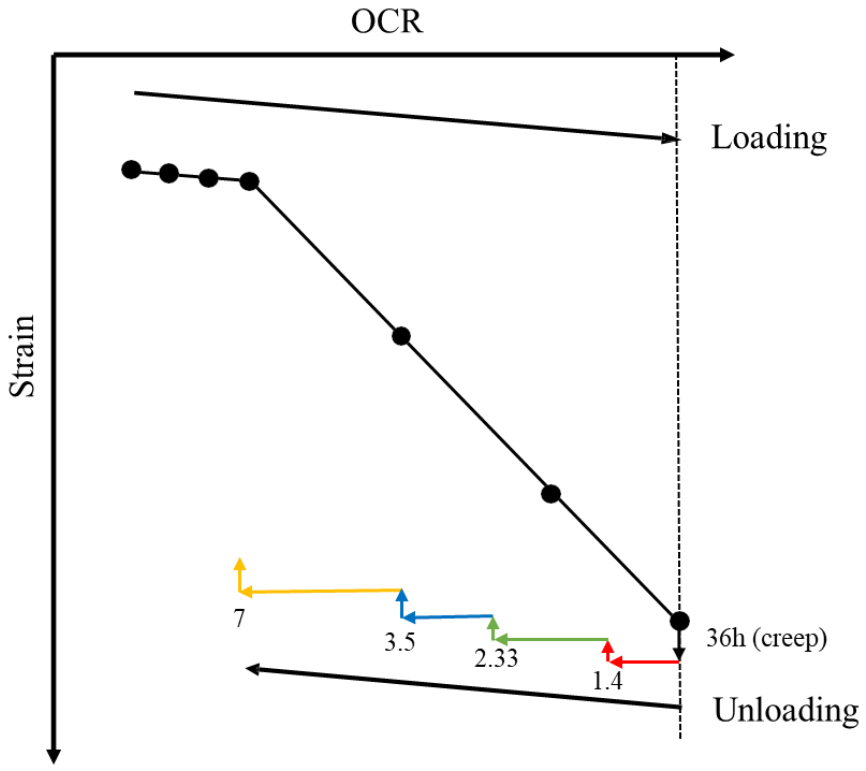

Figure 5-4 Diagram of experimental methods in oedometer test

5.2.2 Test results

The unloading behavior in four unloading steps

The experimental data from the incremental loading oedometer tests recorded by a data logger include the axial displacement and the elapsed time. The strain can be obtained by dividing the axial displacement by the sample's height, and the loading pressure can be calculated from the loaded weight.

Taking the point where the unloading process began as a reference point, the strain is transformed to the incremental void ratio. The relationship between strain and elapsed time during the unloading process of Ariake clay, Louiseville clay, and Onsøy clay measured by incremental loading oedometer test was shown from Figure 5-5 to Figure 5-7. The author utilized a fitting strain-elapsed time curve to fit the experimental data by the Origin program due to much noise in the data. Afterward, calculating the differential of the fitting strain-elapsed time curve as the strain rate-elapsed time curve. The red, green and blue points from Figure 5-5 to Figure 5-7 respectively express the points corresponding to different strain rates of -3.3×10^{-6} s^{-1}, -3.3×10^{-7} s^{-1} and -3.3×10^{-8} s^{-1} in different steps of unloading process.

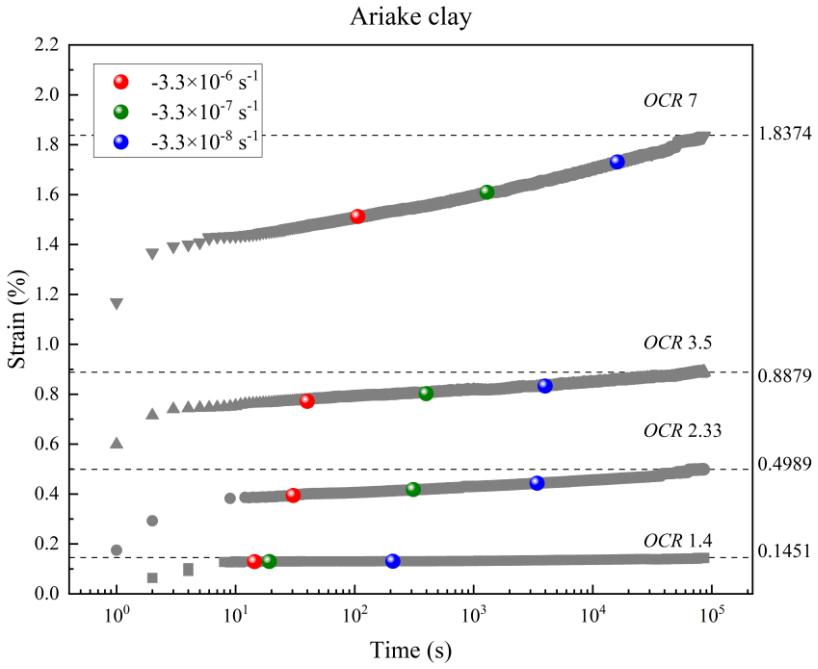

Figure 5-5 Relationship between incremental strain and elapsed time during unloading process measured by oedometer test (Ariake clay)

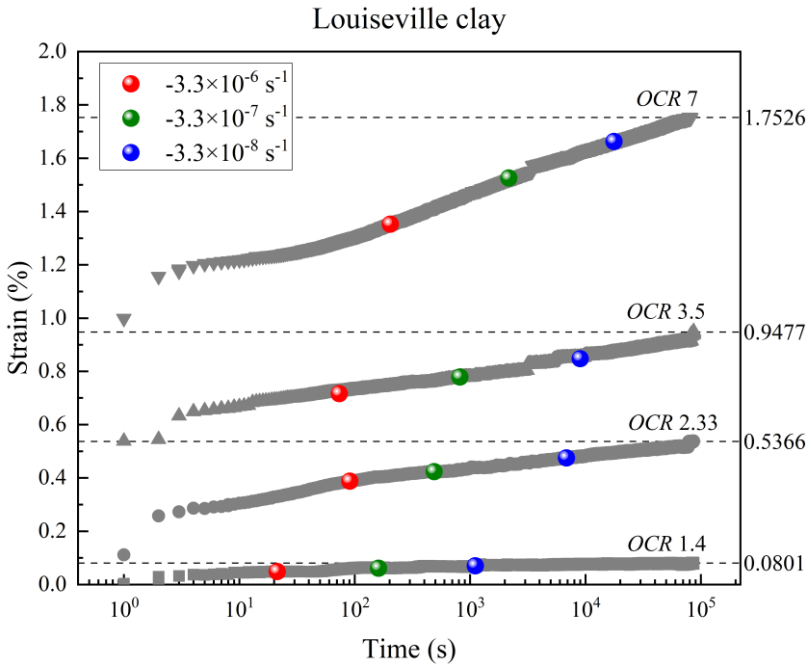

Figure 5-6 Relationship between incremental strain and elapsed time during unloading process measured by oedometer test (Louiseville clay)

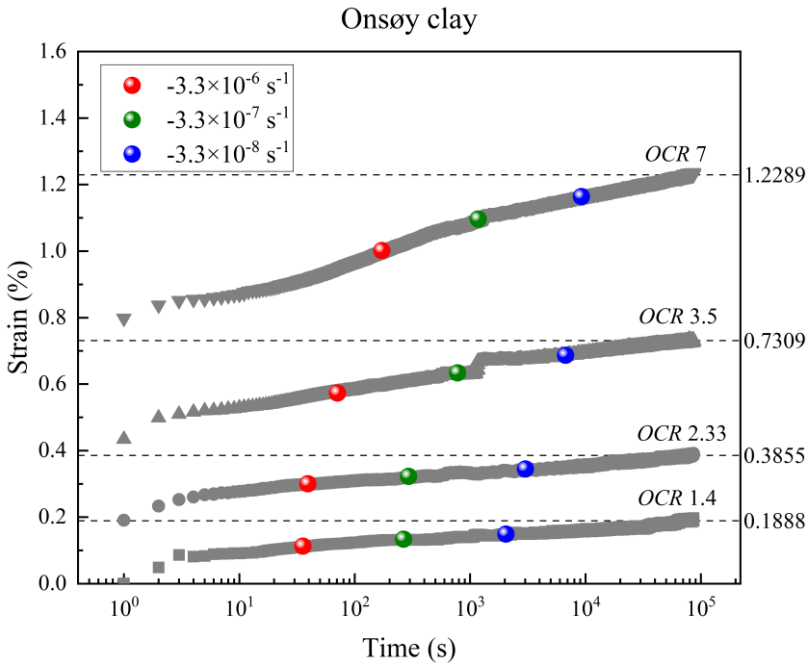

Figure 5-7 Relationship between incremental strain and elapsed time during unloading process measured by oedometer test (Onsøy clay)

The isotache lines compared to multi-stepwise unloading strain rate test results

Figure 5-8, Figure 5-9, and Figure 5-10 show the relationship between incremental strain and p'/p'_{max}, including the same unloading strain rate points in the same kind of marine clay from Figure 5-5 to Figure 5-7. The orange points express the final void ratio according to the different steps. The CRS consolidation test results from the same kind of marine clay were also described in the figures to compare with unloading process data of the incremental loading oedometer test.

However, it appears that the unloading behavior is in the same range between the CRS and IL tests only in the case of Ariake clay. In Louiseville clay and Onsøy clay, the test results are inconsistent during the unloading process. One possible explanation for this inconsistency is that different soil specimens were used in the CRS and IL consolidation tests for Louiseville and Onsøy clays, whereas the Ariake clay specimens for both tests were obtained from the same material sample ID number (i.e., almost the same depth of the same borehole), Saga Ariake 05-2I ④. Although all specimens used in this study are marine clays sampled within a one-meter soil layer, Table 5.1 demonstrates that there are still significant differences in water content and initial void ratio across samples, which may influence the test outcomes.

Another possible reason for the observed inconsistency is the incompatibility between the compression containers and the testing apparatus used in these two sets of experiments. Specifically, it was not possible to directly measure the piston displacement using an LVDT (Linear Variable Differential Transformer) sensor, which is typically required for accurate strain calculation. Instead, vertical displacement was inferred from measurements taken at the top crossbeam. This measurement approach introduced additional possible sources of error. In particular, during the transition from the preloading process to the unloading process, slight mechanical disturbances by the lever caused slippage between the LVDT sensor and the crossbeam, leading to deviations in the recorded data. This is further supported by the fact that most of the deviations are observed during the first unloading stage.

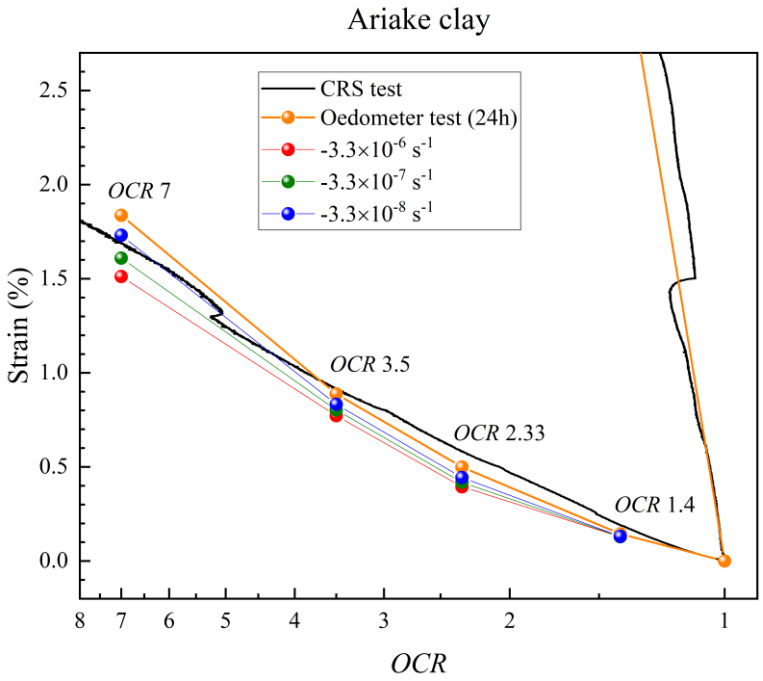

Figure 5-8 Relationship between incremental strain versus *OCR*, including the same unloading strain rate points (Ariake clay)

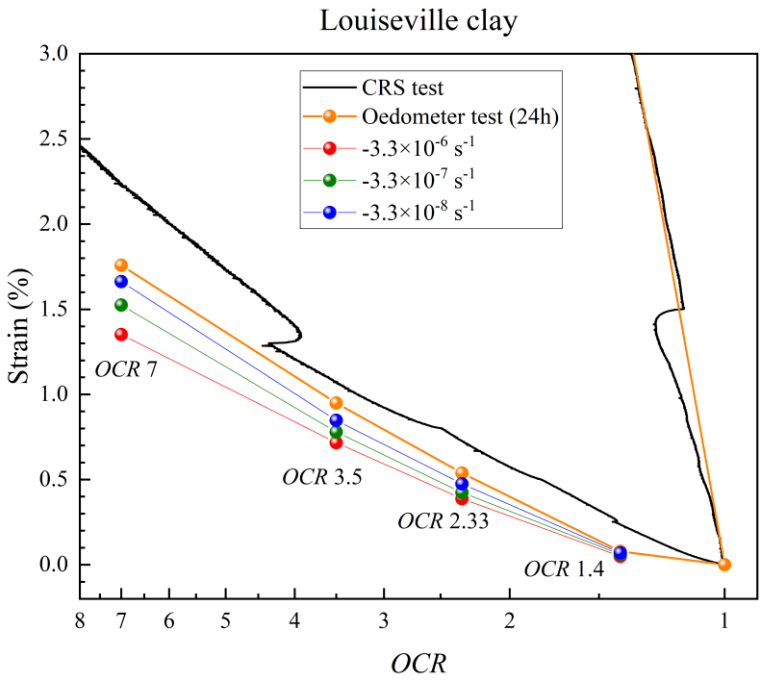

Figure 5-9 Relationship between incremental strain versus *OCR*, including the same unloading strain rate points (Louiseville clay)

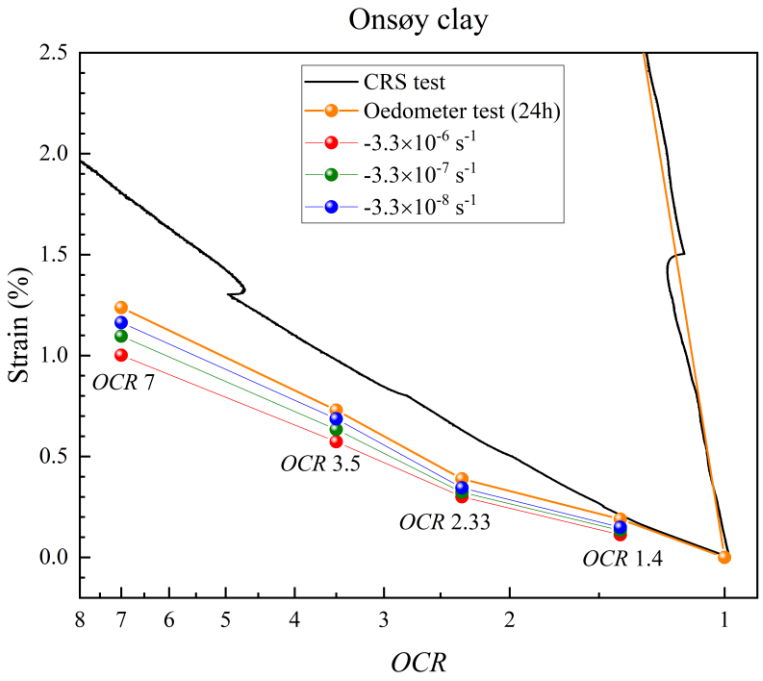

Figure 5-10 Relationship between incremental strain versus *OCR*, including the same unloading strain rate points (Onsøy clay)

Table 5-3 Clay samples' properties in the CRS and Incremental Loading (IL) oedometer tests

Test	Material sample ID number	Depth (m)	w_n (%)	e_0
CRS	Saga Ariake 05-2I ④	7.35-7.45	137.73	3.58
IL	Saga Ariake 05-2I ④	7.35-7.45	137.34	3.55
CRS	Louiseville No.2-13 ④	15.25-15.35	74.27	2.03
IL	Louiseville No.2-13 ②	15.45-15.55	68.42	1.87
CRS	Onsøy Bor.3-13 ②	19.65-19.75	51.48	1.42
IL	Onsøy Bor.3-13 ⑤	19.35-19.45	54.59	1.49

$C_{s\alpha}/C_s$ measured from incremental loading oedometer tests

C_s and $C_{s\alpha}$ can be calculated respectively according to the test results from incremental loading oedometer test, and the values of $C_{s\alpha}/C_s$ are shown in Figure 5-11-Figure 5-13. The values of $C_{s\alpha}/C_s$ tend to increase as *OCR* increases, which means the strain rate dependency becomes stronger when *OCR* becomes higher.

The values of $C_{s\alpha}/C_s$ measured from incremental loading oedometer tests are in the same range with the values from CRS consolidation tests in Table 4-1. Have explained in Chapter 4, it seems the ratio between $\pm 3.3\times10^{-6}$ s^{-1} and $\pm 3.3\times10^{-7}$ s^{-1} is significantly larger, because the unloading strain rate was changed at high *OCR*. In the CRS consolidation tests, the unloading strain rate seems to change from -3.3×10^{-7} s^{-1} to -3.3×10^{-8} s^{-1} at *OCR* 1.25-2.00, and changed from -3.3×10^{-7} s^{-1} and -3.3×10^{-6} s^{-1} at *OCR* 4-7. The values of $C_{s\alpha}/C_s$ from CRS consolidation test have a great agreement with incremental loading oedometer tests in that *OCR* range.

As shown in Figure 5-12 and Figure 5-13, $C_{s\alpha}/C_s$ is larger between -3.3×10^{-6} s^{-1} and -3.3×10^{-7} s^{-1} than that between -3.3×10^{-7} s^{-1} and -3.3×10^{-8} s^{-1}, which means the unloading strain rate dependency tends to become stronger with unloading strain rate increases. This phenomenon is consistent with the loading behavior, yet it seems not apparent as for the results from Ariake clay. This part needs further researches, such as enlarge the evaluate range of the unloading strain rate.

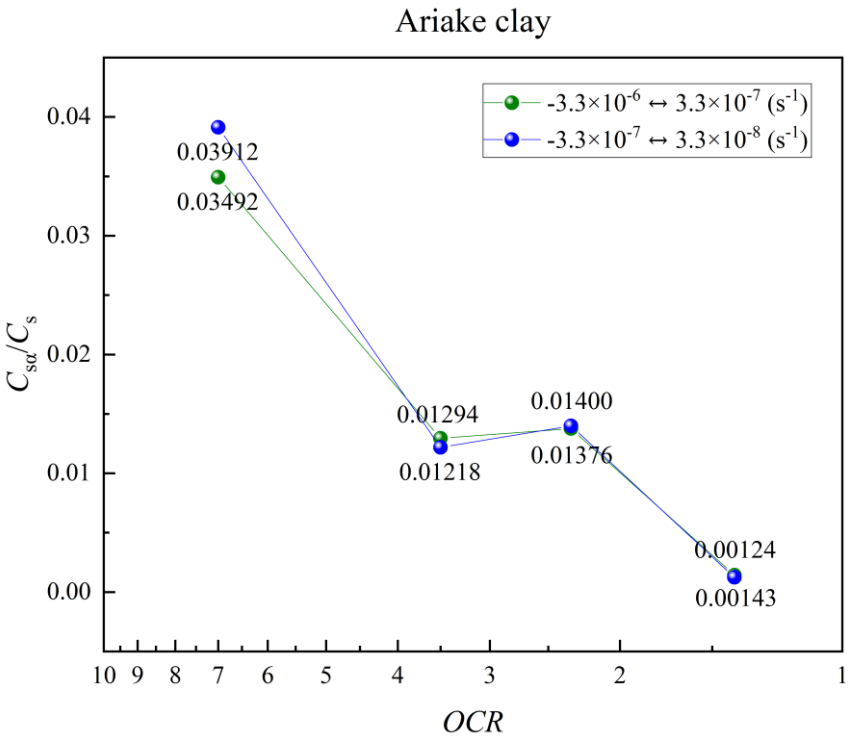

Figure 5-11 $C_{s\alpha}/C_s$ measured by incremental loading oedometer test (Ariake clay)

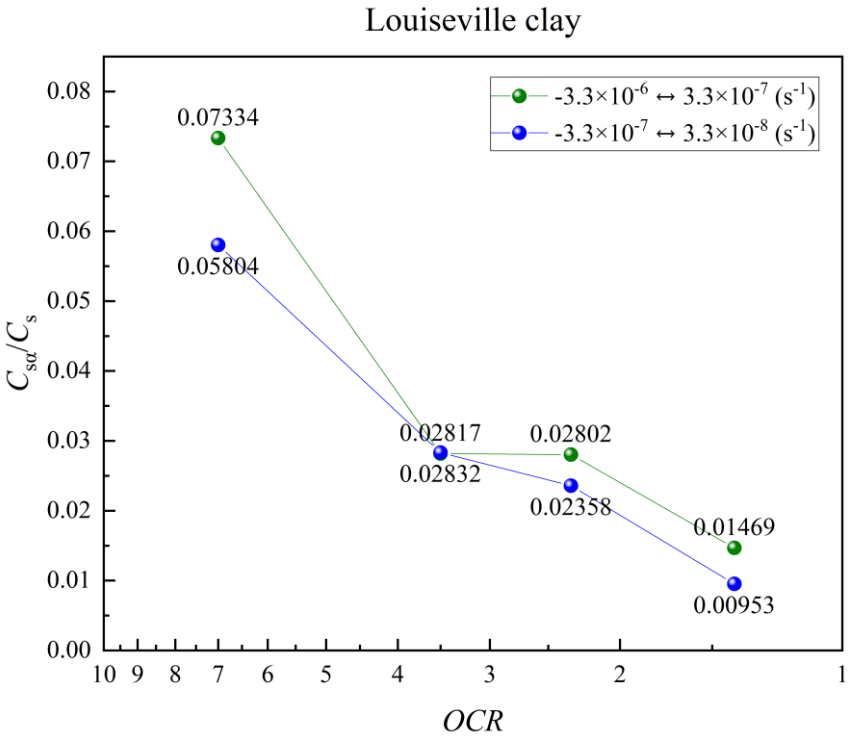

Figure 5-12 $C_{s\alpha}/C_s$ measured by incremental loading oedometer (Louiseville clay)

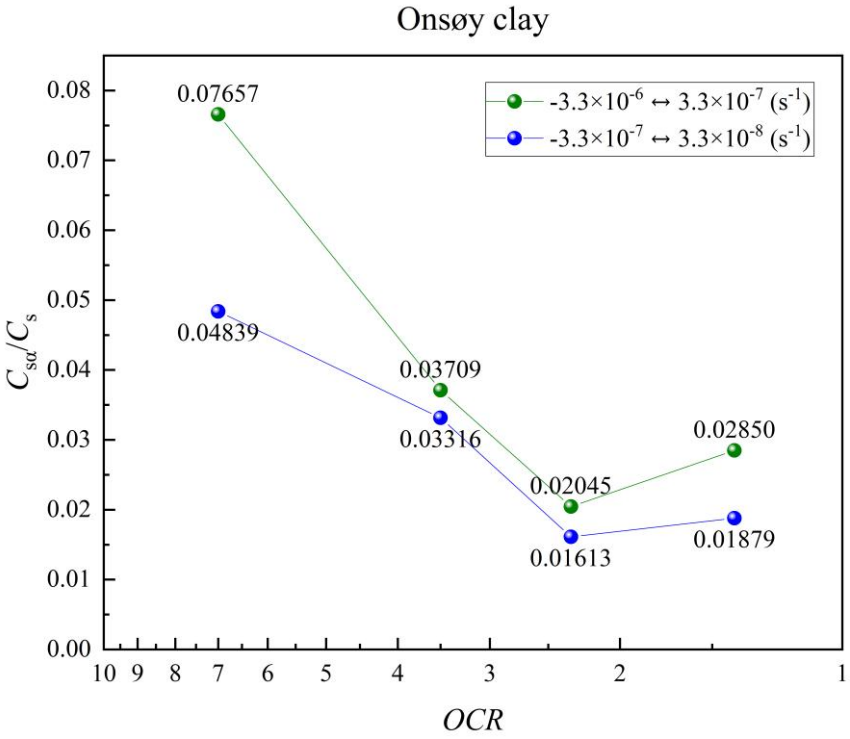

Figure 5-13 $C_{s\alpha}/C_s$ measured by incremental loading oedometer test (Onsøy clay)

Figure 5-14, Figure 5-15 and Figure 5-16 show the incremental strain-elapsed time relationship (black points). The smaller gray points denote the logarithmic unloading strain rate (log $\dot{\varepsilon}$) against the logarithmic elapsed time respectively, in Ariake clay, Louiseville clay, and Onsøy clay.

To calculate the unloading strain rate, firstly, solve the noise from the data of strain by moving average method. Secondly, calculate the differential of strain as the strain rate directly, rather than using the fitting strain-elapsed time curve in Chapter 4.3.1. This method, can avoid overfitting of the unloading strain rate.

The relationship between log $\dot{\varepsilon}$ and log t was fitted by a linear line, which is represented by the red line in Figure 5-14 to Figure 5-16. The fitting parameters R^2 are shown in Table 5-4. Except the *OCR* 1.4 condition of Ariake clay and Louiseville clay, all of the fitting parameters are larger than 0.9. This means that, after the end of the elastic part of expansion, the logarithmic unloading strain rate induced by secondary swelling varies linearly against the logarithmic elapsed time (log t). The fitting parameters perform better in the higher *OCR* conditions because the swelling value are significantly larger.

The data analysis was less influenced by the noise of data logger.

This result demonstrates the strain rate-based behavior induced by viscosity of clays plays an important role in unloading behavior and supports to develop a visco-plastic model for the unloading behavior of marine clays based on the isotache concept.

Table 5-4 Fitting parameters (R^2) for the three kinds of marine clay

	OCR 1.4	*OCR* 2.33	*OCR* 3.5	*OCR* 7
Ariake clay	0.83472	0.94121	0.93559	0.98112
Louiseville clay	0.86204	0.97969	0.96778	0.98241
Onsøy clay	0.92164	0.94092	0.95613	0.99017

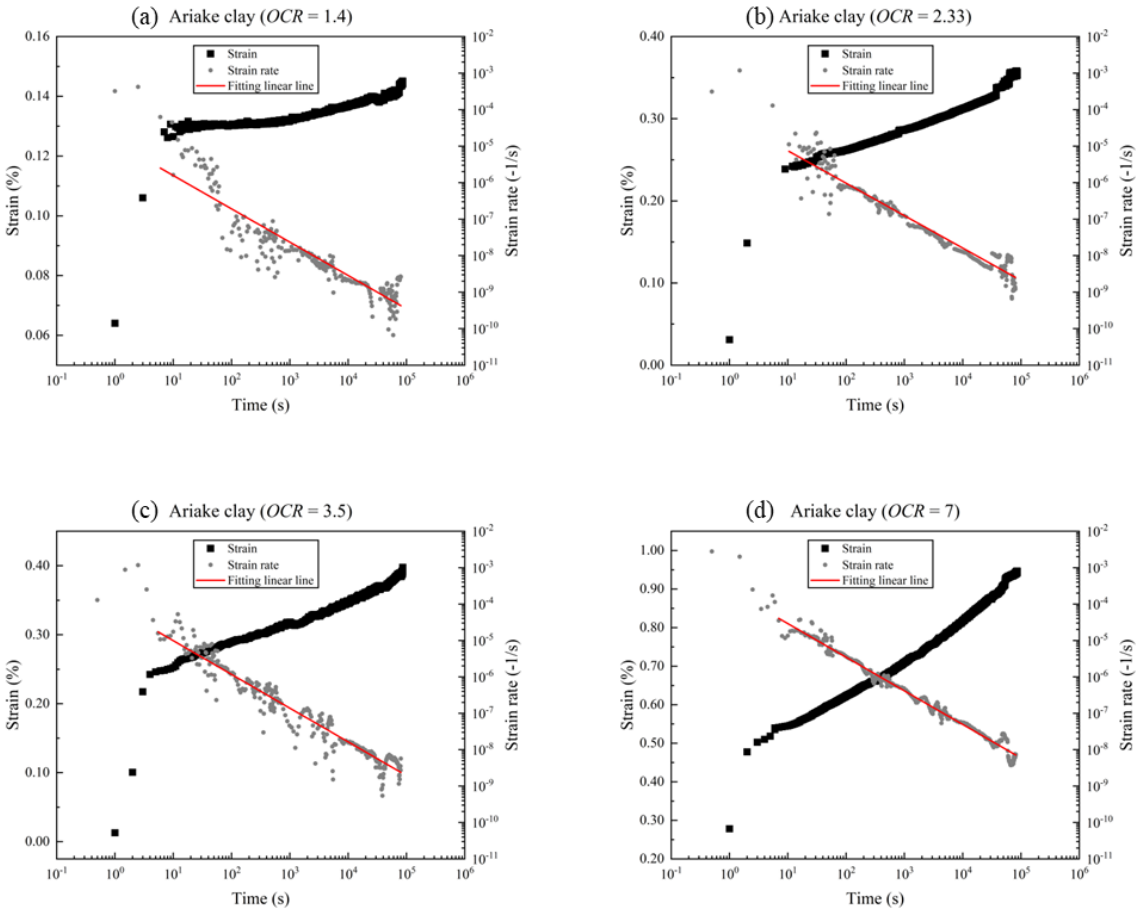

Figure 5-14 Relationship between incremental strain, logarithmic unloading strain rate and log *t* (Ariake clay): (a) *OCR* = 1.4; (b) *OCR* = 2.33; (c) *OCR* = 3.5; (d) *OCR* = 7

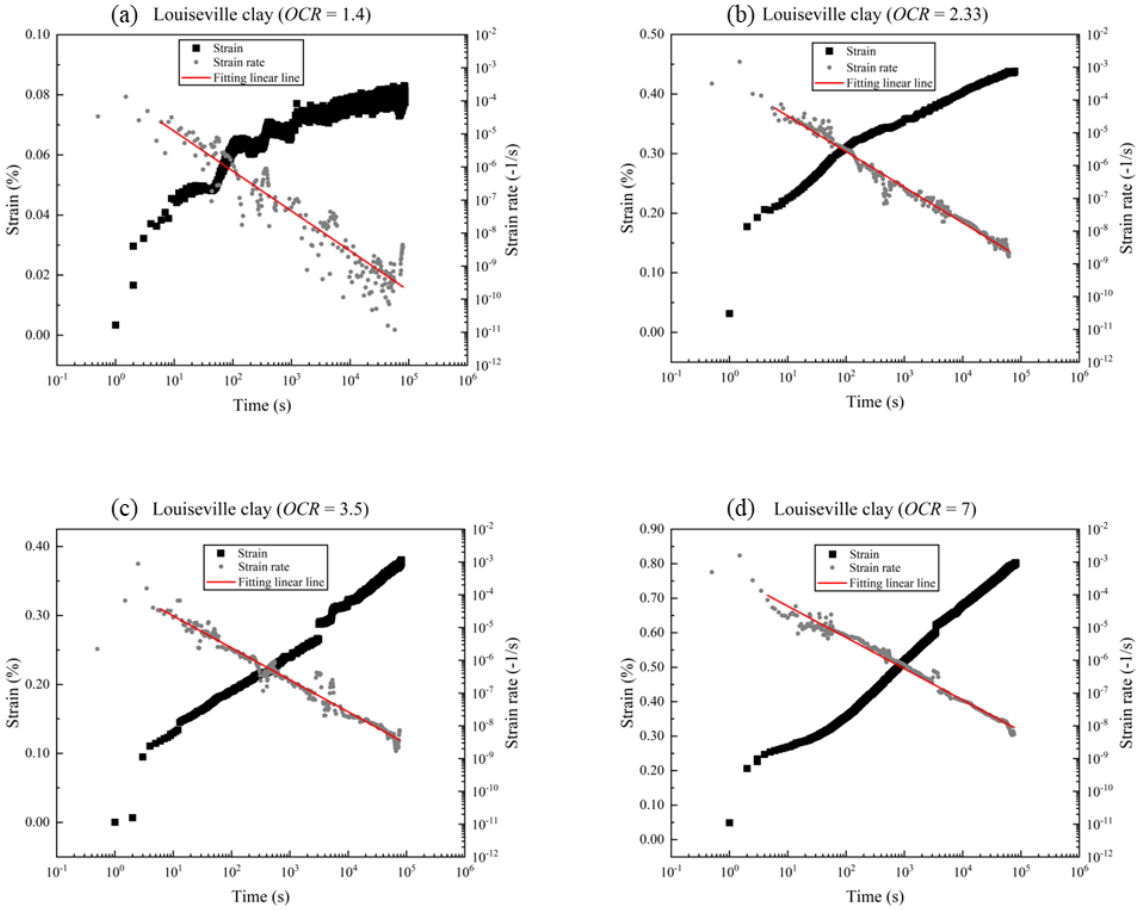

Figure 5-15 Relationship between incremental strain, logarithmic unloading strain rate and log *t* (Louiseville clay): (a) *OCR* = 1.4; (b) *OCR* = 2.33; (c) *OCR* = 3.5; (d) *OCR* = 7

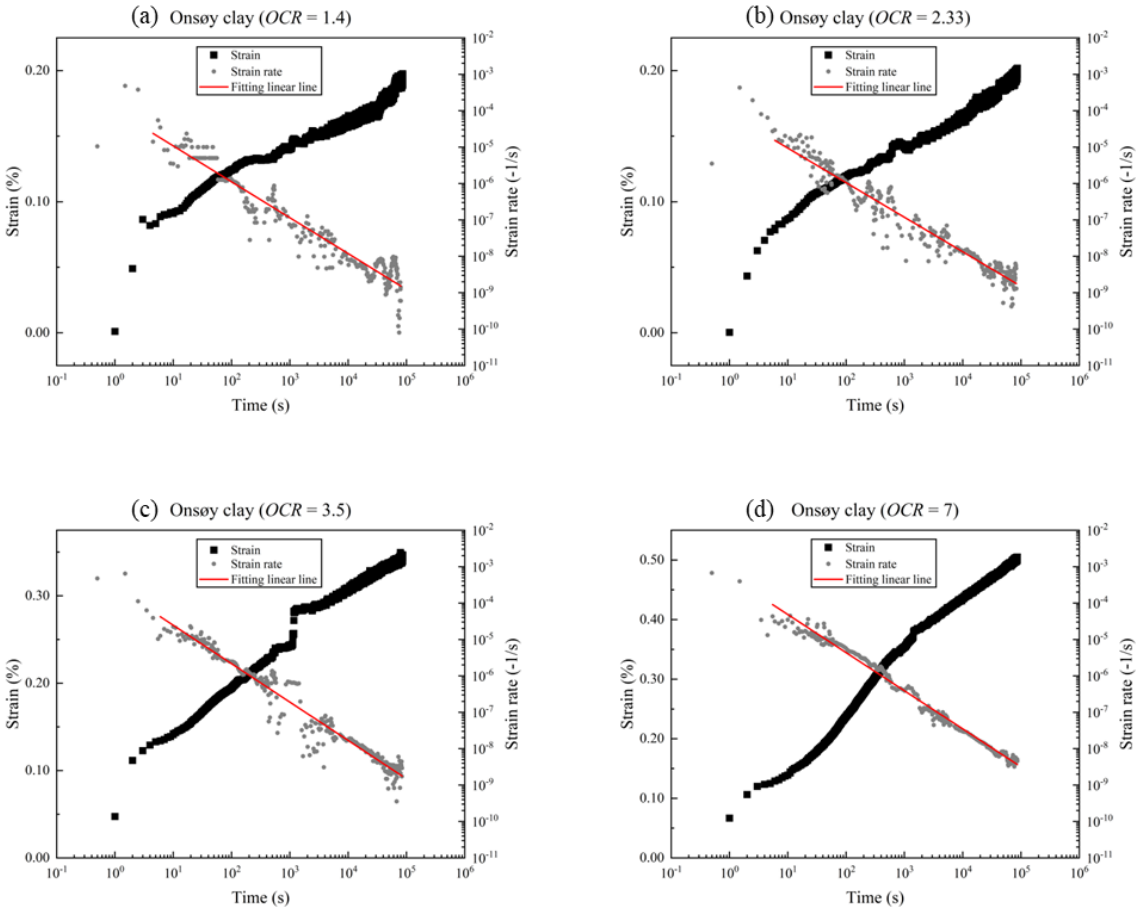

Figure 5-16 Relationship between incremental strain, logarithmic unloading strain rate and log *t* (Onsøy clay): (a) *OCR* = 1.4; (b) *OCR* = 2.33; (c) *OCR* = 3.5; (d) *OCR* = 7

5.3 Long-term unloading oedometer test

5.3.1 Test methodology of unloading behavior for marine clays

Swelling occurs due to the reduction of effective stress. For the large load reduction, long-term swelling occurs (Mesri et al. 1978). The oedometer test result (Alonso and Navarro 2005) showed that the unloading behavior was significantly affected by preloading time. In some published oedometer test results (Tanaka et al. 2014; Mesri et al. 2017), recompression occurred after swelling during unloading process. To observe this behavior, Ariake clay was examined in long-term unloading oedometer tests with a group of *OCR*s (overconsolidation ratio, defined as $\sigma'_{\max}/\sigma'$) and preloading duration.

Figure 5-17 illustrates test processes in long-term unloading oedometer tests. The loading pressure changed in the order as shown in Table 5-5, in long-term unloading oedometer tests.

Table 5-5 The loading procedures in long-term unloading oedometer tests.

Pressure (kPa)	19.6	39.2	78.5	157	314	At the target *OCR*
Loading duration	0.5 h	0.5 h	0.5 h	2 h	0.5, 4 or 36 h	3 weeks

The loading process includes six stages, and the incremental loading ratio is unity. A 24-hour duration is conventionally adopted for incremental loading oedometer tests, despite the lack of a theoretical basis for doing so. This practice probably stems from practical convenience in laboratory testing procedures. However, to shorten the experimental time, the preliminary three stages (19.6 kPa, 39.2 kPa and 78.5 kPa) were carried out for 0.5 hours each and the stage before the final loading stage (the 4th stage, loading to 157 kPa) was conducted for 2 hours to avoid excess water pressure's effect, ensuring all the water pressure dissipated. In the present study, the final loading stage is termed the preloading stage, where clay samples were preloaded until the target strain

rate. Before conducting the series of tests mentioned above, a long-term loading oedometer test without unloading was carried out. Subsequently, the relationship between strain rates at the end of preloading and preloading time became clear as the right graph in Figure 5-17 (EOP is the end of primary consolidation: all the excess pore water pressure dissipates resulting in total stress equals to effective stress. It was calculated by the square root of time method and corresponded to the degree of consolidation equal to 100%). Three kinds of preloading time were used in this study corresponding to different strain rates at the end of preloading, as shown in Table 5-6. During the unloading process of Ariake clay, the clay samples were unloaded to five different overconsolidation ratios (*OCR*s) and kept for three weeks. In total, this series of long-term unloading oedometer tests conducted 16 test cases to investigate the unloading behavior of the Ariake clay, including one reference test (*OCR* = 1).

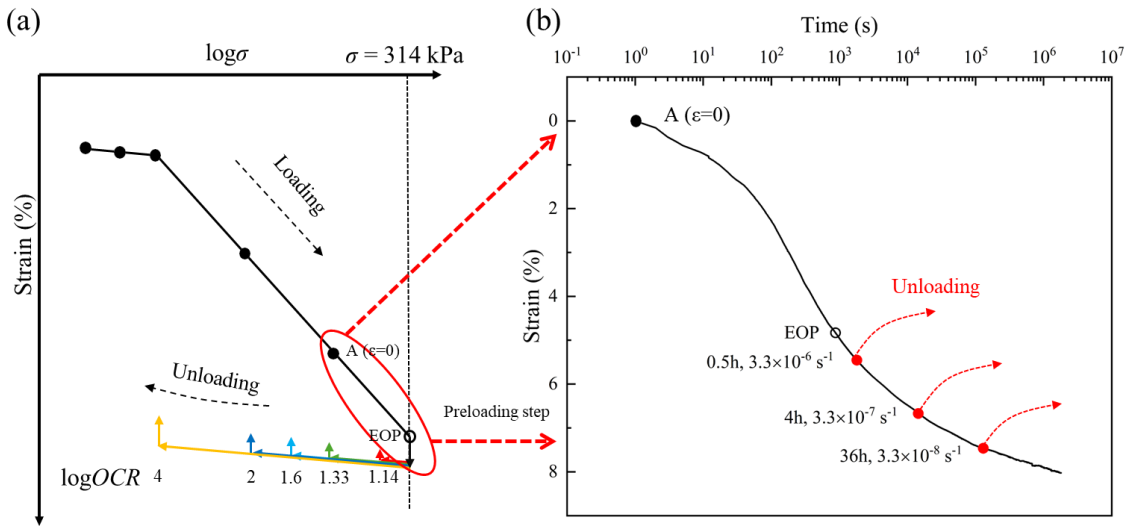

Figure 5-17 Illustration of experimental methods (Long-term unloading oedometer test). (a) Experimental flow of long-term unloading oedometer; (b) Unloading in the preloading stage corresponding to different loading strain rates

Table 5-6 Relationship between strain rates at the end of preloading and preloading time

Strain rate at the end of preloading \ Preloading time (h)	Ariake	Onsøy	Louiseville
$+3.3\times10^{-6}$ s^{-1}	0.5	0.5	1
$+3.3\times10^{-7}$ s^{-1}	4	4	4
$+3.3\times10^{-8}$ s^{-1}	36	36	24

5.3.2 Unloading test results and discussion

Figure 5-18, Figure 5-19 and Figure 5-20 show the long-term unloading oedometer test results of Ariake clay, Louiseville clay and Onsøy clay, respectively. The temporal variations of total strain according to three kinds of strain rate at the end of preloading stage (different preloading time) and four or five kinds of *OCR* ($=\sigma'_{max}/\sigma'$) are shown in Table 5-6 and Figure 5-17. Obviously, with increasing of *OCR* or decreasing of the strain rate at the end of preloading stage, the start of recompression of clay will be delayed. Moreover, when the *OCR* is large enough (> approximately 1.8) or the strain rate at the end of preloading stage is small enough, the clay was continuously swelling and recompression never appears.

In the cases of Louiseville clay and Onsøy clay, when *OCR* is 4 and the strain rate at the end of the preloading stage is $+3.3\times10^{-8}$ s^{-1}, the observed swelling behavior is significantly delayed compared to other tests conducted at the same *OCR* value. This discrepancy is because both soil samples were obtained approximately 20 years ago, resulting in limited sample availability. To maximize the use of these scarce samples, a modified constant-rate-of-strain (CRS) consolidation test method was adopted. Specifically, the samples were unloaded at a strain rate of -3.3×10^{-7} s^{-1} until the stress level corresponding to *OCR* 4 was reached. Subsequently, the stress was kept constant, and the specimen turned to a long-term swelling condition. This approach enabled the acquisition

of both the reference unloading curve and the swelling response under constant stress condition associated with *OCR* 4 from a single specimen.

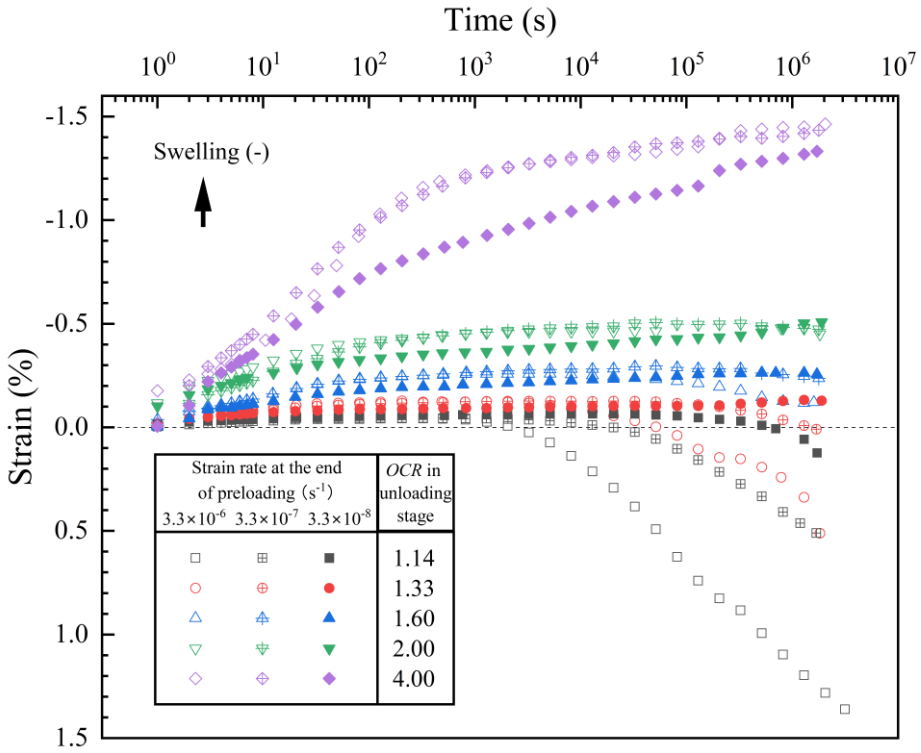

Figure 5-18 The relationship between incremental strain and log *t* in unloading according to different *OCR* and strain rates at the end of preloading (Ariake clay)

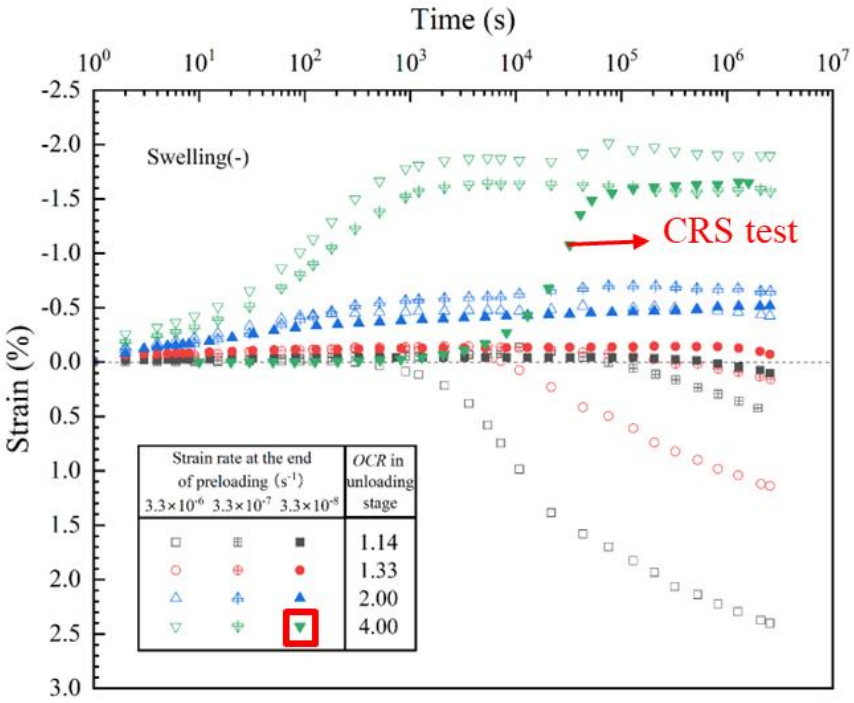

Figure 5-19 The relationship between incremental strain and log *t* in unloading according to different *OCR* and strain rates at the end of preloading (Louiseville clay)

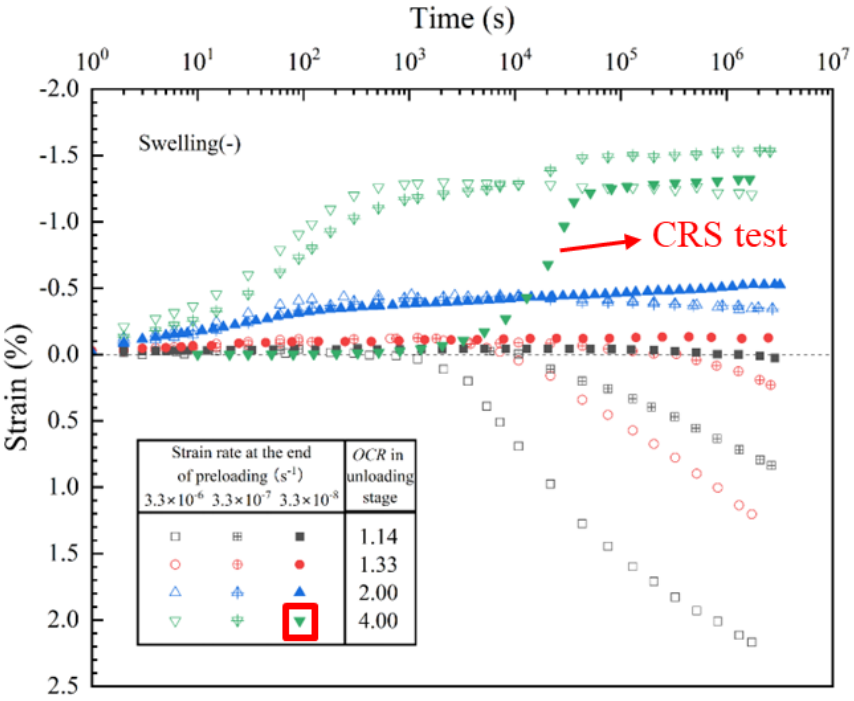

Figure 5-20 The relationship between incremental strain and log *t* in unloading according to different *OCR* and strain rates at the end of preloading (Onsøy clay)

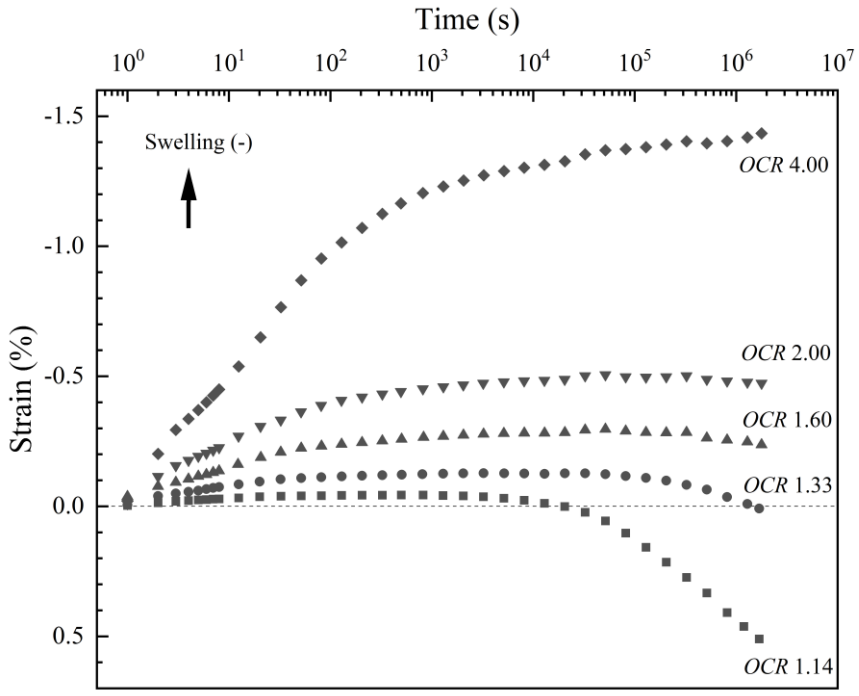

Figure 5-21 Unloading behavior after preloading 4h, Ariake clay (Strain rate at the end of preloading = $+3.3\times10^{-7}$ s^{-1})

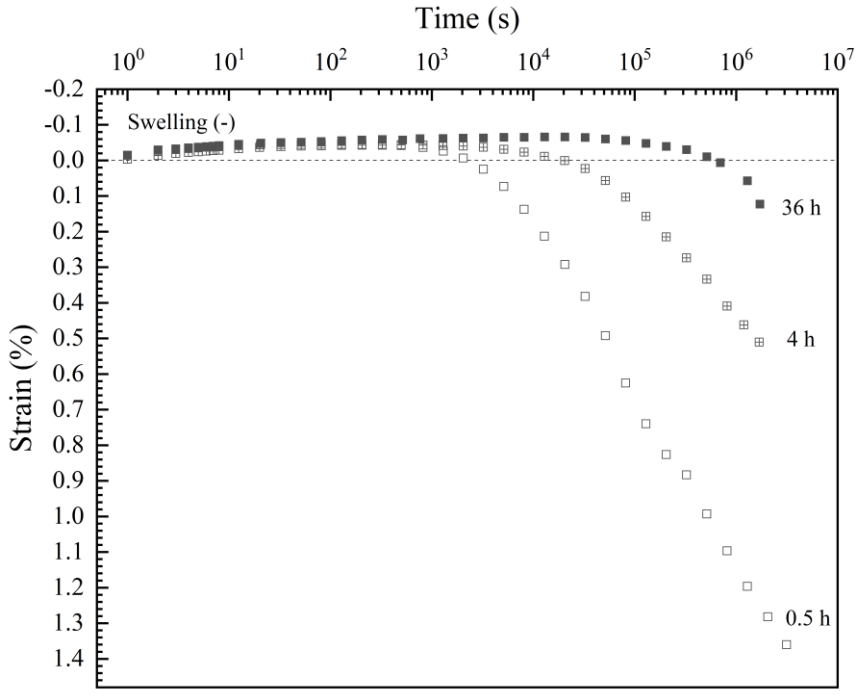

Figure 5-22 Unloading behavior of defferent preloading duration, *OCR* 1.14 condition (Ariake clay)

Figure 5-21 and Figure 5-22 illustrate the cases of preloading 4 hours condition and an *OCR* 1.14 condition, respectively, in order to investigate the influence of one factor while keeping another one constant. Figure 5-21 shows that not only does the swelling strain increase due to the removal of high stress, but the recompression phenomenon is also progressively delayed and eventually disappears. On the other hand, Figure 5-22 demonstrates that, as the preloading duration increases, the residual recompressive strain is significantly reduced and the recompression phenomenon is progressively delayed, although the swelling strain remains relatively consistent among different preloading durations. These results suggest that, comparatively, the magnitude of swelling strain is primarily governed by the overconsolidation ratio (*OCR*), while the occurrence and magnitude of the recompressive settlement are jointly influenced by both *OCR* and the preloading duration.

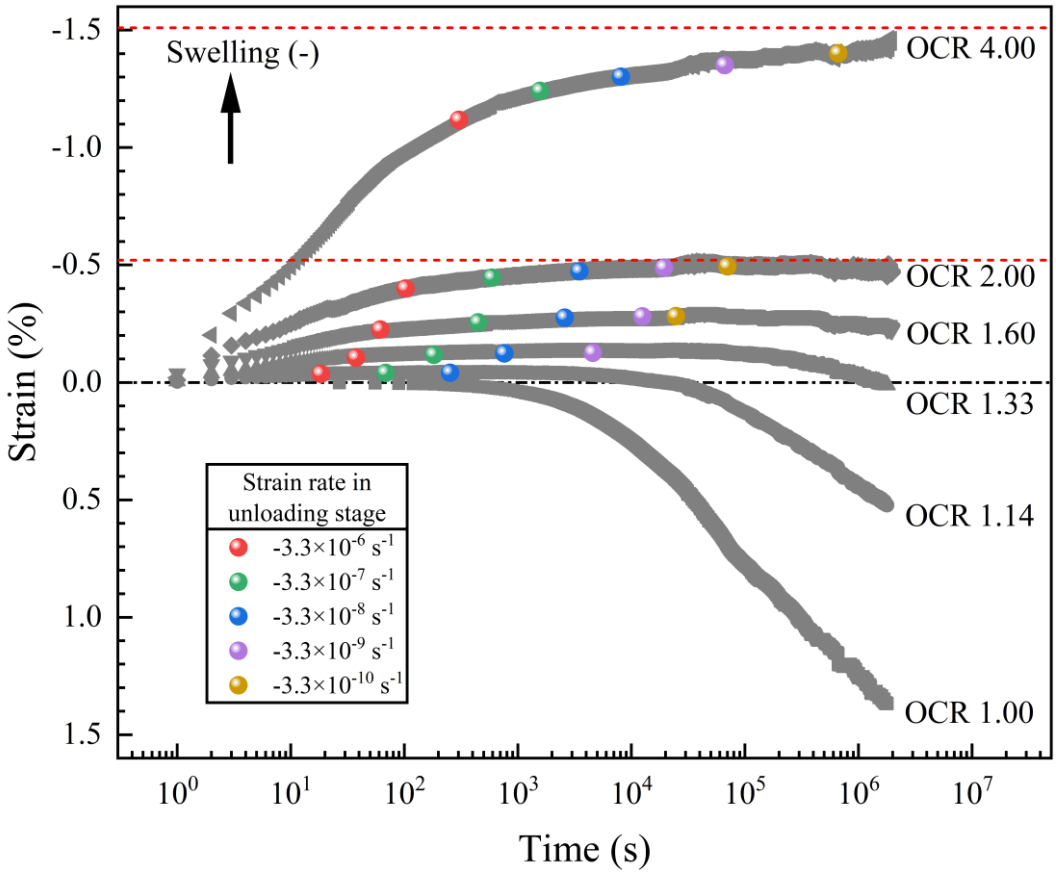

Figure 5-23 Relationship between strain and elapsed time according to different *OCR*

The relationships between incremental strain and logarithmic time of long-term unloading oedometer test, which was unloaded to different *OCR* after 4-hour preloading are shown in Figure 5-23. At elapsed time of 4 hours in preloading, the marine clay's strain rate is about $+3.3\times10^{-7}$ s^{-1}, then unload. Different swelling strain rate points were plotted as different colors in the figure, which were directly calculated using the data presented in Figure 5-23. The test result without unloading was also plotted on the figure as *OCR* 1 and offset the elapsed time ($t = 0$) and strain ($\varepsilon = 0$) at which the strain rate was $+3.3\times10^{-7}$ s^{-1} for comparison with the unloading test result. Similar to the constant stress loading process, the swelling strain during unloading also tends to approach a swelling limit, as indicated by the red dashed line in Figure 5-23. These two lines for *OCR* 2 and *OCR* 4 are calculated from the new model, which will be discussed in later chapters.

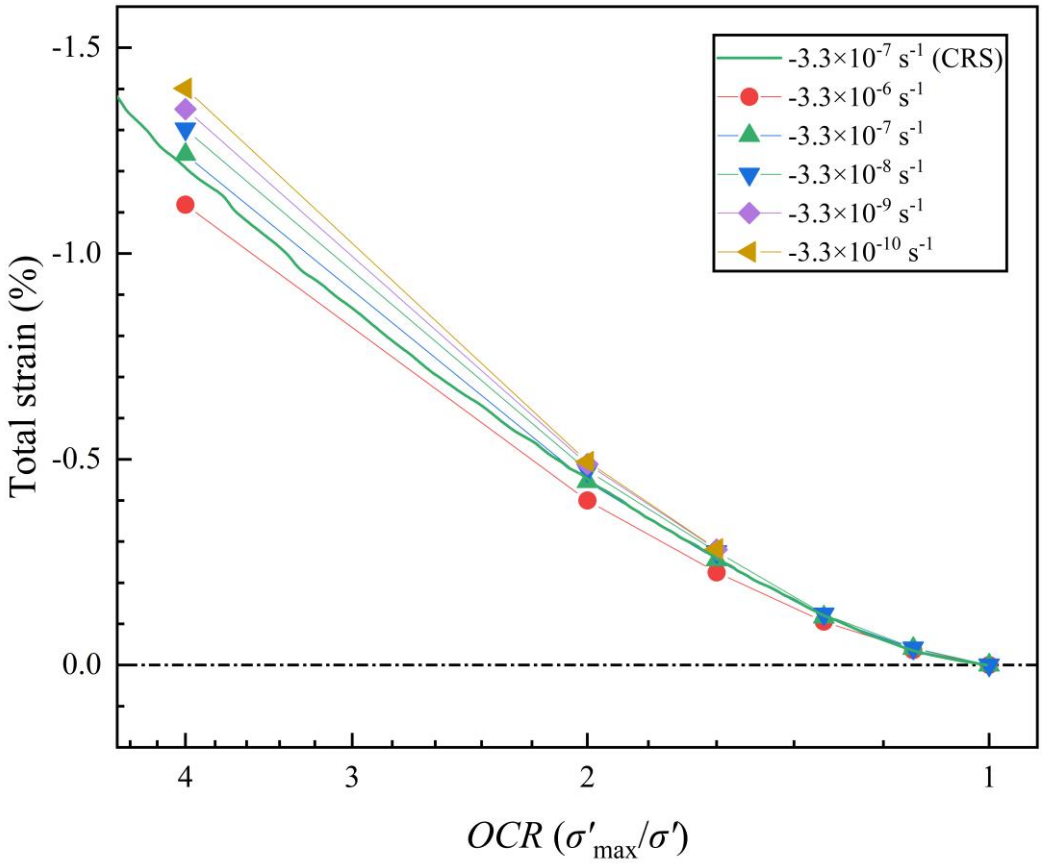

Figure 5-24 Relationship between strain and *OCR* in terms of the same unloading strain rate points.

The relationship between incremental total strain and *OCR* is shown in Figure 5-24, with the constant strain rate of -3.3×10^{-7} s^{-1} unloading curve obtained from the CRS (constant rate of strain) consolidation test drawn as the green curve. The unloading curve obtained from CRS consolidation test has a remarkable agreement with the strain rate point obtained from long-term unloading oedometer test started from the same strain rate at the end of preloading ($+3.3\times10^{-7}$ s^{-1}). As time progresses, the swelling strain rate of the clay sample gradually slows down. Therefore, the lower strain rate points are plotted upper than the larger strain rate points. The distance between different unloading strain rate curves grows with the increase in *OCR*, while the normal consolidation domain, in which the different loading strain rate curves (isotache compression curves) are parallel. The following sections will first quantitatively describe this characteristic behavior in swelling different from normal consolidation, and then based on the results of the quantitative description, a simulation model for swelling will be established in the following section.

Chapter 6 Visco-plastic model for marine clay

6.1 Visco-plastic model for normal consolidation domain

Watabe et al. (2008; 2012) investigated the long-term consolidation behavior of Pleistocene clays at Kansai International Airport in order to enhance the settlement prediction accuracy and proposed a new equation to express the strain rate dependency of consolidation yield stress σ'_{p} by applying the isotache concept (Šuklje 1957). The experimental data (Watabe et al. 2012; Watabe and Leroueil 2015) show that the $C_{c\alpha}/C_c$ ($C_{c\alpha}$ generally denotes as C_{α}, the coefficient of secondary consolidation in void ratio (= $\Delta e/\Delta \log t$) to differentiate it from unloading behaviors, this paper employs "$C_{c\alpha}$" instead of the traditional "C_{α}") is not constant during long-term loading oedometer test. Moreover, the constant $C_{c\alpha}/C_c$ concept suggests that settlement would continue indefinitely over an infinite elapsed time, which is not consistent with common sense. There is a comparison with constant $C_{c\alpha}/C_c$ concept and variable $C_{c\alpha}/C_c$ concept in Figure 6-1. The value of $C_{c\alpha}/C_c$ tends to decrease when strain rate decreases to a small value, as shown in Figure 6-1 (b). Therefore, instead of the constant $C_{c\alpha}/C_c$ concept proposed by Mesri and Castro (1987), a nonlinear relationship between $C_{c\alpha}/C_c$ and strain rate was adopted in the new equation, as Eq. (6-1). When $\dot{\varepsilon}_{\mathrm{vp}}$ decreases toward zero in Eq. (6-1), σ'_{p} converges toward σ'_{pL} as shown in Figure 6-1 (a). It has a great agreement with the test result under constant loading stress conditions such as incremental loading oedometer test as the Figure 5-17 (b) shows that there is a limit value for compression because the slope of log t-ε curve ($C_{c\alpha}$) decreases with the strain rate becomes slower. The strain will close to the limit value with time elapsed.

$$\ln\left(\frac{\sigma'_{\mathrm{p}}}{\sigma'_{\mathrm{pL}}}-1\right)=c_1+c_2\ln\dot{\varepsilon}_{\mathrm{vp}} \tag{6-1}$$

$$c_2=\frac{\ln\left(\frac{\sigma'_{\mathrm{p0}}}{\sigma'_{\mathrm{pL}}}-1\right)-c_1}{\ln 10^{-7}} \tag{6-2}$$

where c_1 and c_2 are constants, representing the value and slope of the preconsolidation pressure at a great strain rate ($\dot{\varepsilon} = 1$); $\dot{\varepsilon}_{vp}$ is visco-plastic strain rate; σ'_p is preconsolidation pressure; σ'_{pL} = lower limit of σ'_p at infinitesimal strain rate ($\dot{\varepsilon} = 0$); $\sigma'_{p0} = \sigma'_p$ at $\dot{\varepsilon}_{vp} = +1.0 \times 10^{-7}$ s^{-1}.

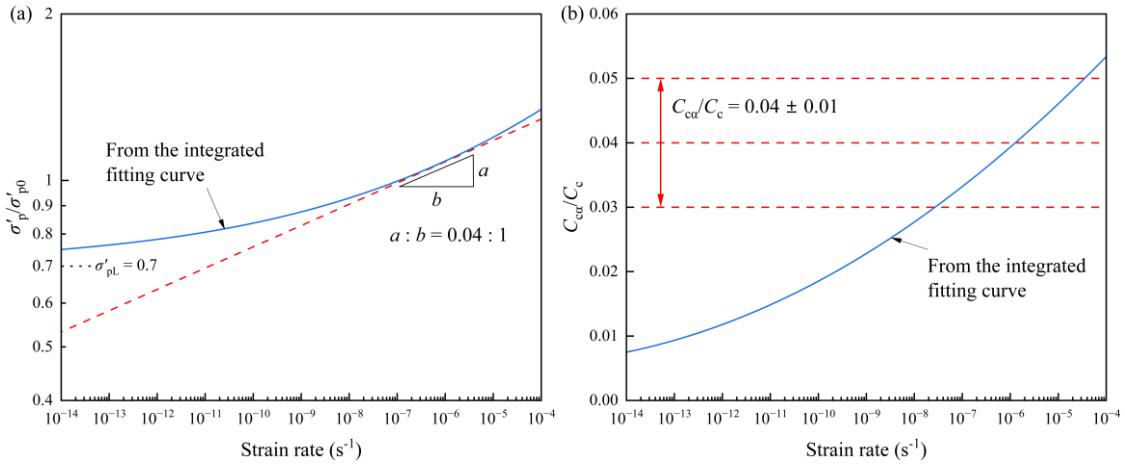

Figure 6-1 Comparison of the integrated fitting curve with the constant $C_{c\alpha}/C_c$ concept: (a) relationship between σ'_p/σ'_{p0} and strain rate; (b) relationship between and $C_{c\alpha}/C_c$ and strain rate (data from Watabe et al. 2012)

Figure 6-2 illustrates the method for evaluating the strain-rate dependency in the normal consolidation domain of marine clay. This model utilizes the constant rate of strain (CRS) consolidation test results as the reference compression curve. The reference compression curve undergoes horizontal adjustment to fit with the strain rate data derived from long-term loading oedometer tests. Following this, Eq. (6-1) articulates a mathematical relationship among the preconsolidation pressure corresponding to different strain rates. This demonstrates a unique relationship among effective stress, strain, and strain rate, i.e., “isotache” during the normal consolidation behavior. Equation (6-1) can be transformed into power-law creep as Eq. (6-3), which is in conjunction with overstress visco-plastic theory (Perzyna 1963). In this study, the authors further develop this model into the swelling stage of marine clay in unloading behavior. Additionally, the study applied a common parameter $\sigma'_{pL}/\sigma'_{p0} = 0.7$ for normal consolidation behavior.

$$\dot{\varepsilon}_{vp} = c_3 \left(\frac{\sigma'_p}{\sigma'_{pL}} - 1\right)^{c_4} \tag{6-3}$$

where $c_3 = \exp(-c_1/c_2)$ and $c_4 = 1/c_2$.

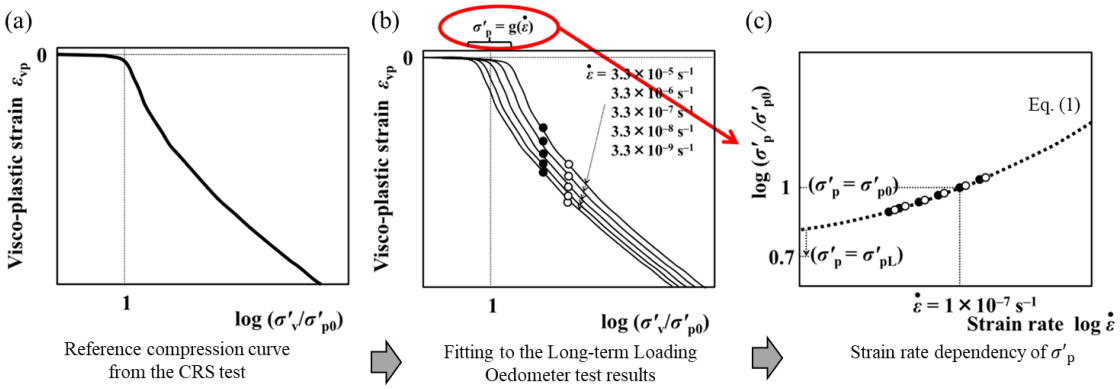

Figure 6-2 Illustration of the method to evaluate the strain-rate dependency of σ'_p from the CRS consolidation test and the long-term loading cosolidation test results (Watabe and Leroueil 2015)

6.2 Developing the visco-plastic model into the swelling stage

There are two distinct cases presented in unloading behavior, as shown in Figure 6-3:

Case 1: Here, if the preloading duration is sufficiently long or the overconsolidation ratio (*OCR*) is sufficiently large, recompression does not occur, leading to the generation of visco-plastic swelling strain. This is illustrated in Figure 6-3 (a), which includes only primary and secondary swelling.

Case 2: Recompression becomes evident under a more minor *OCR* condition. Figure 6-3 (b) shows an example where elastic swelling occurs, followed by visco-plastic swelling and subsequent recompression, as described in Vergote et al. (2021; 2022). However, the current model does not yet incorporate the visco-plastic recompression component, which remains a subject of future work.

In the present study, the visco-plastic model proposed by Watabe et al. (2008; 2012) has been developed to include the swelling behavior in unloading. The new model adopts

the overconsolidation ratio (OCR=$\sigma'_{\max}/\sigma'$) to replace the original effective stress of compression for facilitating understanding and computation.

Initially, Eq. (6-1) can simulate the relationship between the preconsolidation pressure and various strain rates in the normal consolidation domain, as shown in Figure 6-4. This relationship enables the delineation of isotache lines for the loading stage, depicted as the gray lines in Figure 6-5, and the determination of the limiting line for the compression zone, which is called the limit compression line in this paper. During the normal consolidation behavior of marine clays, generally, parameter $\sigma'_{\mathrm{pL}}/\sigma'_{\mathrm{p0}}$ is taken as constant, usually equal to 0.7 according to Watabe et al. (2012), with the c_1 value adjusted to fit the test result. For Ariake clay used in this study, c_1 = 1.06 and subsequently, according to Eq. (6-2), c_2 = 0.118.

In this context, the new model defines the elastic strain during unloading, identified by the slope of two key points: the beginning point of unloading and the intersection of the limit compression line with the unloading curve. The new model applied the plastic rebound concept (Amerasinghe and Kraft 1983; Tachibana et al. 2020) to describe the swelling behavior of soil. The limit compression line of the loading stage is considered a critical boundary to distinguish whether the recompression occurs and visco-plastic swelling will appear for unloading behavior in the new model. Figure 6-6 elucidates the unloading behavior after preloading, visco-plastic strain after a deduction of elastic strain.

Condition 1 in Figure 6-6 corresponds to Case 1 shown in Figure 6-3 (a): The unloading stress decrement is large enough that the OCR exceeds the unloading plastic boundary (the limit line for compression in normal consolidation domain). There is only visco-plastic swelling strain and elastic strain induced by stress reduction. Condition 2 in Figure 6-6 corresponds to Case 2 shown in Figure 6-3 (b): The OCR value after unloading does not exceed the unloading plastic boundary and remains within the elastic domain. Subsequently, visco-plastic recompression strain occurs after swelling. However, it is necessary to mention that the swelling process following unloading is not purely elastic. There is a small visco-plastic part, as the secondary swelling process in Figure 6-3 (b), the development of swelling occurs progressively over time. While the proposed model cannot capture this component, the measured plastic strain in such cases is typically minimal.

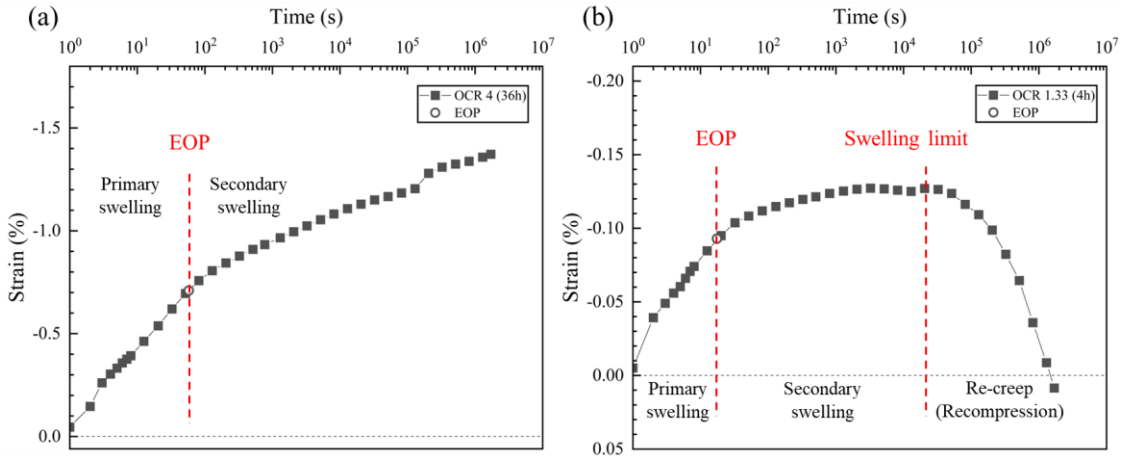

Figure 6-3 Two distinct cases in unloading behavior: (a) Case 1: Left zone of the limit line for compression; (b) Case 2: Right zone of the limit line for compression during the unloading process

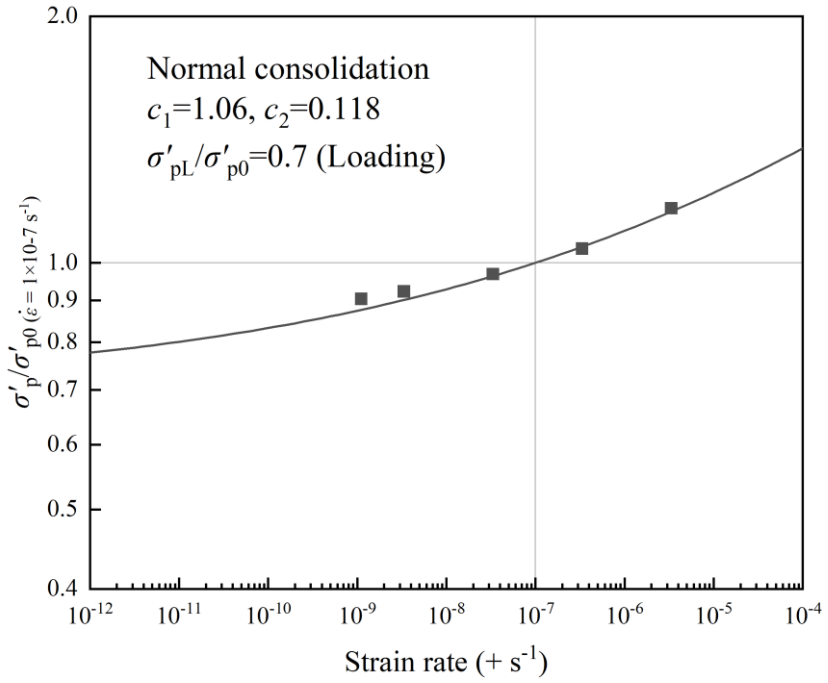

Figure 6-4 Relationship between σ'_p/σ'_{p0} and strain rate in normal consolidation domain

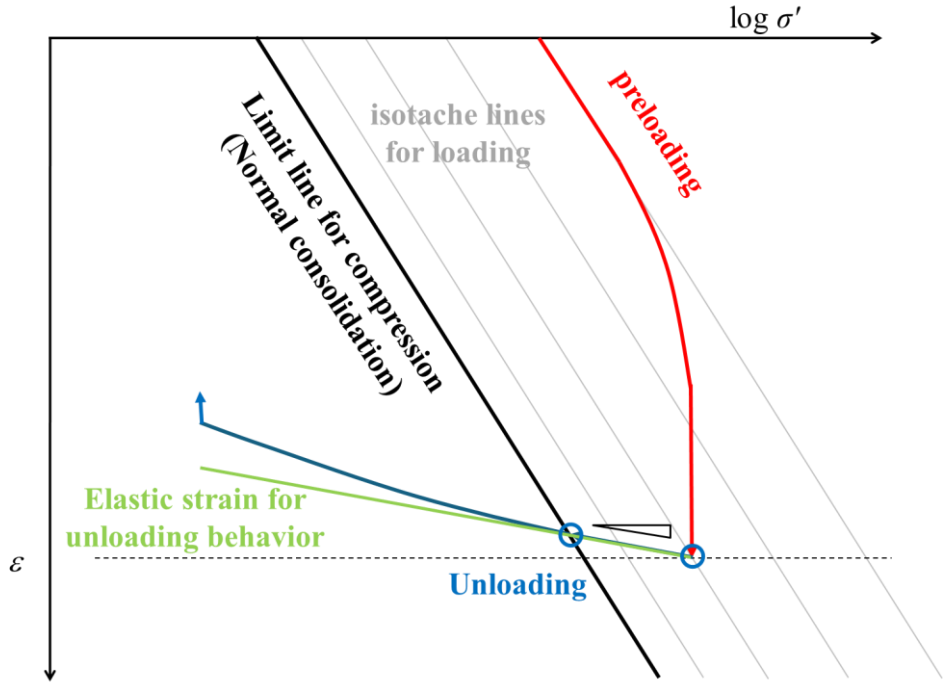

Figure 6-5 The definition of elastic strain for unloading behavior in the new visco-plastic model

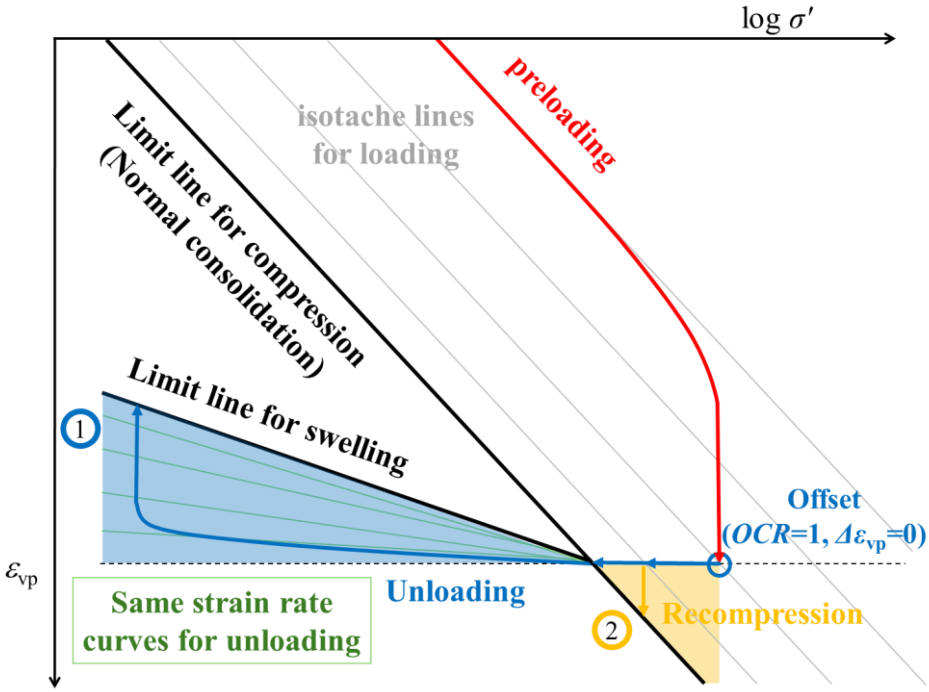

Figure 6-6 Illustration of the unloading behavior by the new simplified visco-plastic model

Fan and Watabe (2024) set a parameter $C_{s\alpha}/C_s$ ($C_{s\alpha}$ (= $\left|\Delta e/\Delta \log t\right|$, analogous to $C_{c\alpha}$ in loading behavior, the coefficient of secondary swelling in void ratio in unloading behaviors) to evaluate the strain rate dependency during the unloading behavior of marine clays as depicted in Figure 6-7. Geometrically, the values of $C_{s\alpha}/C_s$ quantify the horizontal distance equal to the increment of log σ' for one log cycle of strain rate at a constant void ratio (i.e., $x\log \sigma'$) as detailed in (Watabe et al. 2013 and Fan and Watabe 2024). Based on the experimental data, $C_{s\alpha}/C_s$ is strongly affected by overconsolidation ratio (OCR= σ'_{max}/σ') as shown in Figure 6-8. This indicates that as the OCR increases, the distance between different strain rate lines (on log cycle) increases. This behavior contrasts with normal consolidation behavior of soil, in which the same strain rate lines remain parallel. However, the difference between one log cycle strain rate lines in swelling decreases with the strain rate decreases. This is similar to the normal consolidation behavior. As a result, the swelling behavior of Ariake clay also can be modeled by a similar form of Eq. (6-1). In the new viscoplastic model for swelling behavior in unloading, OCR was used instead of σ'_p.

In order to describe the above characteristics of swelling behavior, in this study, the authors novelly developed a new model that based strain-rate effect for simulating the swelling behavior in unloading as illustrated in Figure 6-9. The lines with the same strain rate tend to become close to a limit swelling curve with the strain rate decreases. The newly developed Eq. (6-4) for swelling is similar to Eq. (6-1) in the loading stage because the difference between one log cycle strain rate lines in swelling decreases with the strain rate decreases in the same manner as the loading stage. This modification allows the model to describe the phenomenon that the distance between different strain-rate curves increases linearly with the OCR in the swelling behavior of marine clay. Furthermore, swelling plastic strain only occurs when the OCR exceeds $OCR_{Boundary}$; at values below this threshold ($OCR < OCR_{Boundary}$), solely elastic strain occurs, and there is no strain rate dependency in elastic behavior.

The absolute values of $\dot{\varepsilon}_{vp}$ are used in all equations related to swelling behavior in unloading for simplification and uniformity in the formulas.

$$\ln\left(\frac{\log\left(\frac{OCR}{OCR_{Boundary}}\right)}{\log\left(\frac{OCR_L}{OCR_{Boundary}}\right)}-1\right)=s_1+s_2\ln\dot{\varepsilon}_{vp} \tag{6-4}$$

where s_1 and s_2 are common parameters in the swelling stage; OCR_L is the swelling limit of OCR at infinitesimal swelling strain rate ($\dot{\varepsilon} = 0$ s^{-1}), like σ'_{pL} ; OCR_0 = OCR corresponding to $\dot{\varepsilon}_{vp}$ = -1.0 × 10^{-7} s^{-1}, $OCR_{Boundary}$ is the OCR value of the intersection of the limit compression line with the unloading curve, the boundary of visco-plastic stage and elastic stage during unloading behavior in this model (yield point along the unloading curve).

The following equations adopted the following definitions to simplify the new equation.

$$R = \frac{\log\left(\frac{OCR}{OCR_{Boundary}}\right)}{\log\left(\frac{OCR_0}{OCR_{Boundary}}\right)} \tag{6-5}$$

Here, $R_0 = 1$ at $\dot{\varepsilon}_{vp}$ = -1.0 × 10^{-7} s^{-1} and $R_L = \frac{\log\left(\frac{OCR_L}{OCR_{Boundary}}\right)}{\log\left(\frac{OCR_0}{OCR_{Boundary}}\right)}$ at $\dot{\varepsilon}_{vp}$ = 0 s^{-1}.

Subsequently, Eq. (6-4) can be reformulated as Eq. (6-6):

$$\ln\left(\frac{R}{R_L} - 1\right) = s_1 + s_2 \ln\dot{\varepsilon}_{vp} \tag{6-6}$$

In the new model for swelling, a new parameter R_L/R_0 instead of the parameter $\sigma'_{pL}/\sigma'_{p0}$. s_1 is equal to $\ln\left(\frac{R}{R_L} - 1\right)$ at $\dot{\varepsilon}_{vp} = 1$, i.e., it represents the relative position of the log R–log $\dot{\varepsilon}_{vp}$ curve, parameter s_2 represents the level of strain-rate dependency during swelling behavior. When $\dot{\varepsilon}_{vp}$ = -1.0 × 10^{-7} s^{-1}, Eq. (6-3) was turned to the following equations:

$$\ln\left(\frac{R_0}{R_L} - 1\right) = s_1 + s_2 \ln 10^{-7} \tag{6-7}$$

$$s_2 = \frac{\ln\left(\frac{R_0}{R_L} - 1\right) - s_1}{\ln 10^{-7}} \tag{6-8}$$

The s_2 value can be directly calculated by Eq. (6-8) while s_1 is constant in the same manner as the loading stage and adjusting R_L to fit the test result. Equation (6-7) also can turn to the power-law creep form:

$$\dot{\varepsilon}_{vp} = s_3 \left(\frac{R}{R_L} - 1\right)^{s_4} \tag{6-9}$$

where s_3 = exp (-s_1/ s_2) and s_4 = 1/ s_2.

Figure 6-9 illustrates the proposed visco-plastic model for swelling behavior in

unloading. The isotache lines for loading and the limit line for compression are derived from Equation (6-1). The "Unloading" path, shown in light blue, represents the stress-strain path of long-term unloading oedometer test, which is the main experimental test in this study. The symbol corresponding to the arrowed line denotes the distance between the stress state and the plastic rebound boundary, and it also represents the normalized ratio of the distance between the stress state corresponding to the reference strain rate of 1×10^{-7} s^{-1} and the plastic rebound boundary. In this model, the swelling lines associated with different strain rates form a radial pattern (but not necessary in straight lines), providing a more accurate representation of swelling behavior.

In this model, both the constant rate of strain (CRS) test results and the long-term unloading oedometer (creep) test results can be delineated. During the CRS consolidation tests, the response curve progressively shifts rightward as the strain rate decreases, approaching the limit swelling line where the swelling strain rate reaches zero. In the creep tests, the strain gradually increases over time while the strain rate progressively decreases, asymptotically approaching the limit swelling line.

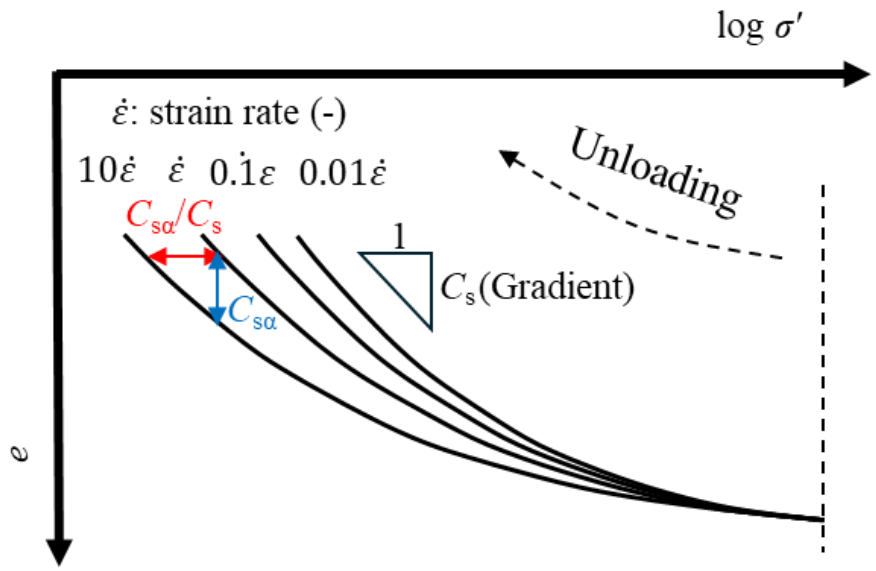

Figure 6-7 Illustration of geometrical relationship between the parameters

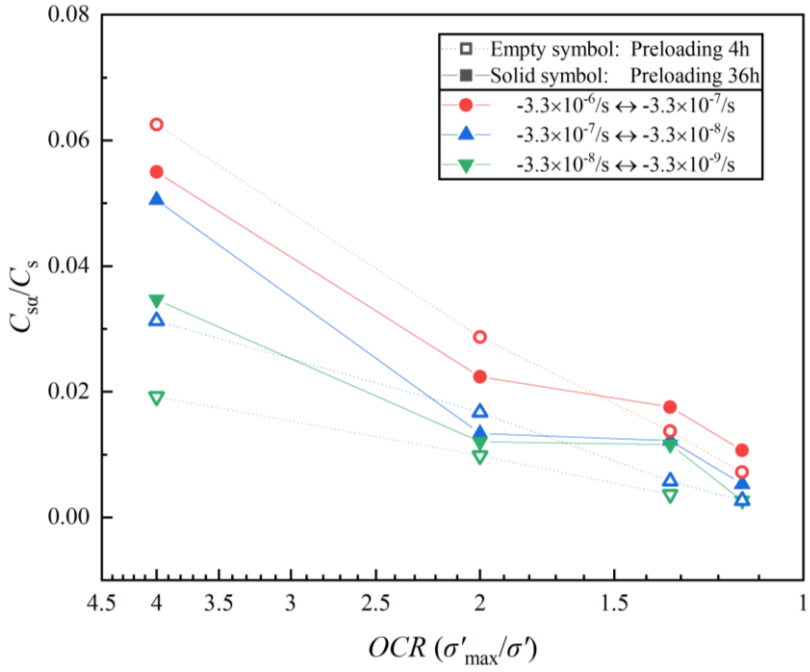

Figure 6-8 $C_{s\alpha}/C_s$ versus *OCR*, measured by long-term unloading oedometer test (Fan and Watabe 2024)

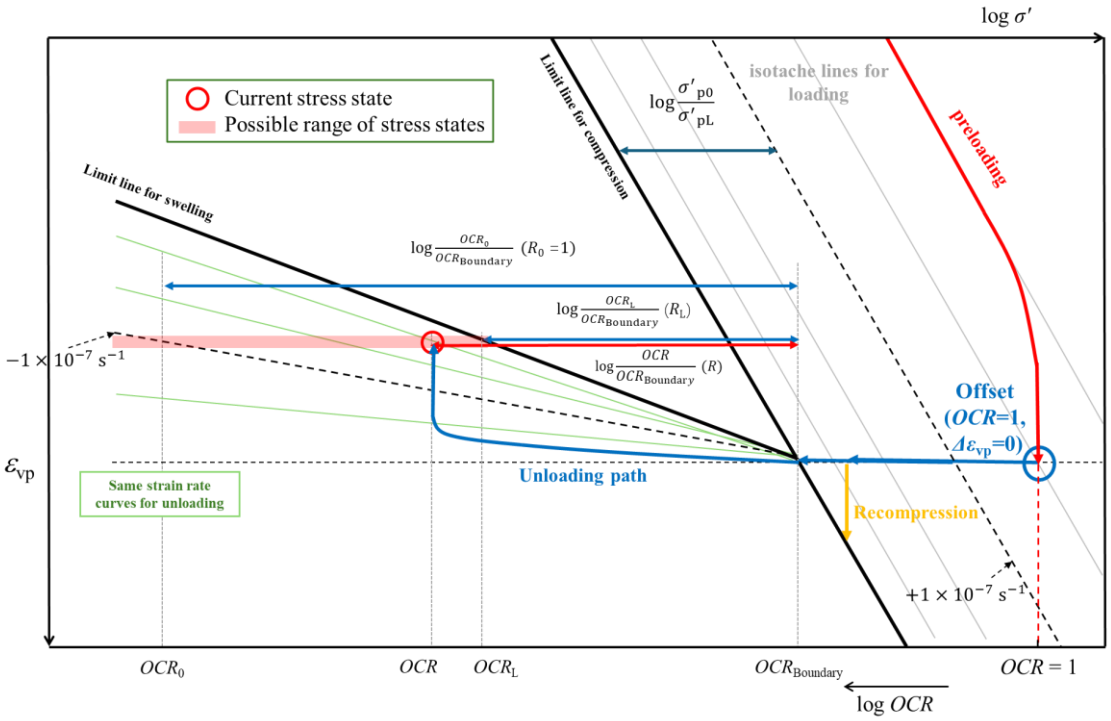

Figure 6-9 Illustration of the new visco-plastic model for swelling behavior in unloading

6.3 Simulation of the swelling behavior in unloading

Here is an example for the application of the new model to simulate the swelling behavior in unloading. The test results are measured for Ariake clay, preloading for 4 hours, already shown in Figure 5-23 and Figure 5-24.

The elastic strain during the unloading procedure is shown in Figure 6-10. Elastic modulus in this model is given by the slope of the beginning point of unloading and the intersection of the limit compression line with the unloading curve. The points corresponding to different swelling strain rates are also plotted in the figure as different colors, which were directly calculated from the oedometer test data. The -3.3×10^{-7} s^{-1} unloading curve from CRS consolidation test results is also plotted as the dark green curve, which is taken as the reference swelling curve. By deducting the elastic strain, the visco-plastic strain obtained is drawn in Figure 6-11.

The simulation results were calculated by Eq. (6-6) based on the reference swelling curve from CRS consolidation test and the relationship between incremental visco-plastics strain and *OCR* of experimental data is also plotted in Figure 6-11. By keeping s_1 constant in the same manner as c_1 in Eq. (6-1) and adjusting R_L/R_0 value to fit the experimental data utilizing the least square method, the s_2 parameter for swelling behavior is obtained. The R_L value of Ariake clay is determined to be 0.854. As shown in Figure 6-12, parameter c_1 is equal to $\ln\left(\frac{\sigma'_p}{\sigma'_{pL}}-1\right)$ at $\dot{\varepsilon}_{vp}=1$, i.e., it represents the relative position of the $\log \sigma'_p$–$\log \dot{\varepsilon}_{vp}$ curve. Parameter c_2 represents the level of strain-rate dependency. Similarly, parameter. s_1 is equal to $\ln\left(\frac{R}{R_L}-1\right)$ at $\dot{\varepsilon}_{vp}=1$, i.e., it represents the relative position of the $\log R$–$\log \dot{\varepsilon}_{vp}$ curve, parameter s_2 represents the level of strain-rate dependency during swelling behavior. Both $\left(\frac{\sigma'_p}{\sigma'_{pL}}-1\right)$ and $\left(\frac{R}{R_L}-1\right)$ are the bases in the overstress theory equation. According to the test result of Ariake clay, it is reasonable to conclude that the parameter values $c_1 = s_1 = 1.06$ are appropriate. What's more, maintaining consistent relative positions is intended to facilitate parameter determination.

A comparison between the model's calculation and experimental data reveals that the newly proposed simplified visco-plastic model shows an agreement with the experimental results for the same preloading duration. The fitting parameter values are

presented in Table 6-1.

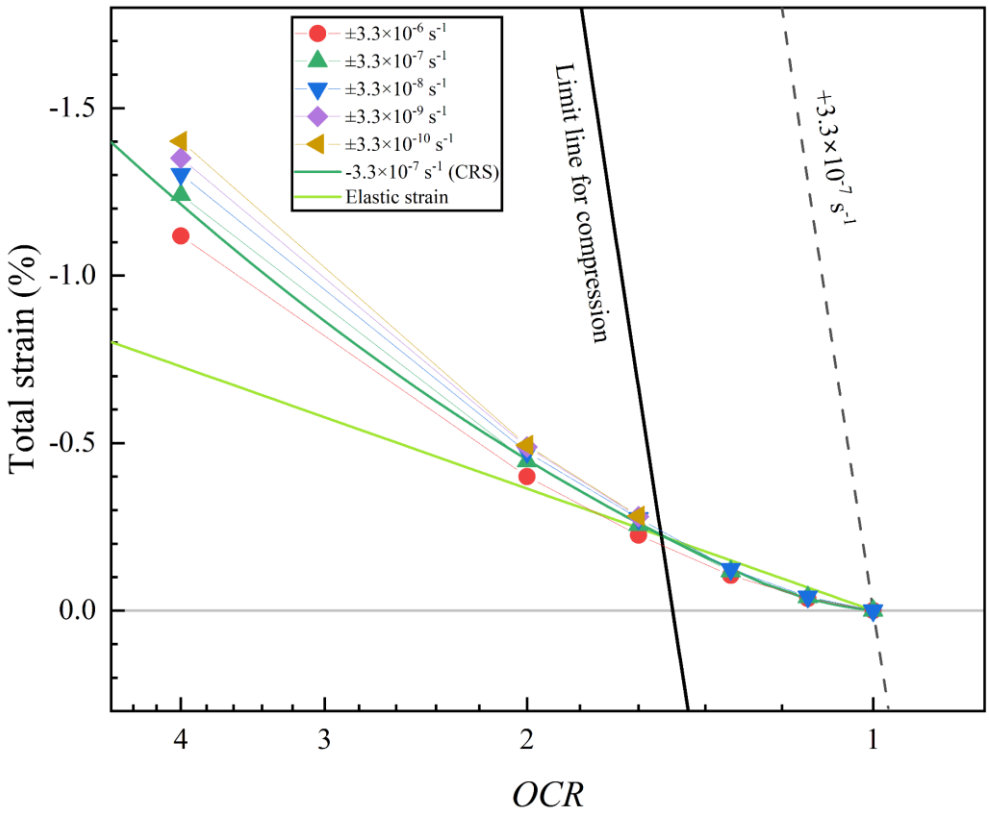

Figure 6-10 Elastic strain during the unloading procedure

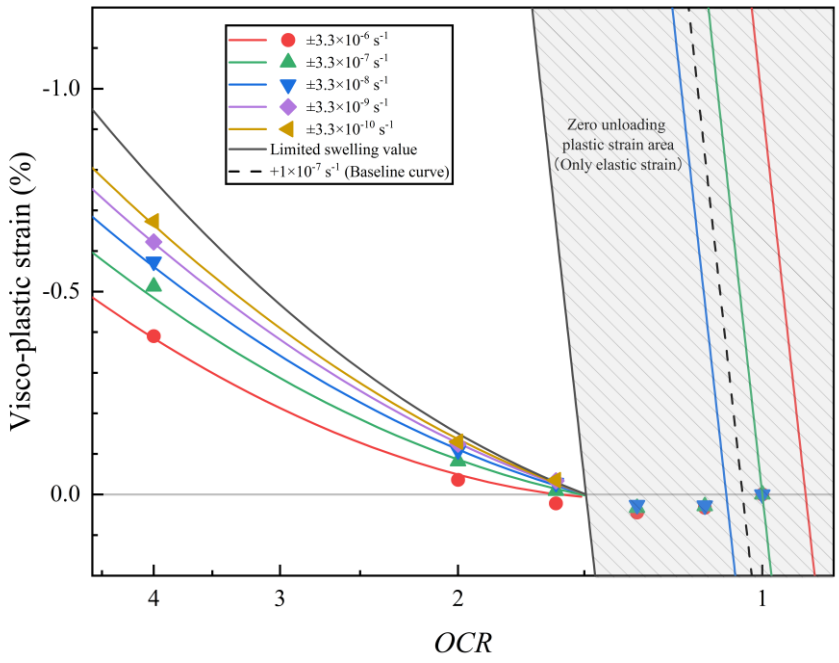

Figure 6-11 Comparison of calculation results with experimental data (Swelling stage)

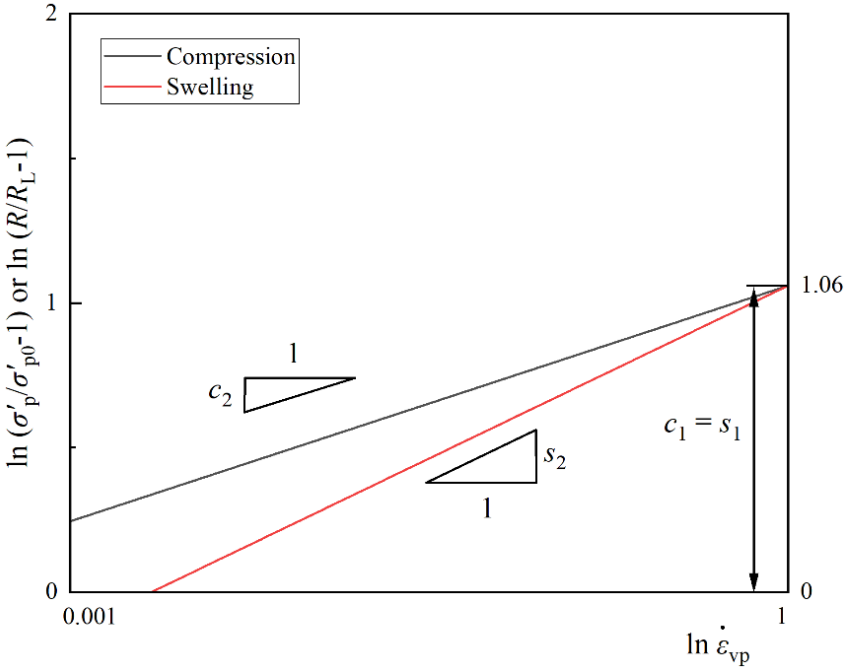

Figure 6-12 Ilustration of the meaning of parameters in the new model

Table 6-1 Fitted parameters for loading and unloading behavior

Parameters	Value	Procedure
c_1	1.06	Loading
c_2	0.118	Loading
$\sigma'_{pL}/\sigma'_{p0}$	0.7	Loading
s_1	1.06	Unloading
s_2	0.173	Unloading
R_L/R_0	0.854	Unloading

6.4 Normalization by OCR_{ref}

Overconsolidation ratio (OCR) represents the ratio of the historical maximum effective stress to the current effective stress. The traditional definition of the overconsolidation ratio does not consider the creep-induced increase in the preconsolidation pressure. Vergote et al. (2022) introduced a parameter named reference overconsolidation ratio (OCR_{ref}), given by Eq.(6-10), as shown in Figure 6-13.

$$OCR_{ref} = \frac{\sigma'_{p,ref}}{\sigma'} \tag{6-10}$$

where the subscript "ref" denotes the reference state, but does not give a clearly defined strain rate. It should also be noted that while the subscript "p" refers to the preconsolidation pressure in this study, its meaning in Vergote's model more closely approximates the maximum past effective stress.

In the current study, to consider the effect of the strain rate at the end of preloading stage (preloading time) in the new model, a similar parameter, OCR_{ref}, was applied. In engineering practice, the consolidation settlement is generally estimated based on the e-log σ' curve obtained from 24-hour incremental loading oedometer tests, corresponding to a strain rate of approximately $+1\times10^{-7}$ s^{-1} (Watabe et al. 2012). The strain rate curve of $+1\times10^{-7}$ s^{-1} is accepted as a reference isotache curve for the loading stage. Equation (6-

11) defines OCR_{ref} based on the strain rate curve of $+1\times10^{-7}$ s^{-1}, as shown in Figure 6-14. As a result, the OCR_{ref} value of the point that started to unload does not need to equal 1. The value of OCR_{ref} depends on the strain rate at the end of preloading stage, which can be calculated by Eq. (6-1) for the loading stage. According to this method, the application of OCR_{ref} can compare the data from different strain rates at the end of preloading stage corresponding to different preloading durations.

$$OCR_{\mathrm{ref}} = \frac{\sigma'_{\mathrm{ref}\,(\dot{\varepsilon} = +1\times10^{-7}\ \mathrm{s}^{-1})}}{\sigma'} \tag{6-11}$$

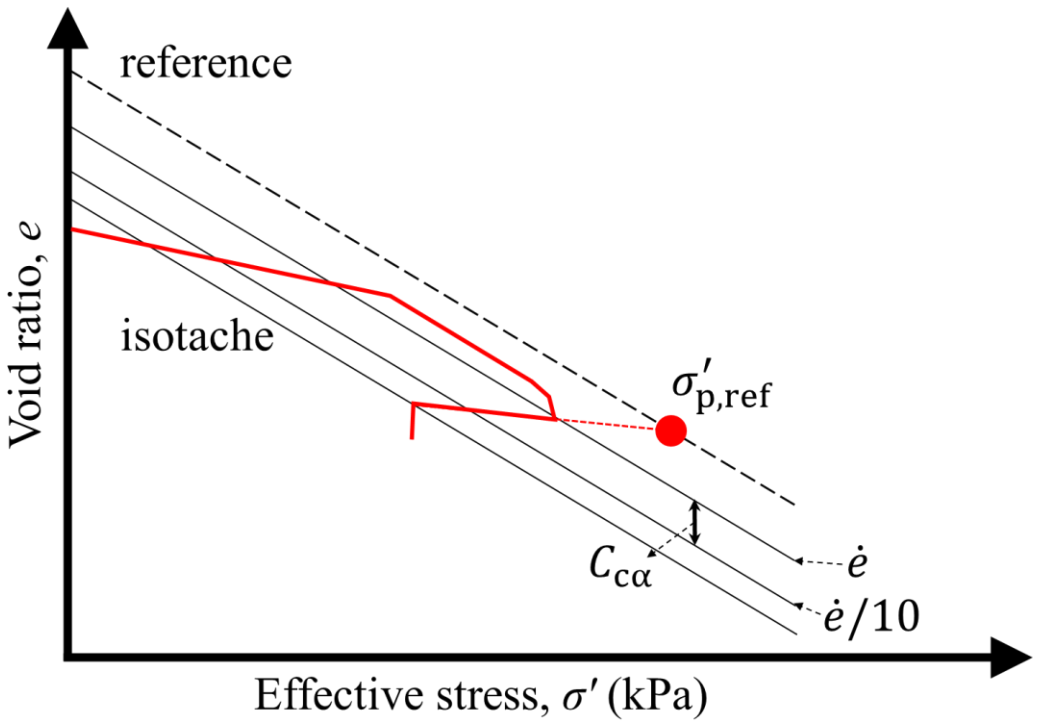

Figure 6-13 Isotache model with reference isotache curves and reference preconsolidation stress (Vergote et al. 2022)

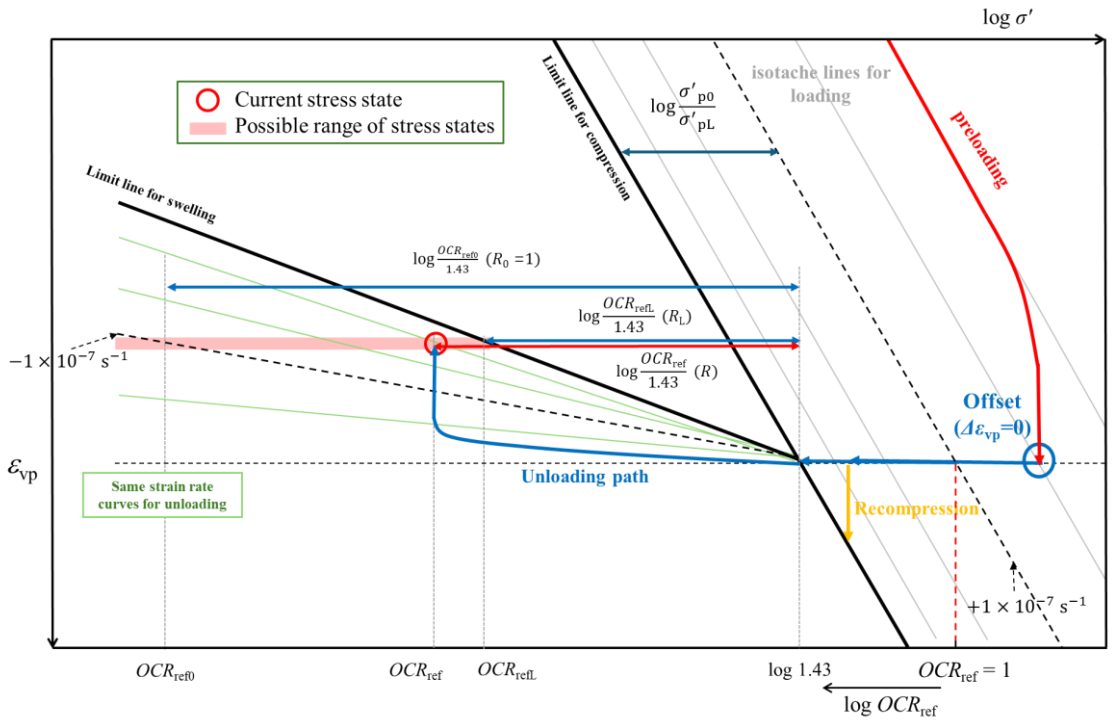

Figure 6-14 Illustration of the new visco-plastic model for unloading behavior after normalization by OCR_{ref}

After introducing the new concept of OCR_{ref}, Eq. (6-4) and Eq. (6-5) are turned into the following Eq. (6-12) and Eq. (6-13), respectively:

$$\ln\left(\frac{\log\left(\frac{OCR_{ref}}{1.43}\right)}{\log\left(\frac{OCR_{refL}}{1.43}\right)}-1\right)=s_1+s_2\ln\dot{\varepsilon}_{vp} \tag{6-12}$$

$$R=\frac{\log\left(\frac{OCR_{ref}}{OCR_{refL}}\right)}{\log\left(\frac{OCR_{ref0}}{1.43}\right)} \tag{6-13}$$

Here, $R_0=1$ at $\dot{\varepsilon}_{vp}$ = -1.0 × 10^{-7} s^{-1} and $R_L=\frac{\log\left(\frac{OCR_{refL}}{1.43}\right)}{\log\left(\frac{OCR_{ref0}}{1.43}\right)}$ at $\dot{\varepsilon}_{vp}=0\ s^{-1}$.

where OCR_{refL} is the high limit of OCR_{ref}, OCR_{ref0} equals to OCR_{ref}, corresponding to $\dot{\varepsilon}_{vp}$ = -1.0 × 10^{-7} s^{-1}.

Substituting (6-13) into (6-12), Eq. (6-6) and Eq. (6-8) are obtained even the calculation is based on OCR_{ref}. The value of $\sigma'_{pL}/\sigma'_{p0}$ equals 0.7 in the model for loading stage. Therefore, in the new form equations, the $OCR_{Boundary}=\frac{p'_L}{p'_0}$ = 1.43 is constant, s_1 remains the same with c_1 in loading stage and s_2 varies with R_L. After introducing the new

concept of OCR_{ref}, the new visco-plastic model can simulate the unloading behavior according to different strain rates at the end of preloading (i.e., preloading duration).

Figure 6-15 illustrates how the new visco-plastic model simulates the swelling behavior in long-term unloading oedometer test and unloading CRS consolidation test. In the CRS consolidation test, the value of OCR_{ref} increases as the unloading CRS consolidation test progresses, while the R value remains the same because $\log\frac{OCR_{ref0}}{1.43}$ increases proportionally with $\log\frac{OCR_{ref}}{1.43}$. Consequently, if a constant strain rate curve is obtained by CRS consolidation test, the swelling strain rate lines can be obtained according to the value of strain rate and Eq. (6-6). On the other hand, for the long-term unloading oedometer test, the value of OCR_{ref} remains the same during the swelling process, while the R value decreases as the corresponding strain rate decreases. This is because $\log\frac{OCR_{ref0}}{1.43}$ increases as the swelling strain becomes larger, while $\log\frac{OCR_{ref}}{1.43}$ remains the same. Finally, the R value approaches R_L and the swelling value of the clay reaches a swelling limit. As described in Eq. (6-9), in the power-law function, when the R value becomes R_L, the visco-plastic strain rate will be zero.

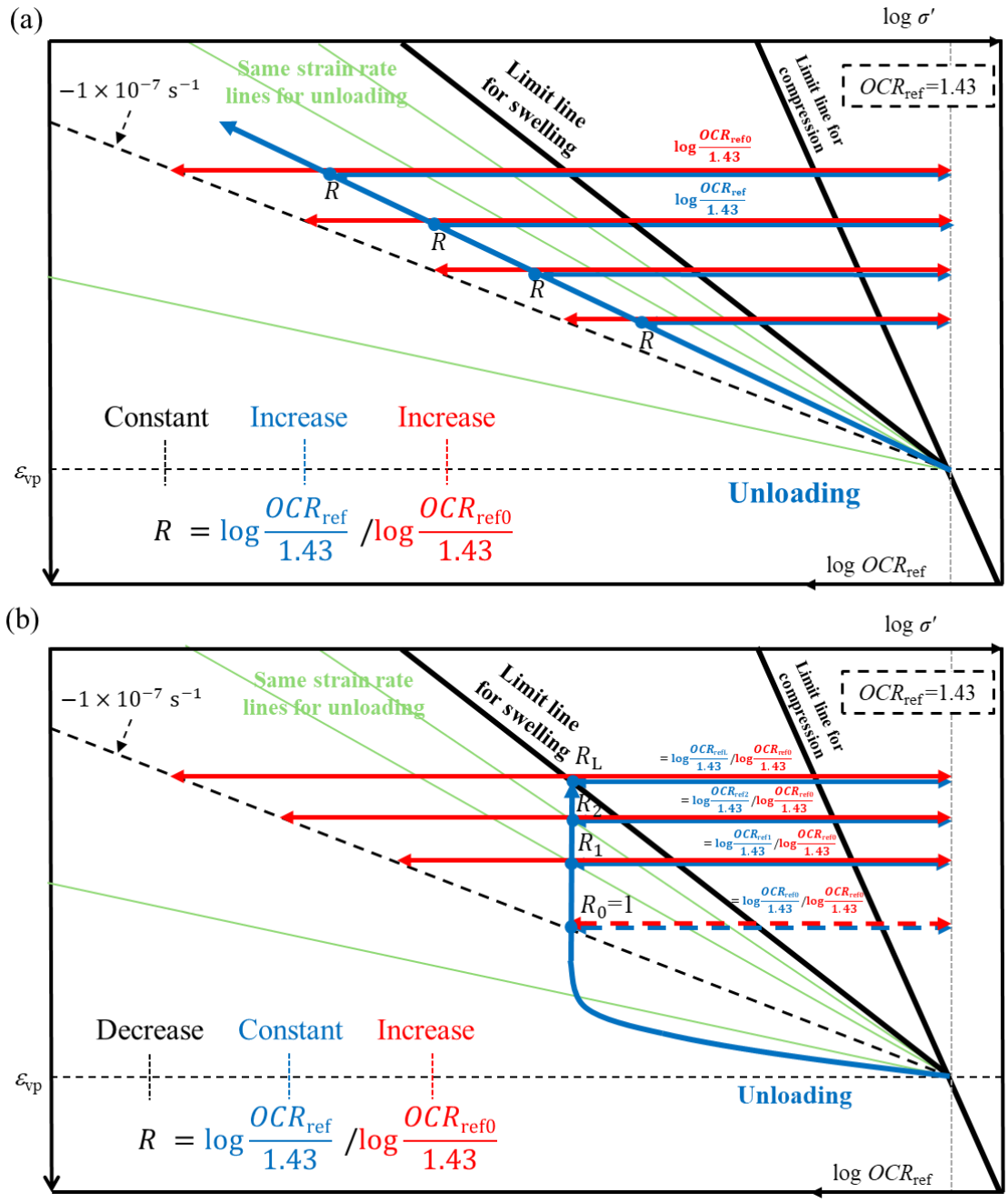

Figure 6-15 Schematic illustration of the new visco-plastic model: (a) Constant rate of strain (CRS) consolidation test; (b) Long-term unloading oedometer test

A comparison of calculation results with experimental data of Ariake clay is shown in Figure 6-16. The solid curves represent the same swelling strain-rate lines calculated from the new model, and the points are the experimental data. Different colors mean different strain rates. The hollow markers, cross markers and solid markers in the figure represent the data of unloading behavior after preloading for 0.5 h, 4 h and 36 h, corresponding to the strain rate at the end of preloading stage $+3.3\times10^{-6}$ s^{-1}, $+3.3\times10^{-7}$ s^{-1} and $+3.3\times10^{-8}$ s^{-1} respectively. The new model also performs well compared to the experimental data after different preloading time.

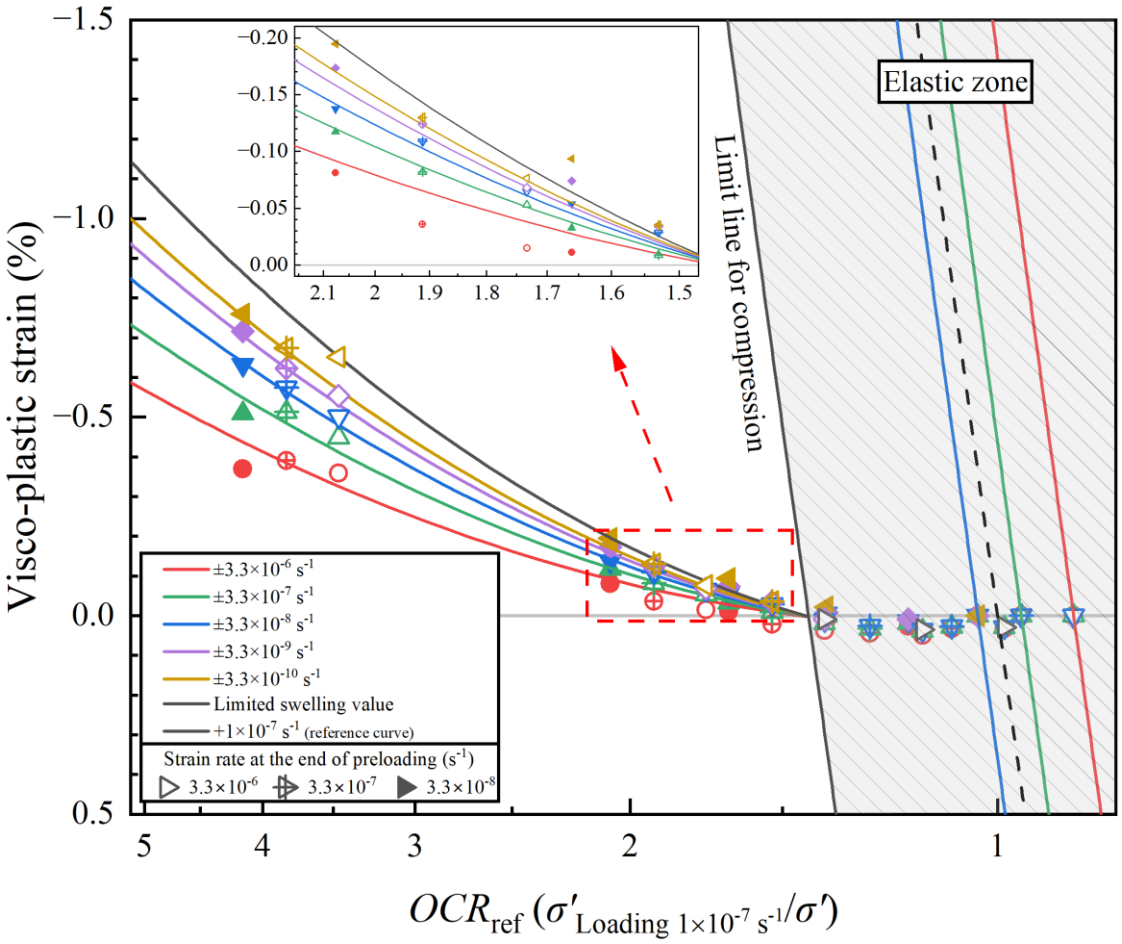

Figure 6-16 Comparison of calculated different unloading strain-rate curves with experimental data from three kinds of preloading time

6.5 Effects of parameters on unloading strain-rate curves

Figure 6-17 illustrates the effect of the model parameter R_L/R_0 on the unloading strain-rate behavior as predicted by the proposed model under a fixed model parameter s_1 = 1.06. Figure 6-17 (a) illustrates the relationship between R/R_0 and strain rate, demonstrating that higher values of R_L/R_0 indicating that the unloading behavior of clays exhibit stronger strain-rate dependency as R_L/R_0 increases. Figure 6-17 (b) and (c) present the model-predicted unloading strain-rate curves corresponding to $R_L/R_0 = 0.7$ and R_L/R_0 = 0.9, respectively. Obviously, the strain-rate dependency becomes increasingly significant as R_L/R_0 increases, as reflected by the larger spacing observed between the unloading strain-rate curves. This means, under constant stress following unloading, more swelling strain occurs with higher R_L/R_0 values. By the value of R_L/R_0, the proposed model is capable of effectively capturing the strain rate dependency of marine clays, suggesting its suitability for describing time-dependent deformation in such rate-sensitive geomaterials.

Figure 6-18 illustrates the effect of the model parameter s_1 on the unloading strain-rate behavior predicted by the proposed model under a fixed parameter $R_0/R_L = 0.7$. Figure 6-18 (a) shows how parameter s_1 influences the strain rate dependency in unloading behavior. The s_1 value's effect on the unloading behavior around the reference strain rate of 1×10^{-7} s^{-1} is minimal, but exhibits stronger influence at both very slow and very fast strain rates. Figure 6-18 (b), (c), and (d) present the model-predicted unloading strain-rate curves for s_1 = 0.6, s_1 = 1.06 and s_1 = 2.0, respectively.

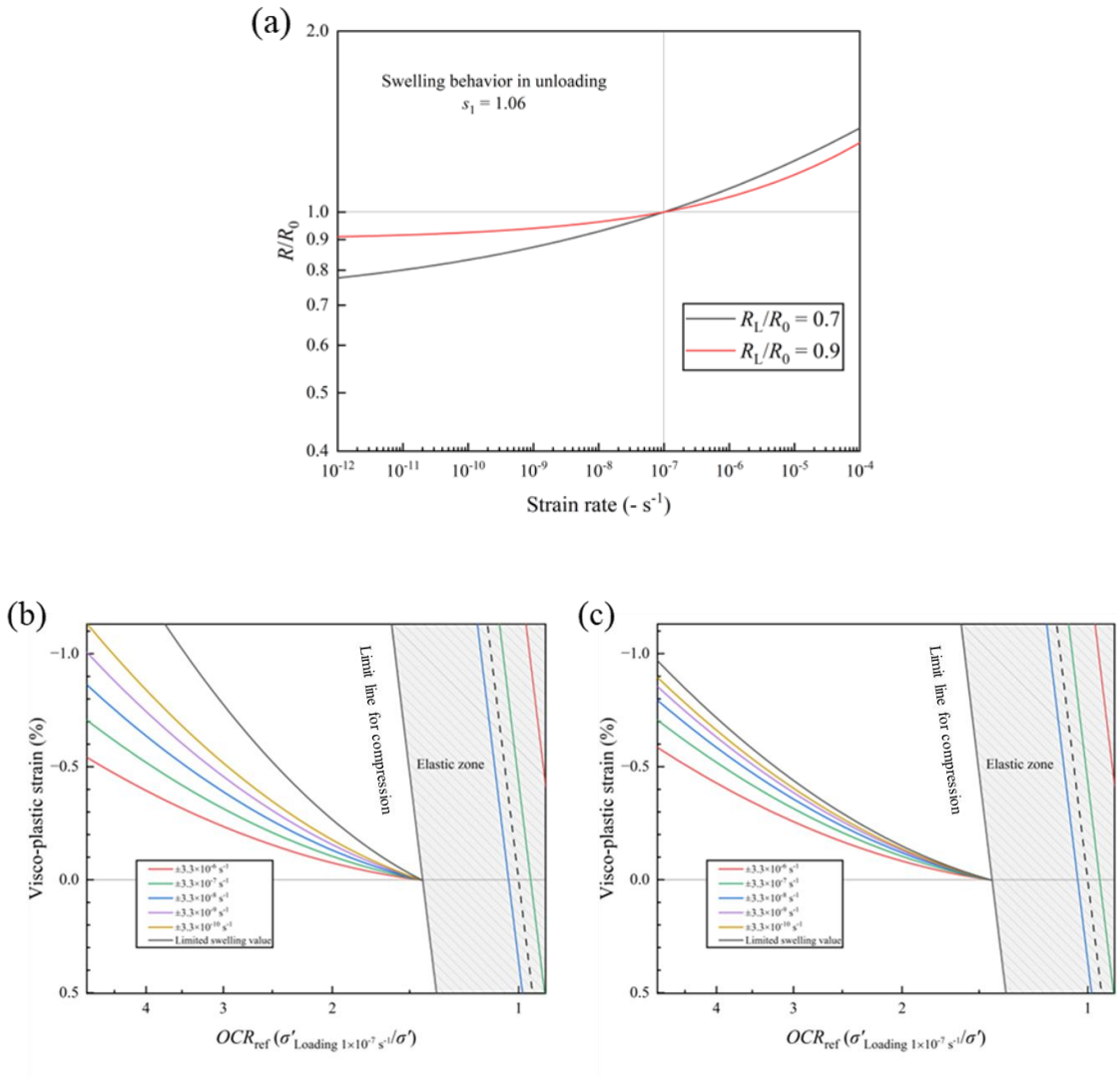

Figure 6-17 Effect of R_L/R_0 on unloading strain-rate curves with s_1 = 1.06: (a) Strain rate dependency of R/R_0 under constant s_1; (b) Unloading strain-rate curves at R_L/R_0 = 0.7; (c) Unloading strain-rate curves at R_L/R_0 = 0.9

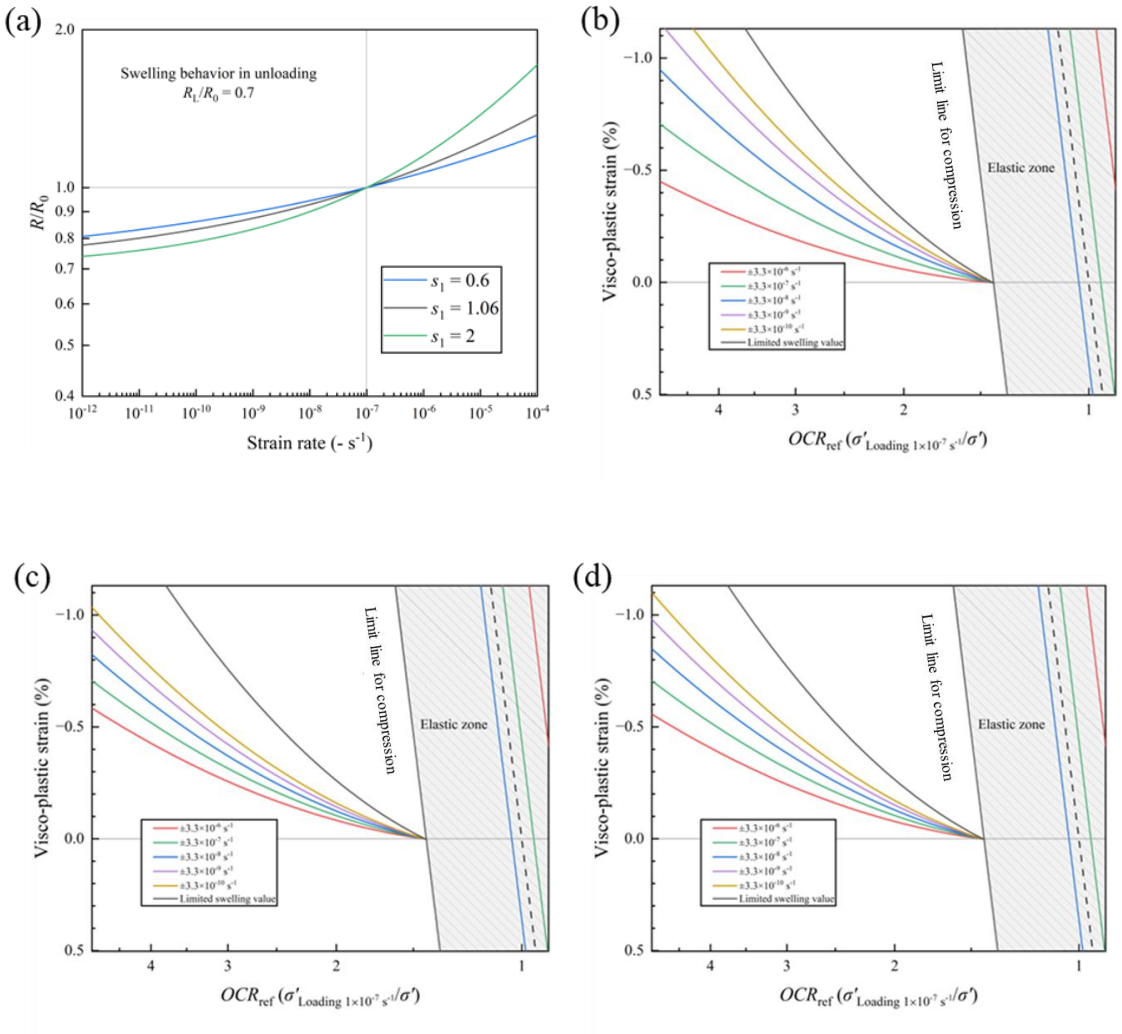

Figure 6-18 Effect of s_1 on unloading strain-rate curves with $R_0/R_L = 0.7$: (a) Strain rate dependency of s_1 under constant R_0/R_L; (b) Unloading strain-rate curves at $s_1 = 0.6$; (c) Unloading strain-rate curves at $s_1 = 1.06$; (d) Unloading strain-rate curves at $s_1 = 2.0$

Chapter 7 Discussion of swelling behavior and other models

7.1 Swelling behavior in unloading and comparison with loading part

Compared to the normal consolidation behavior of clays, there is a lack of experimental unloading tests of marine clays, in which viscosity plays an important role in long-term consolidation behavior. Few one-dimensional tests have been carried out by researchers to study the viscous behavior during the unloading stage (Mesri et al. 1978; Yin and Tong 2011; Feng et al. 2017). In response to this research gap and the scarcity of experimental data on marine clay's swelling behavior after preloading in unloading, this paper systematically conducted a series of experiments, considering the effects of the strain rate at the end of preloading and the *OCR* (overconsolidation ratio) on the unloading behavior of marine clay. The results indicate that two factors significantly influence the unloading behavior of clay.

As illustrated in Figure 5-24 and Figure 6-8, a larger *OCR* leads to a greater swelling strain and viscosity plays a more prominent role. Even with the same *OCR*, different strain rates at the end of preloading induced the unloading behavior of marine clays differently as described in Figure 5-18. According to Eq. (6-1) at the loading stage, different strain rates at the end of preloading of clay result in varying distances between the limit line for compression and the unloading points, as shown in Figure 7-1. For example, when the strain rate at the end of preloading is 3.3×10^{-7} (preloading time = 4 hours), OCR_{Boundary} equals the distance to limit line for compression ($\Delta\log \sigma' = 1.49$). In other words, according to the new model, $OCR > 1.49$: elastic unloading strain and visco-plastic unloading (swelling) strain generated; $OCR = 1.49$: there is only elastic unloading strain; $OCR < 1.49$: elastic unloading strain and visco-plastic recompression (re-creep) strain generated. The closer to the limit line for compression, the smaller the residual settlement value, which explains why recompression develops more slowly. Based on experimental results, we would like to note that a small amount of visco-plastic deformation still occurs

under lower *OCR* conditions. To simplify the model for practical applications, this aspect has not been explicitly included and is instead treated as part of elastic unloading deformation.

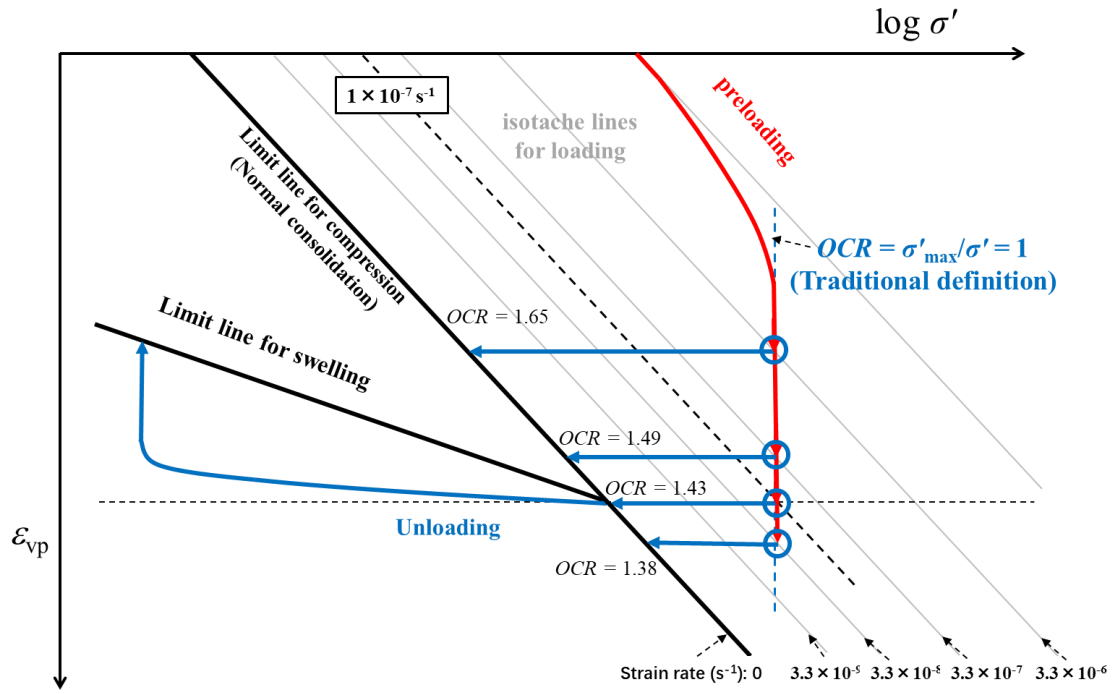

Figure 7-1 Illustration of the weakness of traditional *OCR* in describing the unloading behavior

If the traditional definition of *OCR* is used, the $OCR_{Boundary}$ values corresponding to different loading duration (i.e., different loading strain rate) are different and it also is not able to illustrate the effect of strain rate at the end of preloading, which limits the description of unloading behavior and highlights the limitations of the traditional *OCR* definition. Therefore, to address this limitation, the authors introduced the concept of reference overconsolidation ratio (OCR_{ref}). The definition of OCR_{ref} is corresponding to the loading strain rate (1×10^{-7} s^{-1}) at 24 hours in the incremental loading oedometer test (Watabe et al. 2008) as shown in Eq. (6-10). Compared to the traditional parameter *OCR* corresponding to the maximum effective stress without considering the loading strain rate,

the new OCR_{ref} can describe the clay's stress history reasonably. The new model with OCR_{ref} is enabled to compare the long-term unloading oedometer test data from different preloading times or strain rates in the preloading stage and simulate test data.

Normal consolidation behavior and unloading behavior are significantly different. During normal consolidation behavior, different strain rate lines (isotaches) are parallel. In the other way, during swelling behavior in unloading, the distance among different strain rate lines tends to increase as *OCR* becomes larger. The long-term unloading oedometer test results indicate that the swelling behavior caused by clay's viscosity is nonlinear, which is similar to the normal consolidation behavior of marine clays. The relationship between the compression strain and log t is not a straight line (Berre and Iversen 1972; Leroueil et al. 1985; Watabe et al. 2008).

In the normal consolidation region of marine clay, there is a unique series of strain rate lines (i.e. isotaches). Similarly, to establish a unique relationship among OCR_{ref}, strain, and strain rate during the swelling behavior of marine clay, it is necessary to reset the intersection point of the unloading curve and the elastic rebound boundary. This point should be set to OCR_{ref}=1.43, $\Delta\varepsilon$=0, as depicted in Figure 7-2. By resetting this intersection point, the swelling behavior of marine clay in the left region of the plastic boundary (limit line for compression in normal consolidation domain) in the model can be accurately described using a unique set of OCR_{ref}, strain, and strain rate. This model provides a comprehensive interpretation of the influence of strain rate at the end of preloading.

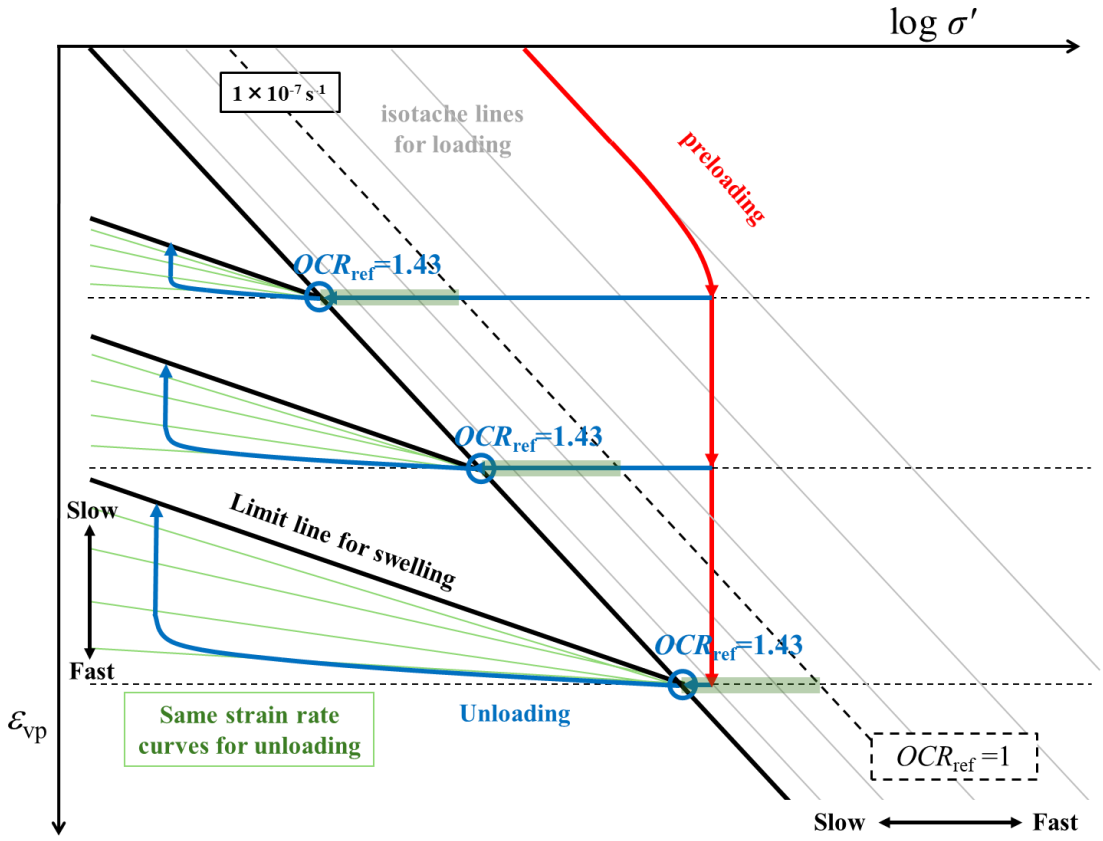

Figure 7-2 Interpretation of the effect of strain rate at the end of preloading in the new model

7.2 Comparison with other models

Many researchers have modeled the unloading (stress-strain) behavior of clays. Tachibana et al. (2020) proposed a constitutive model incorporating a concept of plastic rebound for saturated expansive soils, and Ito et al. (2022) further developed this model to simulate the swelling properties of unsaturated expansive soils during saturation. Their model can simulate the final volume changes and the effective stress paths for both consolidation and swelling in axial and radial problems. However, the model cannot consider the strain rate-time effect. Moreover, the slope of plastic rebound line is identical

to the normal consolidation line ($\lambda = 0.434C_c$) which overestimates the swelling value, as evidenced by the experimental results of saturated clays in this study. While Tachibana et al. (2020)'s model can simulate a wide range of stress states, the proposed model in this study focuses specifically on the relationship between vertical stress and void ratio or vertical strain, mainly applicable in one-dimensional consolidation or unloading. The new model proposed in this study solves this problem by introducing a limit swelling line with a slope smaller than the normal consolidation lines, thus better simulating the swelling behavior observed in the test results.

The MIT-SR model proposed by Yuan (2016) with consideration of strain rate can accurately predict the unloading behavior after surcharge (preloading) in the condition that a small weight surcharge is removed ($OCR < 1.5$), while at higher *OCR* the viscous swelling is not modeled. The EVPS model (Feng et al. 2017) effectively captures non-linear creep and swelling behavior, especially large viscous swelling under the large *OCR* conditions. However, the model assumes that recompression and swelling in unloading are mutually exclusive processes. Additionally, in their experimental methodology, the applied stress was reduced by half per time during the unloading process, which resulted in a minimum *OCR* of 2. As a result, both their experimental tests and model did not consider the recompression phenomenon (as shown in Figure 6-3 (b)). In contrast, this study conducted unloading oedometer tests according to different *OCR*s, and the proposed model effectively simulates and explains the long-term unloading behavior under a wider *OCR* range.

Vergote et al. (2022) developed the C+S model, which accurately simulates both constant stress loading and unloading behavior well, similar to the author's model. However, one limitation of the C+S model is that it requires a large set of experimental data to calibrate its parameters (m_1, b_1, m_2, and b_2), which makes it less practical for applications with limited experimental resources. In contrast, the proposed model requires fewer soil-specific parameters and does not rely on extensive calibration data, making it more convenient for practical engineering applications. Furthermore, the integrated and fully coupled model by Vergote et al. (2021) introduced an novel method by using a distorted isotache concept to explain and predict the visco-plastic recompression (referred to "recreep" in their work) behavior, and considering viscous swelling behavior as a

transient phenomenon. This enables the model to simulate complex stress paths, including relaxation tests and reloading. Vergote et al. (2021) suggest that a rate-based reinterpretation of experimental data shows that swelling and creep often occur sequentially, which requires that at least one of these processes must exhibit non-isotache behavior. The proposed model follows this principle as well but utilizes a plastic rebound boundary (the limit line for compression in the loading stage) to separate the compression isotache and swelling isotache. This allows the proposed model to perform better under high *OCR* conditions.

The newly proposed model in this study requires the determination of only two parameter values for the normal consolidation stage: c_1 and $\sigma'_{pL}/\ \sigma'_{p0}$, as well as one additional parameter, R_L/R_0, for the swelling stage in unloading. These parameters can be determined by fitting the experimental results to the new model. Furthermore, this study novelly modeled the swelling behavior from the perspective of constant unloading strain rate test results, reflecting the impact of clay viscosity and improving the prediction accuracy of swelling behavior during unloading.

Chapter 8 Conclusions and recommendations

8.1 Conclusions of this study

In Chapter 4 and Chapter 5 of the present study, to clarify the effect of the strain rate of clay during the unloading process, Ariake clay, Louiseville clay and Onsøy clay were subjected to unloading by means of the CRS consolidation test, and incremental loading oedometer test was also applied to these three kinds of clays. Long-term unloading oedometer tests were conducted to observe the unloading behavior with several *OCR* values and preloading times (determined by different strain rates at the end of preloading stage). Moreover, the ratios of $C_{c\alpha}/C_c$ and $C_{s\alpha}/C_s$ were calculated to quantitatively compare the strain rate dependency of these kinds of clays during loading and unloading. It appears that basic phenomena remain the same for the different kinds of marine clays and can be modeled based on strain rate. The loading behavior's formulation proposed by Watabe et al. (2008; 2012) was developed into swelling in unloading. The simulated results by the new model show good agreement with the observed unloading behavior of marine clays. The main findings from experimental tests are written hereunder:

(1) The increase in void ratio depends on the strain rate: the lower strain rate leads to the more swelling strain during the unloading CRS consolidation tests.

(2) The ratios of $C_{s\alpha}/C_s$ to $C_{c\alpha}/C_c$ are from 0.25 to approximately 1.00. However, it seems that the ratio between 3.3×10^{-6} s^{-1} and 3.3×10^{-7} s^{-1} is significantly larger. The results from these three kinds of marine clays appear to be within the same range. It means that in some marine clays, the strain rate dependency of compression and swelling has a similar relationship.

(3) After the end of the elastic part of expansion, the logarithmic unloading strain rate induced by secondary swelling varies linearly against the logarithmic elapsed time (log t). This result supports the establishment of a visco-plastic model based on the isotache concept.

(4) The unloading curve from CRS consolidation test has a reasonable agreement with the strain rate point from long-term unloading oedometer due to the same strain rate at the end of preloading stage condition ($\dot{\varepsilon} = +3.3\times10^{-7}$ s^{-1}).

(5) From the incremental loading oedometer test results, $C_{s\alpha}/C_s$ tends to increase as the *OCR* increases, which means the strain rate dependency becomes larger when *OCR* is higher. This also means that the distance between different unloading strain rate curves grows with *OCR* increase; unlike the normal consolidation domain, the different loading strain rate curves are parallel.

(6) A new simplified visco-plastic model was developed to improve the accuracy of marine clay's swelling behavior in unloading and prediction for the maximum swelling value. This study introduced a plastic unloading boundary (Amerasinghe and Kraft 1983; Tachibana et al. 2020) and extended the visco-plastic model proposed by Watabe et al. (2008; 2012) into the swelling stage in unloading to better characterize the swelling behavior in unloading by modifying a new constant parameter R_L/R_0 instead of a constant parameter $\sigma'_{pL}/\sigma'_{p0}$. This new model also adopts a strain rate curve of -3.3×10^{-7} s^{-1} as the reference swelling curve to derive additional swelling strain rate curves. The model demonstrates excellent concordance compared to experimental test results.

(7) The concept of OCR_{ref}, which corresponds to the loading strain rate (1×10^{-7} s^{-1}) at 24 hours in incremental loading oedometer test (Watabe et al. 2008), was introduced in this paper. Instead of the traditional parameter *OCR* which is defined by maximum effective stress without considering the loading strain rate, the new OCR_{ref} can describe the clay's stress history reasonably. The new model with OCR_{ref} is enabled to compare the long-term unloading oedometer test data from different preloading times (or strain rate in preloading stage) and simulate test data. By defining this parameter, it became possible to construct a model that successfully explains the swelling behavior in unloading.

8.2 Recommendations for further research

Following ground improvement methods such as the surcharge method, construction is typically carried out on the treated foundation. Therefore, the reloading behavior of clays plays an important role in understanding their deformation characteristics. The compressive response of clays after different unloading paths requires further model development and targeted experimental investigation to capture the relevant mechanical behavior.

This study includes a substantial amount of experimental data and the proposed model can effectively simulate the swelling behavior of marine clays during unloading. However, it should be noted that the scale of materials used in laboratory tests differs significantly from that in the field. The field scale is significantly larger than the 20 mm-height and 6 mm-diameter samples in the laboratory test. As a result, the effect of layer thickness becomes important. Moreover, the strain rates in actual engineering applications are generally lower than those applied in laboratory conditions. It is recommended to conduct experiments using a large test set-up or other devices that are capable of studying the effect of layer thickness, such as the inter-connected consolidation test. Furthermore, it is better to explore the application of these findings in some case studies.

The constitutive models developed in this study are formulated based on one-dimensional, single-layer soil conditions, as commonly adopted in laboratory settings, with either one-way or two-way drainage. To enhance the applicability of the model, several numerical developments are suggested. For large-scale soil improvement applications, the new model could be integrated into an axisymmetric model that considers prefabricated vertical drains and multiple soil layers. In more complex geotechnical applications such as large-scale excavations, a three-dimensional framework may be required to capture the unloading behavior. In such cases, the model could be embedded within a three-dimensional elasto-viscoplastic formulation, incorporating a swelling rule and refined treatment of the compressive viscous response to better simulate unloading effects. To generalize the one-dimensional model into the three-dimensional form, further experimental studies are also recommended to clarify the long-term unloading behavior of soils under triaxial stress conditions.

From the perspective of experimental fundamental research, it is recommended to begin with remolded clays. In this study, all three types of clay used were undisturbed samples. While undisturbed clays better reflect conditions encountered in practical engineering applications, their behavior tends to be more complex. Therefore, initiating the research with remolded clays, which exhibit more uniform and simplified properties, would be a more reasonable approach in the early stages of experimental investigation.

References

[1] Alonso, E.E., Navarro, V., 2005. Microstructural model for delayed deformation of clay: loading history effects. Can. Geotech. J. 42, 381–392. https://doi.org/10.1139/t04-097

[2] Amerasinghe, S.F., Kraft, L.M., 1983. Application of a Cam–Clay model to overconsolidated clay. Num Anal Meth Geomechanics 7, 173–186. https://doi.org/10.1002/nag.1610070204

[3] Berre, T., Iversen, K., 1972. Oedometer test with different specimen heights on a clay exhibiting large secondary compression. Géotechnique 22, 53–70. https://doi.org/10.1680/geot.1972.22.1.53

[4] Bjerrum, L., 1967. Engineering Geology of Norwegian Normally-Consolidated Marine Clays as Related to Settlements of Buildings. Géotechnique 17, 83–118. https://doi.org/10.1680/geot.1967.17.2.83

[5] Cascone, E., Biondi, G., 2013. A case study on soil settlements induced by preloading and vertical drains. Geotextiles and Geomembranes 38, 51–67. https://doi.org/10.1016/j.geotexmem.2013.05.002

[6] Chu, J., Bo, M., Choa, V., 2006. Improvement of ultra-soft soil using prefabricated vertical drains. Geotextiles and Geomembranes 24, 339–348. https://doi.org/10.1016/j.geotexmem.2006.04.004

[7] Chu, J., Yan, S.W., Yang, H., 2000. Soil improvement by the vacuum preloading method for an oil storage station. Géotechnique 50, 625–632. https://doi.org/10.1680/geot.2000.50.6.625

[8] Degago, S.A., Grimstad, G., Jostad, H.P., Nordal, S., Olsson, M., 2011. Use and misuse of the isotache concept with respect to creep hypotheses A and B. Géotechnique 61, 897–908. https://doi.org/10.1680/geot.9.P.112

[9] Degago, S. A., Jostad, H. P., Olsson, M., Grimstad, G., Nordal, S., 2010. Time-and stress-compressibility of clays during primary consolidation. Proceedings of the 7th European Conference Numerical Methods in Geotechnical Engineering, Trondheim, 125-130.

[10] Den Haan, E.J., Kamao, S., 2003. Obtaining Isotache Parameters from a C.R.S. K_0-

Oedometer. Soils and Foundations 43, 203–214. https://doi.org/10.3208/sandf.43.4_203

[11] Fan, Z., Watabe, Y., 2024. Evaluation of Marine Clays' Strain Rate Dependency During the Unloading Process, in: Duc Long, P., Dung, N.T. (Eds.), Proceedings of the 5th International Conference on Geotechnics for Sustainable Infrastructure Development, Lecture Notes in Civil Engineering. Springer Nature Singapore, Singapore, pp. 2401–2412. https://doi.org/10.1007/978-981-99-9722-0_165

[12] Feng, T. W., 1991. Compressibility and permeability of natural soft clays and surcharging to reduce settlements. PhD thesis, University of Illinois at Urbana-Champaign.

[13] Feng, W.-Q., Lalit, B., Yin, Z.-Y., Yin, J.-H., 2017. Long-term Non-linear creep and swelling behavior of Hong Kong marine deposits in oedometer condition. Computers and Geotechnics 84, 1–15. https://doi.org/10.1016/j.compgeo.2016.11.009

[14] Hanzawa, H., Fukaya, T., Suzuki, K., 1990. Evaluation of Engineering Properties for an Ariake Clay. Soils and Foundations 30, 11–24. https://doi.org/10.3208/sandf1972.30.4_11

[15] Hinchberger, S.D., Rowe, R.K., 1998. Modelling the rate-sensitive characteristics of the Gloucester foundation soil. Can. Geotech. J. 35, 769–789. https://doi.org/10.1139/t98-037

[16] Hong, Z., Liu, S., Shen, S., Negami, T., 2006. Comparison in Undrained Shear Strength between Undisturbed and Remolded Ariake Clays. J. Geotech. Geoenviron. Eng. 132, 272–275. https://doi.org/10.1061/(ASCE)1090-0241(2006)132:2(272)

[17] Indraratna, B., Rujikiatkamjorn, C., Sathananthan, I., 2005. Radial consolidation of clay using compressibility indices and varying horizontal permeability. Can. Geotech. J. 42, 1330–1341. https://doi.org/10.1139/t05-052

[18] Ito, S., Tachibana, S., Takeyama, T., Iizuka, A., 2022. Constitutive model for swelling properties of unsaturated bentonite buffer materials during saturation. Soils and Foundations 62, 101161. https://doi.org/10.1016/j.sandf.2022.101161

[19] JSA (Japanese Standards Association). 2000a. JIS A 1227: Test method for one-dimensional consolidation properties of soils using constant rate of strain loading. JSA, Tokyo. (in Japanese)

[20] JSA (Japanese Standards Association). 2000b. JIS A 1217: Test method for one-

dimensional consolidation properties of soils using incremental loading. JSA, Tokyo. (in Japanese)

[21] Kabbaj, M., Tavenas, F., Leroueil, S., 1988. In situ and laboratory stress–strain relationships. Géotechnique 38, 83–100. https://doi.org/10.1680/geot.1988.38.1.83

[22] Kang, M., Tsuchida, T., Watabe, Y., Tanaka, H., Miyazima, S., 2001. Consolidation behavior of Osaka Pleistocene clay with well-developed structure by separated-type consolidometer of high capacity. Report of the Port and Harbour Research Institute, Vol. 40, No. 2, pp. 23–44. (in Japanese)

[23] Kim, Y.T., Leroueil, S., 2001. Modeling the viscoplastic behaviour of clays during consolidation: application to Berthierville clay in both laboratory and field conditions. Can. Geotech. J. 38, 484–497. https://doi.org/10.1139/t00-108

[24] Ladd, C.C., Foott, R., Ishihara, K., Schlosser, F, Poulos, H.G., 1977. Stress-deformation and strength characteristics. State-of-the-Art Report, Proceedings of the 9th International Conference on Soil Mechanics and Foundation Engineering, Tokyo, 2, 421-494.

[25] Laskar, A., Pal, S.K., 2016. Effect of Anisotropic Flow of Water on Consolidation Behaviour of Silty-Clay Soil. IJET 8, 2895–2901. https://doi.org/10.21817/ijet/2016/v8i6/160806251

[26] Leroueil, S., 2006. The isotache approach. Where are we 50 years after its development by Professor Šuklje? (2006 Prof. Šuklje's Memorial Lecture).

[27] Leroueil, S., Hamouche, K., Tavenas, F., Boudali, M., Locat, J., Virely, D., Roy, M., La Rochelle, P., Leblond, P., 2003. Geotechnical characterization and properties of a sensitive clay from Qu ́ebec. In: Tan (Ed.), Characterisation and Engineering Properties of Natural Soils. Swets & Zeitlinger, Lisse, pp. 363–394.

[28] Leroueil, S., Kabbaj, M., Tavenas, F., Bouchard, R., 1985. Stress–strain–strain rate relation for the compressibility of sensitive natural clays. Géotechnique 35, 159–180. https://doi.org/10.1680/geot.1985.35.2.159

[29] Lunne, T., Long, M., Forsberg, C.F., 2003. Characterisation and engineering properties of Onsøy. In: Tan (Ed.), Characterisation and Engineering Properties of Natural Soils. Swets & Zeitlinger, Lisse, pp. 395–427.

[30] Madaschi, A., Gajo, A., 2017. A one-dimensional viscoelastic and viscoplastic constitutive approach to modeling the delayed behavior of clay and organic soils.

Acta Geotech. 12, 827–847. https://doi.org/10.1007/s11440-016-0518-9

[31] Madaschi, A., Gajo, A., 2015. One-dimensional response of peaty soils subjected to a wide range of oedometric conditions. Géotechnique 65, 274–286. https://doi.org/10.1680/geot.14.p.144

[32] Mesri, G., Ajlouni, M.A., Feng, T.W., Lo, D.O.K., 2017. Surcharging of Soft Ground to Reduce Secondary Settlement, in: Lee, C.F., Lau, C.K., Ng, C.W.W., Kwong, A.K., Pang, P.L.R., Yin, J.-H., Yue, Z.Q. (Eds.), Soft Soil Engineering. Routledge, pp. 55–65. https://doi.org/10.1201/9780203739501-5

[33] Mesri, G., Castro, A., 1987. C_α/C_c Concept and K_0 During Secondary Compression. J. Geotech. Engrg. 113, 230–247. https://doi.org/10.1061/(ASCE)0733-9410(1987)113:3(230)

[34] Mesri, G., Choi, Y.K., 1985. Settlement Analysis of Embankments on Soft Clays. J. Geotech. Engrg. 111, 441–464. https://doi.org/10.1061/(ASCE)0733-9410(1985)111:4(441)

[35] Mesri, G., Ullrich, C.R., Choi, Y.K., 1978. The rate of swelling of overconsolidated clays subjected to unloading. Géotechnique 28, 281–307. https://doi.org/10.1680/geot.1978.28.3.281

[36] Ohtsubo, M., Takayama, M., Egashira, K., 1982. Marine Quick Clays from Ariake Bay Area, Japan. Soils and Foundations 22, 71–80. https://doi.org/10.3208/sandf1972.22.4_71

[37] Onoue, A., 1988. Consolidation of Multilayered Anisotropic Soils by Vertical Drains with Well Resistance. Soils and Foundations 28, 75–90. https://doi.org/10.3208/sandf1972.28.3_75

[38] Perzyna, P., 1963. The constitutive equations for rate sensitive plastic materials. Quart. Appl. Math. 20, 321–332. https://doi.org/10.1090/qam/144536

[39] Qu, G., Hinchberger, S.D., Lo, K.Y., 2010. Evaluation of the viscous behaviour of clay using generalised overstress viscoplastic theory. Géotechnique 60, 777–789. https://doi.org/10.1680/geot.8.P.031

[40] Rowe, R.K., Hinchberger, S.D., 1998. The significance of rate effects in modelling the Sackville test embankment. Can. Geotech. J. 35, 500–516. https://doi.org/10.1139/t98-021

[41] Rujikiatkamjorn, C., Indraratna, B., 2007. Soft ground improvement by vacuum-

assisted preloading.

[42] Shirako, H., Sugiyama, M., Tonosaki, A., Akaishi, M., 2009. Behaviors of one-dimensional consolidation settlement after the removal of surcharge. Journal of Japan Society of Civil Engineers, Ser. C (Geotechnical Engineering) 65 (1), 275–287. https://doi.org/10.2208/jscejc.65.275 (in Japanese)

[43] Šuklje, L., 1957. The analysis of the consolidation process by the isotache method. Proc., 4th Int. Conf. on Soil Mechanics and Foundation Engineering, Vol. 1, Butterworths, London, 200–206.

[44] Tachibana, S., Ito, S., Iizuka, A., 2020. Constitutive model with a concept of plastic rebound for expansive soils. Soils and Foundations 60, 179–197. https://doi.org/10.1016/j.sandf.2020.02.007

[45] Tanaka, H., 2000. Sample Quality of Cohesive Soils: Lessons from Three Sites, Ariake, Bothkennar and Drammen. Soils and Foundations 40, 57–74. https://doi.org/10.3208/sandf.40.4_57

[46] Tanaka, H., Locat, J., Shibuya, S., Soon, T.T., Shiwakoti, D.R., 2001. Characterization of Singapore, Bangkok, and Ariake clays. Can. Geotech. J. 38, 378–400. https://doi.org/10.1139/t00-106

[47] Tanaka, H., Tsutsumi, A., Ohashi, T., 2014. Unloading behavior of clays measured by CRS test. Soils and Foundations 54, 81–93. https://doi.org/10.1016/j.sandf.2014.02.001

[48] Tanaka, H., Udaka, K., Nosaka, T., 2006. Strain Rate Dependency of Cohesive Soils in Consolidation Settlement. Soils and Foundations 46, 315–322. https://doi.org/10.3208/sandf.46.315

[49] Vergote, T.A., Leung, C.F., Chian, S.C., 2022. Modelling creep and swelling after unloading under constant load and relaxation with Bayesian updating. Géotechnique 72, 496–509. https://doi.org/10.1680/jgeot.20.P.106

[50] Vergote, Thomas A., Leung, C.F., Chian, S.C., 2021. Elastoviscoplastic modelling with distorted isotaches and swelling for constant strain rate and incremental loading. International Journal for Numerical and Analytical Methods in Geomechanics 45, 1920–1933. https://doi.org/10.1002/nag.3248

[51] Vergote, Thomas Alexander, Leung, C.F., Chian, S.C., 2021. Predicting sequential swelling and creep after unloading. In Proceedings of the 20th International

Conference on Soil Mechanics and Geotechnical Engineering, Sydney, pp. 4019–4026.

[52] Vergote, T.A., Leung, C.F., Chian, S.C., 2019. Creep after unloading: A comparison and validation of constitutive models. In Proceedings of the 16th Asian Regional Conference on Soil Mechanics and Geotechnical Engineering. Taipei, Taiwan.

[53] Watabe, Y., Kobayashi, M., Emura, T., Udaka, K., Watabe, A., 2009. Effect of layer thickness on the swelling behavior of Osaka Bay clay during unloading, The 44th Annual National Conference of Japanese Geotechnical Society. (in Japanese)

[54] Watabe, Y., Kobayashi, M., Emura, T., Udaka, K., Watanabe, N., 2010. The strain rate dependency on swelling process of Osaka Bay clay, The 45th Annual National Conference of Japanese Geotechnical Society. (in Japanese)

[55] Watabe, Y., Leroueil, S., 2015. Modeling and Implementation of the Isotache Concept for Long-Term Consolidation Behavior. Int. J. Geomech. 15, A4014006. https://doi.org/10.1061/(ASCE)GM.1943-5622.0000270

[56] Watabe, Y., Miyata, Y., Ishioka, M., 2021. Discussion on the strain rate dependency in consolidation behavior based on the isotache law and the power-law creep, The 56th Annual National Conference of Japanese Geotechnical Society. (in Japanese)

[57] Watabe Y., Tanaka M., Sassa S., Kobayashi M., Udaka K., 2009. Effects of specimen thickness and skeletal structure on consolidation behavior around consolidation yield stress, in: Proceedings of the 17th International Conference on Soil Mechanics and Geotechnical Engineering. IOS Press. https://doi.org/10.3233/978-1-60750-031-5-696

[58] Watabe, Y., Udaka, K., Morikawa, Y., 2008. Strain Rate Effect on Long-Term Consolidation of Osaka Bay Clay. Soils and Foundations 48, 495–509. https://doi.org/10.3208/sandf.48.495

[59] Watabe, Y., Udaka, K., Nakatani, Y., Leroueil, S., 2013. “Long-term consolidation behavior interpreted with isotache concept for worldwide clays” by Watabe, Y., Udaka, K., Nakatani, Y., Leroueil, S. [Soils and Foundations 52 (3) (2012) 449–464]. Soils and Foundations 53, 360–362. https://doi.org/10.1016/j.sandf.2013.01.003

[60] Watabe, Y., Udaka, K., Nakatani, Y., Leroueil, S., 2012. Long-term consolidation behavior interpreted with isotache concept for worldwide clays. Soils and Foundations 52, 449–464. https://doi.org/10.1016/j.sandf.2012.05.005

[61] Watabe, Y., Yoneda, A., Hashizume, H., Ono, Y., 2020. Multi-Stepwise Strain-Rate Loading Consolidation Test to Evaluate Strain Rate Dependency, in: Duc Long, P., Dung, N.T. (Eds.), Geotechnics for Sustainable Infrastructure Development, Lecture Notes in Civil Engineering. Springer Singapore, Singapore, pp. 1253–1258. https://doi.org/10.1007/978-981-15-2184-3_165

[62] Yamazoe, N., Nishimura, S., Tanaka, H., Ogino, T., Kochi, T., 2025. Long-term settlement behavior of peat after unloading and applicability of isotach law. Soils and Foundations 65, 101560. https://doi.org/10.1016/j.sandf.2024.101560

[63] Yao, Y.-P., Fang, Y.-F., 2020. Negative creep of soils. Can. Geotech. J. 57, 1–16. https://doi.org/10.1139/cgj-2018-0624

[64] Yin, J.-H., Tong, F., 2011. Constitutive modeling of time-dependent stress–strain behaviour of saturated soils exhibiting both creep and swelling. Can. Geotech. J. 48, 1870–1885. https://doi.org/10.1139/t11-076

[65] Yu, H., Lu, C., Chen, W., Tian, H., 2021. An insight into the creep mechanisms of a clayey soil through long-term consolidation tests. Bull Eng Geol Environ 80, 9127–9139. https://doi.org/10.1007/s10064-021-02472-3

[66] Yuan, Y., 2016. A new elasto-viscoplastic model for rate- dependent behavior of clays. PhD thesis, Massachusetts Institute of Technology.

[67] Yuan, Y., Whittle, A.J., 2018. A novel elasto-viscoplastic formulation for compression behaviour of clays. Géotechnique 68, 1044–1055. https://doi.org/10.1680/jgeot.16.P.276

[68] Zhou, Y., Sun, L., Ren, Y., 2023. Consolidation analyses of PVD-improved marine clay considering long-term natural sedimentation. Applied Ocean Research 141, 103795. https://doi.org/10.1016/j.apor.2023.103795

[69] Zhu, W., Yan, J., Yu, G., 2018. Vacuum preloading method for land reclamation using hydraulic filled slurry from the sea: A case study in coastal China. Ocean Engineering 152, 286–299. https://doi.org/10.1016/j.oceaneng.2018.01.063

Notations

C_c compression index

$C_{c\alpha}$ secondary compression index in normal consolidation behavior

C_s swelling index

$C_{s\alpha}$ secondary swelling index in unloading behavior

c_1, c_2 common model parameters for Eq. (6-1) in normal consolidation behavior

c_3, c_4 common model parameters for Eq. (6-3) in normal consolidation behavior

s_1, s_2 common model parameters for Eq. (6-4), Eq. (6-6) and Eq. (6-12) in unloading behavior

s_3, s_4 common model parameters for Eq. (6-9) in unloading behavior

ε_{vp} visco-plastic strain = total strain – elastic strain

$\dot{\varepsilon}_{vp}$ visco-plastic strain rate

σ'_p preconsolidation pressure (consolidation yield stress p'_c)

σ'_{pL} lower limit of σ'_p

σ'_{p0} σ'_p corresponding to $\dot{\varepsilon}_{vp} = +1.0\times10^{-7}$ s^{-1}

OCR overconsolidation ratio = σ'_{max}/σ'

OCR_L the high limit of OCR

OCR_0 OCR corresponding to $\dot{\varepsilon}_{vp} = -1.0\times10^{-7}$ s^{-1}

OCR_{ref} reference overconsolidation ratio, $OCR_{ref} = \frac{\sigma'_{p,+1\times10^{-7}s^{-1}}}{\sigma'}$

OCR_{refL} higher limit of OCR_{ref}

OCR_{ref0} OCR_{ref} corresponding to $\dot{\varepsilon}_{vp} = -1.0\times10^{-7}$ s^{-1}

$OCR_{Boundary}$ the OCR value of the intersection of the limit compression line with the unloading curve

R equaling to $\frac{\log\left(\frac{OCR}{OCR_{Boundary}}\right)}{\log\left(\frac{OCR_0}{OCR_{Boundary}}\right)}$ based on OCR; $\frac{\log\left(\frac{OCR_{ref}}{OCR_{refL}}\right)}{\log\left(\frac{OCR_{ref0}}{1.43}\right)}$ based on OCR_{ref} expression

R_{L} equaling to $\frac{\log\left(\frac{OCR_{\mathrm{L}}}{OCR_{\mathrm{Boundary}}}\right)}{\log\left(\frac{OCR_{0}}{OCR_{\mathrm{Boundary}}}\right)}$ ($\dot{\varepsilon}_{\mathrm{vp}} = 0\ \mathrm{s}^{-1}$) based on O$CR$; $\frac{\log\left(\frac{OCR_{\mathrm{refL}}}{1.43}\right)}{\log\left(\frac{OCR_{\mathrm{ref0}}}{1.43}\right)}$ based on OCR_{ref} expression

R_0 equaling to 1 ($\dot{\varepsilon}_{vp} = 1 \times 10^{-7}\ s^{-1}$)